APPENDIX II

The Optimal Control Model of a Pilot in V/STOL Aircraft Control Loops

This is a copy of the Final Report

THE INSERTION OF HUMAN DYNAMICS MODELS IN THE FLIGHT CONTROL LOOPS OF V/STOL RESEARCH AIRCRAFT

by

Mark E. Zipf
Department of Electrical Engineering
University of Pittsburgh, 1989.

Final Report for NASA Grant NAG 3-729

Computer Simulation of a Pilot in V/STOL Aircraft Control Loops

Funded By:
NASA Lewis Research Center
21000 Brookpark Road
Cleveland, OH 44135

PRINCIPAL INVESTIGATORS:

William G. Vogt
Professor of Electrical Engineering
University of Pittsburgh
Pittsburgh, PA 15261
(412) 624-9686

Marlin H. Mickle
Professor of Electrical Engineering
University of Pittsburgh
Pittsburgh, PA 15261
(412) 624-9682

PARTICIPANTS:

Mark E. Zipf, Research Assistant
Department of Electrical Engineering
University of Pittsburgh
Pittsburgh, PA 15261

Senol Kucuk, Research Assistant
Department of Electrical Engineering
University of Pittsburgh
Pittsburgh, PA 15261

THE INSERTION OF HUMAN DYNAMICS MODELS IN THE FLIGHT CONTROL LOOPS OF V/STOL RESEARCH AIRCRAFT

A FINAL REPORT FOR NASA GRANT NAG-729

Mark E. Zipf

Department of Electrical Engineering

University of Pittsburgh

Pittsburgh, PA.

ABSTRACT

This report presents an overview of research work focussed on the design and insertion of classical models of human pilot dynamics within the flight control loops of V/STOL aircraft. The pilots have been designed and configured for use in integrated control system research and design. The models of human behavior that have been considered are: 1) McRuer-Krendel - a single variable transfer function model, 2) Optimal Control Model - a multi-variable approach based on optimal control and stochastic estimation theory. These models attempt to predict human control response characteristics when confronted with compensatory tracking and state regulation tasks.

An overview, mathematical description, and discussion of predictive limitations of the pilot models is presented. Design strategies and closed loop insertion configurations are introduced and considered for various flight control scenarios. Models of aircraft dynamics (both transfer function and state space based) are developed and discussed for their use in pilot design and application. Pilot design and insertion are illustrated for various flight control objectives. Results of pilot insertion within the control loops of two V/STOL research aircraft (1) Sikorski Black Hawk UH-60A, 2) McDonnell Douglas Harrier II AV-8B) are presented and compared against actual pilot flight data. Conclusions are reached on the ability of the pilot models the adequately predict human behavior when confronted with similar control objectives.

TABLE OF CONTENTS

TABLE OF CONTENTS - continued

TABLE OF CONTENTS - continued

FIGURE LISTINGS

FIGURE LISTINGS - continued

TABLE LISTINGS

TABLE LISTINGS - continued

PLOT LISTINGS

PLOT LISTINGS - continued

PLOT LISTINGS - continued

PLOT LISTINGS - continued

PLOT LISTINGS - continued

NOMENCLATURE

t	$\triangleq$ Time variable.
S	$\triangleq$ Laplacian complex variable.
$H_n()$	$\triangleq$ Transfer function model of the human's muscular system.
T_n	$\triangleq$ Time constant of the human's muscular system.
$H_p()$	$\triangleq$ Transfer function model of human response dynamics.
K_p	$\triangleq$ Forward path gain of the human response model.
T_D	$\triangleq$ Time delay of the human response model.
T_L, T_L	$\triangleq$ Lead/Lag time constants of the McRuer_Krendel pilot equalization network.
T_K, T_K'	$\triangleq$ Time constants of the general form McRuer_Krendel muscular system.
w_n	$\triangleq$ Undamped natural frequency
ζ, ζ_n	$\triangleq$ Damping ratio
A, F	$\triangleq$ System matrix of a state space representation.
B, G	$\triangleq$ Input distribution matrix of a state space representation.
C, H	$\triangleq$ Measurement matrix of a state space representation.
$\bar{x}$	$\triangleq$ State vector of a state space representation.
$\bar{u}$	$\triangleq$ Input vector of a state space representation.
$\bar{y}, \bar{y}_p$	$\triangleq$ Precieved system output vector of a state space representation.

$\tilde{w}$ $\triangleq$ Disturbance vector of a state space representation.

V_{uu}, Q_u $\triangleq$ Remnant motor noise model.

V_{yy}, R_y $\triangleq$ Remnant observation noise model.

J() $\triangleq$ Cost function associated with the control objectives.

Q,Qopt $\triangleq$ State weighting matrix of the cost function.

R,Ropt $\triangleq$ Input weighting matrix of the cost function.

S,Gopt $\triangleq$ Control rate weighting matrix of the cost function.

q,p,r $\triangleq$ Vehicle pitch, roll, and yaw rates.

θ, ϕ, ψ $\triangleq$ Vehicle pitch, rollm and yaw(heading) Euler angles.

V_u, V_v, V_w $\triangleq$ Forward, lateral, and vertical vehicle velocities.

XX_u, YY_y, ZZ_w $\triangleq$ Longitudinal, lateral and vertical positions.

ALT,ALTDT $\triangleq$ Altitude and vertical rate, respectively.

$X_{(u,\theta,q,w,e,j,T)}$ $\triangleq$ Parameters of the X-directed force components of the longitudinal dynamics.

$M_{(u,q,w,e,j,T)}$ $\triangleq$ Parameters of the pitch rotational moment components of the longitudinal dynamics.

$Z_{(u,\theta,q,w,e,j,T)}$ $\triangleq$ Parameters of the Z-directed force components of the longitudinal dynamics.

NOMENCLATURE - continued

$L_{(p,v,r,a,rr)}$ $\triangleq$ Parameters of the roll rotational moment components of the lateral dynamics.

$N_{(p,v,r,a,rr)}$ $\triangleq$ Parameters of the yaw rotational moment components of the lateral dynamics.

$Y_{(\phi,p,v,r,a,rr)}$ $\triangleq$ Parameters of the Y-directed force components of the lateral dynamics.

δ_e $\triangleq$ Longitudinal stick cockpit control mechanism for the Harrier AV-8B.

δ_a $\triangleq$ Lateral stick cockpit control mechanism for the Harrier AV-8B.

δ_r $\triangleq$ Rudder pedal cockpit control mechanism for the Harrier AV-8B.

δ_j $\triangleq$ Nozzle angle lever cockpit control mechanism for the Harrier AV-8B.

δ_T $\triangleq$ Throttle lever cockpit control mechanism for the Harrier AV-8B.

δ_{mr_c} $\triangleq$ Main rotor collective stick cockpit control mechanism for the Black Hawk.

δ_{tr_c} $\triangleq$ Tail rotor collective pedal cockpit control mechanism for the Black Hawk.

δ_{lo_c} $\triangleq$ Longitudinal cyclic stick cockpit control mechanism for the Black Hawk.

δ_{la_c} $\triangleq$ Lateral cyclic stick cockpit control mechanism for the Black Hawk.

I. INTRODUCTION

The practical problems associated with aircraft flight control system design and evaluation are complex and wide ranging. During the design phase, control system designers are faced with the selection of the control parameters that will best fit the system performance and control objectives, the vehicle configuration, and the particular situation. Powered-lift V/STOL aircraft pose unique problems in controls design since the propulsion controls are an integral part of the overall flight control system. Control system response characteristics and thus the control parameters are typically chosen from analytic evaluations and iterative design methods. Mathematical models of the vehicle and control system are developed. Control parameters are selected by various techniques to achieve the desired response characteristics. Evaluations of the control system performance are carried out in computer simulation environments or by a closed form approaches. Test input deflections (i.e. steps, ramps, disturbances, etc.) are injected into the various control mechanisms to directly excite specific closed loop dynamics. Measurement and subsequent evaluation of the closed loop vehicle and control system responses determine if the desired characteristics have been achieved.

The analysis of the control system and aircraft dynamics, in this typical design approach, provides the designer with valuable insight to the system's general/functional operation, but with only a limited basis to gauge the final selection of the control parameters. These limitations are associated with the lack of the total system response (i.e. the summation of the aircraft, control system, and the human pilot's dynamics). When an actively participating human is introduced to the flight control environment, he brings with him a complex array of control responses, that serve as inputs to the vehicle and control system. These inputs differ significantly from the test inputs used during the initial design

process. Thus the pilot's dynamic behavior must be carefully considered throughout the design and evaluation process.

When actively involved and participating in a flight control environment, the pilot acts as a controls integrator by performing a variety of control tasks via the manipulation of the multiple cockpit control mechanisms (e.g. longitudinal and lateral stick, rudder pedals, throttle, etc.). In addition, some flight scenarios require the pilot to perform tasks other than the control commitments (e.g. communications, navigation, weaponry system, etc.). Because the pilot is such an integral component of the overall flight control structure, pilot opinion tends to be the major criterion for deciding whether control system performance is satisfactory.

Current approaches to incorporating human response characteristics during the control system design involve the use of fixed-base piloted simulators. This phase is a necessary step in the overall system design process and provides the ultimate source of human response characteristics for evaluation purposes. In addition, the pilot's opinion can be directly incorporated as the final gauge of the overall system performance. The direct incorporation of fixed-base human piloted simulation within the design phases provides a safe and effective environment for controls design, but suffers from problems of cost, scheduling, and inconvenience. These stem from the necessity that the development take place at remote sites within the simulator structure and schedule. To further complicate matters, one must also take into account the acquisition of qualified pilots.

An alternative approach, to the direct incorporation of actual human pilots, is the use of analytic models of human behavior within a computer simulation environment. These

"paper pilots" attempt to simulate various aspects of a human's dynamic response characteristics when confronted with certain classes of closed loop control objectives. Analytic pilot models provide the ability to analyze and evaluate the fully integrated, total system response characteristics, before the control system is introduced to a remote manned simulator facility. This approach represents a significant advantage in cost, time, and convenience by allowing the base line control system design to be completed at the home institution and then to be thoroughly tested and adjusted at a remote, manned simulator site.

Human pilot behavior is, however, very complex. Analytic models tend to be limited in their abilities to precisely predictor human behavior in a given situation. These limitations stem from the model's inability to fully simulate the human's methods of deriving information from a variety of sources (e.g. visual, auditory, etc.), the human's complex information processing activities, and his physical methods of applying the control commands. In addition, individual human pilots perform/act differently when confronted with identical control objectives. Thus, human pilot models can only attempt to represent human behavior is a very general sense.

I.A. A Piloted Control Simulation Structure

Pilot activities within a flight control environment are directed at a wide variety of operations and objectives. The pilot must provide the necessary control, stabilization, guidance, and navigation, along with any additional tasks associated with a specific mission. The pilot supplies the controls needed to achieve the mission objective by actively analyzing his environment and instituting the appropriate control commands. The pilot

therefore functions as a control integrator, by acting as the center piece of the entire control structure and actively participating in the closed loop control efforts.

A human pilot flies an airplane by a feedback method. He senses by sight or feels by "the seat of the pants", the motion of the aircraft, and manipulates various cockpit control mechanisms to minimize the error between the actual and some desired motion. In other words, the motion of the aircraft is perceived, both directly and indirectly through the visual inspection of cockpit flight instrumentation (e.g. altimeter, artificial horizon, etc), external visual cues, auditory (the manner by which a car driver can shift gears by the sound of the engine), and by physical means. Through his computational mechanisms and thought processes, the pilot assesses the perceived vehicle attitudes/orientations, and determines the necessary compensative corrections. The pilot applies the corrections to the cockpit control mechanisms, through the physical movement of his muscular system. This is a form of negative feedback control, where the controller (pilot), must close the loop to achieve some desired, overall control objective.

To simulate active pilot participation within a closed loop control environment, the control structure illustrated in Figure I.A.-1. has been considered. Within this structure, the pilot appears as a cascaded compensator that is driven by command based vehicle attitudes and orientations from some type of guidance or navigation process. The pilot attempts to orient the vehicle in the manner specified by the command via the manipulation of the appropriate cockpit control mechanisms. The control configuration shown in Figure I.A.-1 assumes that the pilot feedback is based on visual assessments of cockpit instrumentation and external visual cues. The assumption of visual feedback reduces the effectiveness of

the simulated pilot because of the inherent limitations due to the lack of other forms of feedback (i.e. auditory, physical, etc.).

The research work that is presented in this report is focussed on the development of analytic human pilot models, "Paper Pilots", to serve as design tools for controls systems research. The models are tailored for use in computer simulation environments involving V/STOL research aircraft. The control structure of Figure I.A.-1 is used as the basis for the design, analysis, and insertion of the pilot model within the control loops of the V/STOL aircraft that are considered. This report will present an overview of the human models, simulated aircraft environments, and inserted pilot results of the research that has been conducted. Chapter II presents a description of the models of human dynamic behavior that have been utilized. The inherent limitations in their abilities of predicting human behavior are discussed. Chapter III discusses the techniques utilized in the design and insertion of the pilot models. Aircraft simulation environments and some simplified models of vehicle dynamics are introduced for use in the design of the pilot models. Pilot design is demonstrated and control objective considerations are discussed. Finally, configurations for pilot insertion to the control environment are discussed. Chapter IV introduces the concepts involved in the development of the vehicle dynamics models that have been used in the design of the pilots. Model structure and parameter identification are discussed and considered for their compatibility with the specific pilot configuration. Models of specific V/STOL vehicles and regions of the flight envelope are presented. Chapter V illustrates the pilot design and control loop insertion strategies for the specific V/STOL vehicles. Pilot parameters are presented for the various vehicles and flight scenarios. Results of pilot insertion are presented and discussed. Comparisons are made between the pilot models and the flight data of actual human pilots performing similar flight control operations. Chapter

VI presents a discussion of the results and an overall conclusion of the research that has been conducted and poses questions to be considered for future research efforts. Appendix A discusses the general mathematical characteristics of the Optimal Control Model of human behavior. The continuous time OCM is discussed and a discrete time representation is derived. Appendix B presents the derivation of a high order state space model of the V/STOL research aircraft (Harrier II AV-8B) for use with the OCM. Appendix C is a users guide for the OCM software. The general structure of the OCM code is introduced and procedures for installation and application of the OCM are presented and discussed.

II. MODELS OF HUMAN PILOT BEHAVIOR

The human pilot models that have been considered in this research are based on quasi-linear models of human behavior in closed loop compensatory tracking and state regulation tasks. The predicted/simulated human compensative control responses are generated from visual assessments of some displayed error or external visual cue. The models do not consider the other techniques that actual humans utilize to obtain information (i.e. auditory, physical (seat of the pants)). A human's control characteristics can be simulated by a cascade of three linear operators[1,2,3,4,5,6,7], as shown in Figure II.-1, and enumerated below:

1. Neuro-Muscular/Motor Dynamics - This operator describes the lags/bandwidth constraints imposed by the human's muscular system and is approximated by an adjustable, linear, first-order lag given by:

$$H_n(S) = \frac{1}{T_nS+1} \qquad \text{(II.-1)}$$

where T_n is the time constant of the neuro-motor response. It is important to note that the human's muscular bandwidth is often restricted by the rate limitations of the cockpit control mechanism. The time constant of this lag can be selected to accommodate these effects on the bandwidth at which the human can exert control operations.

2. Pure Time Delays - These operators describe various internal time delays associated with visual information processing and neuro-motor signal pathways.

3. Equalization Network - This operator describes the control strategy implemented by the human to close the loop in a manner that best fits a given situation. Typically, the human

will select the equalization network to provide the dominant closed loop control response with a damping ratio (ξ) in the range, 0.5-0.8, and a natural frequency (ω_n) in the range, 3-4 rad/sec.

The inherent unpredictability of the human's response is simulated by a random component called the controller remnant.

In this research, two types of human dynamics models have been considered: 1) McRuer-Krendel - a single variable linear transfer function description, 2) An Optimal Control Model - a multi-variable state space approach based on optimal control and stochastic estimation theory. Each model is based on differing implementations of the three cascaded operator description. This section presents a general overview of the two models, their mathematical foundations and their inherent limitations of simulating/predicting human dynamic behavior.

II.A. - McRuer-Krendel Model of Human Dynamics

The McRuer-Krendel model (MKM) is a single-degree of freedom quasi-linear model based on a best fit analysis of experimental human response data [1,2,3,6,7]. The model uses assessments of visually-based information to produce compensative control mechanism displacements. The general form is given by:

$$H_p(s)=K_p e^{-T_D s}\frac{(T_L s+1)}{(T_I s+1)}\left\{\frac{(T_K s+1)}{(T_K' s+1)}\frac{1}{\left[(s/\omega_N)^2+2(\xi_N/\omega_N)s+1\right]}\right\} \qquad \text{(II.A.-1)}$$

where $H_p(s)$ is the transfer function of the human response, often referred to as the describing function, s is the complex Laplace transform variable, the input is the visually based error signal, while the output is the corresponding control displacement. McRuer and Krendel discuss typical values of the precision model in [1,2,3].

Within this model, human activities are represented by physiological and equalization sections. Physiologic attributes simulate the limitations and abilities of the human's physical mechanisms. The inherent lags associated with the human's visual, information processing, and signal transmission systems are modeled by a pure delay. The restrictions associated with the muscular system are represented by the system within the brackets. The equalization attributes simulate the control strategies employed by the human to achieve the required closed loop responses in the form of a lead-lag network. The primary focus of the research using this type of human pilot model has been directed toward the fundamental control activities of the pilot during various flight control maneuvers. A zero remnant is therefore used during the development of the McRuer/Krendel pilot control strategies. Remnant selection for these types of piloted flight configurations is described in [8].

The model of EQ(II.A.-1) can be simplified to obtain the transfer function,

$$H_p(s)=\frac{K_p e^{-T_D s}(T_L s+1)}{(T_N s+1)(T_I s+1)} \qquad \text{(II.A.-2)}$$

where very low and very high frequency accuracy is not necessary. This transfer function model is illustrated in the simplified block diagram of Figure II.A.-1. The rejection of the very low and high frequency content is a reasonable assumption for the human pilot since, as discussed before, the bandwidth of the closed loop is 3-4 rad/sec (or 0.48-0.64 Hz).

The pure transmission time delay parameter T_D is estimated to be between 0.13-0.23 seconds [1,2,3,6,7]. Although the changes in the time delay can be significant depending on the particular control task, the parameter selected at T_D=0.20 was considered reasonable for the purposes of this research. The term $1/(T_N s+1)$ is an approximation of the neuro-muscular lag of the arm meaning that the pilot can not move his arm faster than the rate of this pole. The value of T_N is assumed to be constant and approximately 0.10 seconds. The remaining term, $K_p(T_L s+1)/(T_I s+1)$, is the equalization part of the model (a time dependent variable gain and a lead-lag compensator) whose parameters are altered by the pilot to the particular flight configuration and control objective. The constraints on the model parameters are as follows:

$$0.0 \leq T_L \leq 2.50 \ (T_L \neq T_N) \qquad \text{(II.A.-3a)}$$

$$0.0 \leq T_I \leq 20.0 \qquad \text{(II.A.-3b)}$$

$$T_N = 0.10 \qquad \text{(II.A.-3c)}$$

$$T_D = 0.20 \qquad \text{(II.A.-3d)}$$

The lead-lag compensator/equalizer is based on the assumption that the human is required to furnish at least one differentiation and one integration to obtain the desired performance, and the constraints on the parameters, T_L and T_I determine how efficiently the integration and differentiation processes are performed by the human. Even though there are only a few parameters to be adjusted, the analysis is still not trivial because of the time delay, time-varying pilot parameters and time-varying aircraft dynamics.

II.B. - The Optimal Control Model

The Optimal Control Model (OCM) [4,5,6,7] is a multi-variable approach to the modeling of human behavior. The OCM is based on the use of modern control and estimation theory to simulate/predict human behavior in closed loop control operations. The OCM is capable of treating multi-variable systems by incorporating a single conceptual framework based on state space techniques. The primary assumption involved in the OCM is that a well trained human pilot/operator behaves in a near optimal manner subject to his inherent limitations, constraints, and control tasks [4]. This optimal behavior is simulated by an analogous optimal control system. The optimal control system operates to minimize a quadratic performance index in the presence of various system inputs, noises, and disturbances.

The system under control consists of the control element and displays which are modeled by a linear state equation and output equation.

$$\dot{\bar{x}}(t) = A\,\bar{x}(t) + B\,\bar{u}(t) + \bar{w}(t) \qquad \text{(II.B.-1)}$$

$$\bar{y}(t) = C\,\bar{x}(t) \qquad \text{(II.B.-2)}$$

The "n" dimensional state vector is defined by:

$$\bar{x} = [x_1, x_2, \ldots, x_n]^T \qquad \text{(II.B.-3)}$$

The human manipulates "m" controls:

$$\bar{u} = [u_1, u_2, \ldots, u_m]^T \qquad \text{(II.B.-4)}$$

and observes "l" system displays (output variables):

$$\bar{y} = [y_1, y_2, \ldots, y_l]^T \qquad \text{(II.B.-5)}$$

It is assumed, from remnant and psychophysical studies of human perception [9] that the human can extract position and rate from a single display or external visual cue, but can not extract higher derivatives. Thus the output "y(t)" contains those quantities explicitly displayed as well as those implicitly derived by the human. This is an important concept because it will be directly incorporated in the organization of the vehicle model and the strategies associated with displayed information. The disturbance, $\bar{w}(t)$, is a vector of zero mean, white gaussian noise processes and is generally associated with atmospheric turbulence when considering aircraft applications.

The OCM models human behavior in two categories: 1) intrinsic human limitations, 2) human control/equalization efforts. Simulation of human limitations is provided by a time delay, a neuro-muscular dynamics model, and a controller remnant. The time delays associated with visual information processing, neuro-muscular signal propagation, and other operations are combined into a lumped equivalent perceptual time delay, T_D. It is assumed that all outputs are delayed by the same amount. Typically, this delay is on the order of 0.2 seconds [4,5,6,7,10,11,12]. Neuro-muscular/motor dynamics are represented by an adjustable lag matrix, T_N. This lag is not directly modeled as an inherent limitation, but is indirectly incorporated by weighting the control rate terms in the cost function of the optimal control strategy. The inclusion of a control rate term results in a first-order lag being introduced in the optimal controller. This term is utilized to indirectly model the physiological limitations of the rate at which a human can perform a control action due to

the neuro-muscular/motor dynamics. Controller remnant is modeled by an observation noise vector, $V_{yy}(t)$, and a motor noise vector, $V_{uu}(t)$, where

$$E\{\bar{V}_{yy}(t),\bar{V}_{yy}^{T}(\sigma)\} = R_y\,\delta(t-\sigma) \qquad \text{(II.B.-6)}$$

$$E\{\bar{V}_{uu}(t),\bar{V}_{uu}^{T}(\sigma)\} = Q_u\,\delta(t-\sigma) \qquad \text{(II.B.-7)}$$

The observation noise models the inherent uncertainty of the human's visual assessments of the displayed information. A separate noise source is associated with each displayed output. The noise processes are modeled as an independent, zero mean, white, gaussian noise sources. The spectral density is proportional to the mean-squared value of the displayed variable, which is basically a signal-to-noise ratio that is on the order of -20dB [5,6,7,8,10]. The motor noise models the inherent uncertainty of the human's control execution. Like the observation noise, the motor noise is assumed to be independent, zero-mean, white, and gaussian. The spectral density is proportional to the mean-squared operator output. The motor signal-to-noise ratio is typically chosen near -25dB [5,6,7,8,10].

The human's equalization network describes the manner in which the human attempts to optimize his control strategy to match a given situation. As shown in Figure II.B.-1, the human perceives a delayed noisy replica of the system output, $y_p(t)$, where:

$$y_p(t) = y(t-d) + V_{yy}(t-d) \qquad \text{(II.B.-8)}$$

Estimation of the delayed state vector, $\hat{\bar{X}}(t-T_D)$, is accomplished via a Kalman filter. The Kalman filter models the human's deduction of the system states from the displayed information. A least mean-squared predictor generates a present time state estimate, $\hat{\bar{X}}(t)$,

from the delayed estimate, $\hat{\bar{X}}(t-T_D)$. The predictor models the human's compensation for his inherent time delay. The optimal gain matrix, K^*, is generated by the solution, in steady state, of the optimal regulator problem [13] for the cost function of the form:

$$J(u) = \lim_{T \to \infty} E \left\{ \frac{1}{T} \int_0^T [\, \bar{x}(t)^T Q \bar{x}(t) + \bar{u}(t)^T R \bar{u}(t) + \dot{\bar{u}}(t)^T S \dot{\bar{u}}(t)] dt \; y_p(\sigma) \right\} \tag{II.B.-9}$$

where

$\sigma \leq t$

Q and R are positive semi-definite

S is positive definite

The application of the optimal control, Kalman filter, and predictor require the use of an internal reference model (i.e. the model of the vehicle as perceived by the operator) to generate their appropriate gains and parameters. Thus the model of the system under control plays an important role in the response actions of the OCM. Appendix A.1 presents a mathematical overview of the OCM in a continuous time representation. For use in the simulation model program, the continuous time model is converted to a discrete time representation. The concepts involved and the resulting discrete time OCM are presented in Appendix A.2.

III. STRATEGIES OF PILOT MODEL APPLICATION

The inherently different structures of the McRuer-Krendel model (MKM) and the Optimal Control Model (OCM) require different approaches in parameter selection and control loop insertion. The MKMs are specifically designed for each control objective and region of the flight envelope. The equalization parameters are selected off-line, by Root-Locus techniques and arranged in a gain table format. The multi-variable aspects of the OCM are directly incorporated in high order control configurations. Cost function weightings are selected according to parameters extracted from actual piloted flight data and arranged for the specific control situation. This section will discuss the techniques utilized to select the pilot's control parameters and the configurations used to insert the pilots within the simulated control environment.

III.A. Aircraft Simulation Environments

Before introducing the techniques utilized to select and insert the pilot models, it is important to discuss the computer-based aircraft simulation environments that were used in this research. The principle tools utilized to examine the V/STOL vehicles and evaluate the performance of the pilot models were two computer simulation programs [14,15,16,17] provided by NASA Lewis. These programs implement nonlinear, total force, large angle representations, in six degrees of freedom. These programs provide full flight envelope operation and incorporate all on-board stability augmentations systems.

III.B. McRuer-Krendel Pilot Models with Static Parameters

The static MKM pilots are based on the selection of the equalization parameters, for specific regions of the flight envelope, through the use of off-line application of Root-Locus techniques. In this approach, low order transfer function models of the aircraft dynamics are developed for regions of the flight envelope that are of interest. The regions of the flight envelope are designated by the vehicle's forward velocity. Pilot equalization parameters are selected from the use of a delayed Root-Locus and the direct incorporation of the pilot's physically limiting factors. Pilot parameters are then arranged in gain tables according to the flight envelope region. This design process is carried out for all cockpit control mechanisms (e.g. Lateral and Longitudinal Stick, Rudder Pedals, etc.) and for the vehicle attitudes and orientations that are relevant to the flight control objectives. This creates a set of Single Variable Pilot Mechanisms (SVPM). The insertion of a static MKM pilot is achieved by selecting an appropriate group of SVPMs for the objectives associated with the flight scenario. The insertion group has a SVPM defined for each cockpit control mechanism and thus has a unique feedback structure. The insertion group is therefore valid for only a limited number of flight control objectives.

III.B.1. - Structure of Aircraft Dynamics Models

The models of aircraft dynamics for use in the design of the MKM pilots, are based on single variable low order, linear transfer functions. The transfer function models are derived from the dominant response characteristics of the vehicle dynamics due to the injection of test inputs (e.g. impulses, steps, etc.) to the cockpit controls. The dominant responses refer to the most pronounced (primary) vehicle attitude reaction due to the deflection of a single cockpit control mechanism. The remaining vehicle reactions (i.e. the

coupled responses occurring in the other attitudes due to the operation of the cockpit control mechanism), are considered secondary. This definition of primary and secondary vehicle responses is illustrated in Figure III.B.1.-1. During SVPM development, the secondary reactions are ignored and considered as disturbances. The secondary reactions are, however, considered in the selection of an insertion group.

The dominant aircraft dynamics responses were identified by the direct evaluation of the time and frequency domain responses of the simulation model programs due to the test input deflections of the cockpit control mechanisms. Time based responses were utilized to match simplified low order responses. The frequency responses were obtained by Fast Fourier Transforms of the time responses. Attempts at the determination of ultra-low frequency response characteristics were hampered by the presence of parasitic low frequency response modes (Phugoid Modes) and distortions associated with the cross-couplings of the secondary variables. Solutions to these problems are considered in [19,20].

Along with the initial decoupling of the primary and secondary responses, the control and response characteristics of each vehicle were separated into two groups: 1) Longitudinal Control Set, and 2) Lateral-Directional Control Set. These sets consider the effects of the control mechanisms on the overall orientations of the vehicle to the primary orthogonal planes [18,19,20]. These sets simplify the selection of the SVPM when constructing an insertion group.

III.B.2. - Development of SVPM Equalization Parameters

The development of the Single Variable Pilot Mechanisms are based on the single loop control structure shown in Figure III.B.2.-1. This single variable control configuration is organized in such a way that the manipulation of a specific cockpit control mechanism is based on the assessment of visual feedback obtained from the observation of a single cockpit instrument or external visual cue. The relationship of aircraft dynamics to the specific cockpit control is obtained from the analysis of the aircraft dynamics discussed previously, and the desired control variable.

The MKM equalization parameters are selected via Root-Locus techniques. A problem that complicates this approach is the pure time delay associated with the human's visual, computational, and signal conduction delay model. In the continuous time domain, a pure time delay corresponds to an infinite number of poles positioned at $S = -\infty$ on the real axis. These poles introduce an infinite number of asymptotes that are parallel to the real axis. The presence of these asymptotes (specifically the primary asymptote) create significantly destabilizing distortions of the asymptotic behavior of the Root-Locus, as shown in Figure III.B.2.-2. An additional problem that is presented by the delayed Root-Locus is that many of the non-delayed assumptions are no longer valid.

To overcome the complications associated with the delayed Root-Locus, an approximation to the infinite pole set was applied in a non-delayed format. The pure delay approximation is given by:

$$e^{-T_D S} \sim \frac{1}{(1 + \frac{T_D}{N} S)^N} \qquad \text{(III.B.2.-1)}$$

where $T_D = 0.2$ seconds for this application.

This approximation not only simulates asymptotic behavior, but also permits all non delayed assumptions. To remain within computational limits (Quad Precision), 20 poles were placed at S = -100 on the real axis, as shown in Figure III.B.2.-3. The primary asymptote of this pole set has a 9° angle of incidence and has an imaginary axis intercept at 15.84 rads/sec (15.71 rads/sec for the ideal pure delay). This pole set serves as a reasonable approximation to the pure delay when considering the closed loop natural frequency of the piloted control ($W_N \sim 3.5$ rads/sec).

Incorporating the delay approximation and the muscular system limitation pole, a modified transfer function for design purposes only) can be given by:

$$G_{PILOT}^{DESIGN}(s) = \frac{K(S + a)}{(S + b)} \left\{ \frac{(100)^{20}}{(S + 10)(S + 100)^{20}} \right\} \qquad \text{(III.B.2.-2)}$$

where $a \geq 0.8$

$b \geq 0.0$

III.B.3. Multi-variable McRuer-Krendel Pilot Insertion Techniques

When a participating human pilot is introduced into the control loops, he uses all cockpit control mechanisms to provide an operational control by employing visual, audio, and other forms of feedback cues. For the purpose of simulation, a comprehensive human

response pilot model is constructed by integrating various single variable pilot mechanisms (SVPM) into a multi-variable structure (an insertion group), as shown in Figure III.B.3.-1.

The multi-variable pilot structural configuration is defined by the manner in which visual feedback is interpreted and applied to the cockpit control mechanisms via a specific set of Single Variable Pilot Mechanisms (SVPM). The intrinsic limitations of each configuration (insertion set) make it applicable to only a specific set of flight control maneuvers. This is primarily due to the limited number of feedback paths that are available (i.e. the number of feedback paths equals the number of cockpit control mechanisms). Each type of flight maneuver or command sequence is therefore associated with a specific multi-variable pilot configuration. In general, a command maneuver will be described by a set of vehicle attitudes and/or rates that define the new orientation that the vehicle is required to attain. The intricacy of the maneuver defines the number of attitudes and/or rates that are simultaneously involved in the operation.

The flight control objectives associated with simple maneuvers require the control of only one primary vehicle attitude or rate. The remaining secondary variables are monitored and regulated (regulation set) to preserve the stabilized aspects of the vehicle orientation (e.g. level flight). This type of operation can be performed by the configuration shown in Figure III.B.3.-2. A regulation set is defined by the single variable pilot mechanisms that are associated with the flight control variables needed to maintain a stabilized operation in a specific maneuver. The selection of the regulation set is based on the primary command attitude and the general operations involved in the execution of the maneuver. Large scale secondary responses must be compensated, proper feedback paths must be allocated, and the appropriate SVPMs must be utilized. This is similar to the manner in which a well

trained pilot reconfigures his feedback for a given situation. An additional concern in the selection of an insertion set is the use of multi-function cockpit control mechanisms. These controls are utilized differently depending on the control objectives. A good example of a multi-function control mechanism is the rudder pedals. During level forward flight, the pedals are used to make minor heading corrections, while during coordinated turns, they are used to minimize sideslip. This type of control mechanism is handled through the assignment of the feedback path and equalization network.

III.C. - Optimal Control Model

The multi-variable structure of the OCM makes it's insertion to the control loop relatively simple. The application of the OCM is based on parameter selection in two basic categories: 1) Control task related, 2) Pilot model related. This section will provide an overview of the general construction of the OCM.

III.C.1. - Control Task Description

The first concern is the description of the control task. The control task must be described analytically, this includes the specifications of the system under control (vehicle) and the objective of the control activity (trajectory). As indicated previously, the vehicle is represented by a state space model. Care must be taken in selecting the vehicle model due to its implicit use in the formulation of the optimal control gains, Kalman filter and predictor. The state and output vectors must be chosen in such a way as to not limit the manner in which the OCM will extract estimates of vehicle orientation from the visually displayed

information. Control objectives are reflected in the cost function parameters. The controller's specific task is to choose a control input, on the basis of observing the displays, so as to minimize a weighted sum of the averaged state and control variables.

Once the vehicle and the control task have been specified, determination of the displayed variables is relatively straight forward. The control task, can at times, indicate the variables that are considered, or the displayed variables can be concluded from the available cockpit instrumentation. In certain control tasks a marked target, in the form of an external visual cue, is used. The variables available from the target are therefore related to it's markings and are thus described by the display vector associated with the target. As mentioned previously, the displayed variables include the quantities explicitly displayed plus their first derivatives.

III.C.2. - Pilot Description

The OCM pilot is described by four parameters: 1) Time delay, 2) Observation noise, 3) Motor noise, 4) Neuromuscular lag. The overall structure of the OCM is based on optimal control theory, but the theory does not provide the parameter selection. This information is typically obtained from human performance data.

The time delay in simple compensatory tracking and state regulation tasks is generally on the order of 0.1 to 0.3 seconds [4,5,6,7,10,11,12]. In complex tasks, the time delay is difficult to determine. Values near 0.2 seconds have shown to be reasonable choices from human performance data [7,10,12].

Observation noise plays an important role in the estimation problem, because it tends to be the dominant source of controller remnant. Various experiments have been performed [8] to obtain reasonable estimates of the observation noise spectral density. Typical values, for simple tracking tasks are on the order of -20dB while for complex operations -10dB has shown good results [10].

Motor noise is a difficult quantity to extract from human performance information. Typically, model matching techniques are incorporated to determine reasonable values. Spectral density signal-to-noise ratios on the order of -25dB have been indicated for relatively simple tasks [5,6,7] and near -10dB for complex tasks [10]. The effects of motor noise, however, do not appear to be great and have even been neglected in some cases [5].

The muscular system model of the OCM is based on the subjective weighting of the control rate terms of the cost function. The values of the lag matrix, T_N, must be chosen for the specific muscular activity and cockpit control dynamics. Classical values of T_N=0.1 do not appear to be valid when considering complex control tasks or stiff control mechanisms. Time constants on the order of T_N=1.4 - 0.2 have been shown to more closely agree with pilot data [6,7,10,11,12]. In addition, the muscular system involved with the use of the legs (for executing control manipulation of the rudder pedals) must take into consideration the inherent reduction in bandwidth.

III.C.3. - Difficulties in applying the OCM

The OCM provides a great many algorithmic and computational advantages in the quantitative estimation of a human operator's dynamics. There are, however, some difficulties that arise during the application of the OCM. The first relates to the explicit

requirement that the human pilot description be based on an internal model of the human's inherent characteristics, the dynamics of the system under control, and external disturbances. To provide a present time state estimate, $\hat{\underline{X}}(t)$, the system matrices (A,B,C) ,system disturbances, the human time delay, observation and motor noises must all be known. To generate the controller's optimal state variable feedback gains the A and B matrices along with the control objective weights of the cost function are required. Essentially, this amounts to a complete knowledge of the pilot from man-machine system concepts. The OCM requires a very accurate internal model if it is to adequately function in a manner consistent with human behavior within the control environment.

The second difficulty stems from the fundamentally difficult problems associated with identifying the pilot's internal model parameters from experimental data. In addition, the optimal control strategy suffers from a degree of over parameterization. From an identification viewpoint, observation and motor noises are unresolvable and optimal control and state estimation gains can only be determined from the matching of experimental data or through the similarity transformation of the model [6].

The final problem is associated with the specification of the control objective cost function. The cost function parameters must be selected in accordance with the control task and thus the OCM designer must speculate on the parameters that will be of importance to the actual human pilot.

IV. MODELS OF V/STOL RESEARCH AIRCRAFT

Two types of V/STOL research aircraft have been used in this study: 1) Sikorski Black Hawk UH-60A - a modern high performance helicopter and 2) McDonnell Douglas Harrier II AV-8B - a thrust vectored jet fighter. Aircraft dynamics where simulated by nonlinear computer program models [14,15,16,17], provided by NASA-Lewis. Both programs implement total force, large angle, nonlinear representations of the individual aircraft dynamics in time based computer simulation environments. These vehicle definitions provide full flight envelope operation and support the onboard flight stabilization and control systems.

The vehicle models that have been developed in this study are designed to complement the structures of the individual pilot models. The McRuer/Krendel pilots require the use of low order/decoupled transfer function vehicle models , while the OCM model relies on high order/coupled state space representations. Linearized models of the aircraft dynamics (for use in the design of the pilot models) where developed by a mix of analytic models of vehicle motion and direct analysis of the time and frequency responses of the simulation program to test deflections of the cockpit control mechanisms. The following sections provides an overview of the vehicle, the model structures, parameter identification techniques, and the resulting vehicle models.

IV.A. Harrier II AV-8B : A Thrust Vectored Jet Fighter

The Harrier AV-8B's thrust vectoring capabilities make it a truly unique aircraft. The regions of the Harrier's flight envelope can be defined by the direction of the thrust vector, and consists of the three basic flight configurations shown in Figure IV.A.-1. The high

speed configuration, shown in Figure IV.A.-1.a, is characterized by the thrust vector being directed forward (i.e. nozzle jet vectors aft). In this mode, the propulsion system supplies the forward thrust component in a manner that is common to conventional aircraft. The lift and control components are supplied by the aerodynamic surfaces as they are forced through the atmosphere. The magnitude of the thrust vector supplied by the propulsion system is used to control vehicle speed. The stabilator is used to control the angle of attack and altitude.

The transition mode, shown in Figure IV.A.-1.b, is described by a general loss of aerodynamic responsiveness. As forward speed decreases, aerodynamic surfaces loose their ability to provide necessary lift and control functions. As the name implies, the vehicle control actions are in a transition between atmospheric flight and powered-lift activities. In general, sustained flight in this region is avoided by the typical maneuvers associated with acceleration to and deceleration from the high speed envelope.

The low speed configuration, shown in Figure IV.A.-1.c, is characterized by the thrust vector being directed upward (i.e. nozzle jet vectors downward). The lack of sufficient forward velocity requires that the propulsion system provide the lift components (powered-lift). A closer examination reveals that the propulsion system supplies the forward thrust and the primary lift component in a manner similar to a helicopter's main rotor. The magnitude of the thrust vector is primarily utilized to control the altitude and it's direction is used to adjust forward speed.

The interesting region of the Harrier's flight envelope occurs during low speed powered-lift activities. In this region, the aerodynamic properties of the aircraft

significantly differ from those of high speed conventional flight. During low speed flight the components of lift produced by aerodynamic means are small. The vehicle relies primarily on lift components supplied by the propulsion system. In addition, the aircraft's aerodynamic control surfaces (e.g. rudder, ailerons, etc.) no longer function as the primary control mechanisms. The Harrier relies on the Reaction Control System (RCS) to provide the additional control components that are needed to maneuver the aircraft.

The primary focus of the research on pilot models for the Harrier II AV-8B has been directed toward the low speed - powered-lift region of the flight envelope. Dynamic response tests and general use of the simulation model programs were conducted while in trimmed forward flight at speeds ranging from hover to 35 knots. The vehicle was configured with the landing gear down, flaps extended to 60 degrees, and the lift enhancement devices fully extended. The SAS was enabled to provide damping of angular rates.

IV.A.1. - Harrier Control Structure

When operating in the low speed region of the flight envelope, the Harrier's control structure shows signs of a modest decoupling of the longitudinal and lateral dynamics. Longitudinal and lateral control sets are defined by the control strategies that are associated with the cockpit control mechanisms. The longitudinal control set specifies the control mechanisms and their associated reactions that primarily influence vehicle responses in the longitudinal plane (X-Z body plane). The three cockpit control mechanisms that operate within this region are: 1) nozzle angle control, 2) throttle, 3) longitudinal stick.

Nozzle Angle Control

The nozzle angle controls the direction of the propulsion system thrust vector. A typical low speed - powered-lift thrust diagram of a decrease in nozzle angle is shown in Figure IV.A.1.-1. The nozzle angle for this region of the flight envelope is large. The control structure is very similar to that of the longitudinal cyclic of a helicopter. Minor changes in the direction of the thrust vector will tend to dominate the forward thrust component. This indicates that the nozzle angle will dominate the control of the vehicle's forward speed. Small variations of the nozzle angle in low speed flight will have only a small effect on the primary lift components. The moment arm associated with the thrust vector displacement from the vehicle's center of gravity will induce a relatively small pitching torque in the longitudinal plane.

Throttle

The throttle controls the magnitude of the propulsion system's thrust vector. A thrust diagram of an increase in engine speed is shown in Figure IV.A.1.-2. This control behavior is similar to the main rotor collective of a helicopter. Changes in the magnitude of the thrust vector will tend to dominate the lift component and thus the vehicle altitude. Minor changes in the thrust vector magnitude will have only a small impact on the velocity components and the thrust vector displacement from the vehicle center of gravity will induce a relatively small pitching torque in the longitudinal plane.

Longitudinal Stick

The longitudinal stick controls the stabilator angle of attack and the vents of the RCS's forward and aft jets. During powered-lift activities the auxiliary thrust components and the associated moment arms (due to their physical configurations) of the forward and aft RCS jets to induce pitching torque responses about the Y body axis in the longitudinal plane. Figure IV.A.1.-3 illustrates the auxiliary thrust components produced by deflecting the longitudinal stick. Engine air bleed of the RCS will tend to effect the propulsion system performance. The aircraft longitudinal inertial components tend to induce sluggish responses. During low speed flight, the longitudinal stick is primarily used to control longitudinal orientations (e.g. angle of attack, pitch angle). It is important to note that the primary thrust vector of the propulsion system will be redirected during pitching maneuvers if the nozzle angle is fixed. This can result in changes in forward speed and altitude.

The lateral - directional control set specifies the control mechanisms and their associated reactions that influence vehicle responses in the lateral plane (Y-Z body plane) and in the directional plane (X-Y body plane). The two cockpit control mechanisms that operate in this set are: 1) lateral stick, 2) rudder pedals.

Lateral Stick

The lateral stick controls the ailerons and the vents of the wing-tip RCS jets. When operating in the low speed region of the flight envelope the auxiliary thrust components and the moment arms of the wing tip RCS jets are used to induce rolling torques about the X body axis. Figure IV.A.1.-4 illustrates the auxiliary thrust components produced by deflection of the lateral stick. Again, the air bleed of the RCS jets will effect engine

performance. The lateral inertial components and the RCS wing tip geometry create a highly responsive rotational moment about the X body axis. The rolling motion redirects the lateral components of the thrust vector and will therefore tend to dominate the lateral velocity components. The lateral plane components tend to be coupled to reactions in the directional plane.

Rudder Pedals

The rudder pedals control the rudder angle and the vents of the tail-end RCS jets. During powered-lift operations, the thrust components and moment arm of the tail-end RCS jets are used to execute yawing and lateral control maneuvers. Figure IV.A.1.-5 illustrates the auxiliary thrust components produced by deflection of the rudder pedals. Again, RCS air bleed will effect engine performance. The RCS thrust vectors induce rotations about the Z body axis. This allows rudder pedal control of the lateral velocity during turn coordination tasks (sideslip reduction) and heading regulation.

IV.A.2. - Low Order Transfer Function Models of Harrier Dynamics

This section presents the development of a set of low order linear transfer function models (for use in the design of the McRuer/Krendel pilot models) that are based on an investigation of the fundamental behavior of the nonlinear aircraft simulation model. The low order models describe dominant, decoupled, short period vehicle dynamics that are induced by deflections of specific cockpit control mechanisms [20]. These models do not attempt to account for the inherent couplings of the vehicle dynamics or any long term response characteristics (e.g. longitudinal phugoid modes, lateral spiral or dutch roll

modes). Long term dynamic modes and cross couplings are neglected and considered secondary to the dominant responses.

The low order linear transfer function models of the aircraft dynamics where obtained by an analysis of the time and frequency responses of the simulation program to test deflections of the cockpit control mechanisms. To simplify and limit this discussion, several examples of low order model identification will be presented. A comprehensive analysis and evaluation of the transfer function models can be seen in [20].

Pitch Angle/Longitudinal Stick Model

As shown in Figure IV.A.1.-3, the longitudinal stick dominates the pitching motions. The time based, short period pitch rate response while in a near hover, due a 1 inch impulse deflection of the longitudinal stick can be seen in Plot IV.A.2.-1. This type of time response can be modeled by a simple pole residing on the negative real axis of the Laplacian complex plane. A low order transfer function model that describes this type of time response is given by:

$$\frac{q(S)}{\delta_e(S)} \sim \frac{K_{THETDT}}{S + a_{THETA}} \qquad \text{(IV.A.2.-1)}$$

where

$$K_{THETDT} = 0.71 \ \frac{deg}{inch\text{-}sec^2} \qquad \text{(IV.A.2.-2a)}$$

$$a_{THETA} = 1.56 \ sec^{-1} \qquad \text{(IV.A.2.-2b)}$$

The pitch angle model is the direct integral of the pitch rate model and is given by:

$$\frac{\theta(S)}{\delta_e(S)} \sim \frac{K_{THET}}{S(S + a_{THETA})} \qquad \text{(IV.A.2.-3)}$$

The parameters of these equations vary only slightly, due to the relatively small changes in aerodynamic effects within the low speed region of the flight envelope.

Roll Angle/Lateral Stick Model

The lateral stick's dominant effect on rolling motions can be seen in Figure IV.A.1.-4 tends to dominate the rolling motions. The time based response of the roll rate due to a 1 inch impulse on the lateral stick is shown in Plot IV.A.2.-2. The roll rate response is similar to the pitch rate response, but has a much shorter time constant. The transfer function model is given by:

$$\frac{p(S)}{\delta_a(S)} \sim \frac{K_{PHIDT}}{S + a_{PHI}} \qquad \text{(IV.A.2.-4)}$$

where

$$K_{PHIDT} = 1.89 \frac{deg}{inch\text{-}sec^2} \qquad \text{(IV.A.2.-5a)}$$

$$a_{PHI} = 3.45\ sec^{-1} \qquad \text{(IV.A.2.-5b)}$$

The roll angle model is the direct integration of the roll rate model and is given by:

$$\frac{\phi(S)}{\delta_a(S)} \sim \frac{K_{PHIDT}}{S(S + a_{PHI})} \qquad \text{(IV.A.2.-6)}$$

Parameter variations are insignificant within the low speed environment.

Forward Velocity/Nozzle Angle Model

As a final example of the low order transfer function models, consider the response characteristics of the nozzle angles effect on forward velocity. The time based response of the forward velocity due to a 5 degree impulse of the nozzle angle is shown in Plot IV.A.2.-3. The short period response can be modeled as a step function (i.e. integral of the impulse input). The ramping response appearing in the later phases of Plot IV.A.2.-3 is due to the long term phugoid effects. The transfer function model of an integrator is a simple pole residing at the origin of the complex Laplace plane, and is represented by:

$$\frac{V_u(S)}{\delta_T(S)} \sim \frac{K_{VEL}}{S} \qquad \text{(IV.A.2.-7)}$$

where

$$K_{VEL} = -0.017 \frac{\text{knots}}{\text{deg-sec}} \qquad \text{(IV.A.2.-8)}$$

IV.A.3. - High Order State Space Models of Harrier Dynamics

The high order, coupled state space vehicle models that have been developed for use in the design of the OCM pilot's internal reference model, are based on a set of generalized linear, first-order differential equations [21,22], that describe the vehicle motion. The equations of motion are of the form:

$$\dot{\bar{x}}(t) = A\,\bar{x}(t) + B\,\bar{u}(t) \qquad \text{(IV.A.3.-1)}$$

The state vector, $\bar{x}(t)$, represents the perturbations from trim of the vehicle's pseudo-body axis variables. To maximize the overall usefulness of the internal reference model and to apply the control tasks (described in later sections), the state vector of Table IV.A.3.-1 was used. Utilizing this large order state vector provides for a flexible internal reference model. The use of pseudo-body axis variables results from the manner in which the human pilot model will interpret the flight control environment via a mix of external visual cues and instrumental feedback. A close examination of the state vector variable selection and organization shows that the state vector is made up of a set of vehicle body angles and positions, along with their first derivatives (i.e. angular rates and body velocities).

The control vector, $\bar{u}(t)$, represents the deviations from the trim positions of the cockpit control mechanisms and is defined in Table IV.A.3.-2. The use of the cockpit control mechanisms is due to the manner in which the human will institute his control actions upon the vehicle.

The output or measurement equation is of the form:

$$\bar{y}(t) = C\,\bar{x}(t) \qquad \text{(IV.A.3.-2)}$$

This equation provides the relationship of the variables that are displayed to the pilot from a linear combination of states. The structure and organization of the state vector permits the displays to primarily include vehicle positions and body angles. This is indeed a good structure because many of the cockpit displays and information available from external visual cues are in the form of a position indication. It is assumed that the pilot will therefore derive the first derivative information from the displays, and thus the entire state vector can be estimated given the proper display organization.

In the most general aircraft model, the elements of the system matrix A, and the control distribution matrix B, consist of two basic types. The first consists of inertial and gravitational components that are obtained analytically from the equations of motion. The second consists of partial derivatives associated with aerodynamic forces and moments. Due to the use of the low speed region of the flight envelope, many of the aerodynamic terms can be neglected. In addition, no attempt will be made to incorporate the SAS, instrumental, actuation, or cockpit control mechanism dynamics as components external to the state model. Instead, these dynamics will be incorporated directly within the state model.

The total linearized vehicle dynamics can be described by a completely coupled state model given by:

$$\dot{\bar{x}}(t) = \begin{bmatrix} A_{long} & A_{lat\text{-}long} \\ A_{long\text{-}lat} & A_{lat} \end{bmatrix} \bar{x}(t) + \begin{bmatrix} B_{long} & B_{lat\text{-}long} \\ B_{long\text{-}lat} & B_{lat} \end{bmatrix} \bar{u}(t) \qquad \text{(IV.A.3.-3)}$$

In general, the cross coupling terms, $A_{long\text{-}lat}$, $A_{lat\text{-}long}$, $B_{long\text{-}lat}$, and $B_{lat\text{-}long}$, can be ignored because of their limited secondary response characteristics and the low speed assumption [21,22,23]. Extensive testing of the simulation model program showed this to be true (see Appendix B). It is interesting to note that the lateral system did not show any signs of response excitation due to longitudinal activities, which results in:

$$A_{long\text{-}lat} \equiv B_{long\text{-}lat} \equiv 0 \qquad \text{(IV.A.3.-4)}$$

It is believed that this response characteristic is due to the absolute symmetry of the computer simulation model. The lateral system components did, however, induce relatively small reactions within the longitudinal system, thus:

$$A_{\text{lat-long}} \sim B_{\text{lat-long}} \sim 0 \qquad \text{(IV.A.3.-5)}$$

The effects of the lateral components will be discussed in the development of the longitudinal model in Appendix B.

Longitudinal Dynamics Model

A generalized linear representation of the core longitudinal dynamics is given by:

$$\begin{bmatrix} \dot{V}_u \\ \dot{\theta} \\ \dot{q} \\ \dot{V}_w \end{bmatrix} = \begin{bmatrix} X_u & X_\theta & X_q & X_w \\ 0 & 0 & 1 & 0 \\ M_u & 0 & M_q & M_w \\ Z_u & Z_\theta & Z_q & Z_w \end{bmatrix} \begin{bmatrix} V_u \\ \theta \\ q \\ V_w \end{bmatrix} + \begin{bmatrix} X_e & X_j & X_T \\ 0 & 0 & 0 \\ M_e & M_j & M_T \\ Z_e & Z_j & Z_T \end{bmatrix} \begin{bmatrix} \delta_e \\ \delta_j \\ \delta_T \end{bmatrix} \text{(IV.A.3.-6)}$$

The core dynamics are those variables which are the principle components involved in the description of the motions and responses. The remaining variables are the direct integration of the core dynamics. Using various low speed assumptions (see Appendix B), a variety of simplifications were made and verified by an analysis of the responses of the simulation model program. The longitudinal system of EQ(IV.A.3.-6) was simplified to:

$$\begin{bmatrix} \dot{V}_u \\ \dot{\theta} \\ \dot{q} \\ \dot{V}_w \end{bmatrix} = \begin{bmatrix} X_u & X_\theta & 0 & 0 \\ 0 & 0 & 1 & 0 \\ M_u & 0 & M_q & 0 \\ 0 & 0 & 0 & Z_w \end{bmatrix} \begin{bmatrix} V_u \\ \theta \\ q \\ V_w \end{bmatrix} + \begin{bmatrix} 0 & X_j & 0 \\ 0 & 0 & 0 \\ M_e & 0 & 0 \\ 0 & 0 & Z_T \end{bmatrix} \begin{bmatrix} \delta_e \\ \delta_j \\ \delta_T \end{bmatrix}$$

(IV.A.3.-7)

This model describes the generalized low speed dynamics of a thrust vectored aircraft. The response characteristics of this state model were examined and compared against the classical V/STOL responses [21,22] and those of the Harrier simulation program [15,16,17] (see Appendix B). The comparisons showed and explained many interesting response modes associated with the Harrier simulation programs operations. An example of this, can be seen in the long term pitch rate response due to an impulse on the longitudinal stick while operating outside the ground effects region, as shown in Plot IV.A.3.-1. The low frequency oscillatory response characteristics (noticeable in the latter phases of the response) can be attributed to the Phugoid mode [21,22] (see appendix B). The Phugoid response characteristic rarely troubles pilot activities because of it's ultra-low frequency content. This is similar to driving a car that is "out-of-alignment". The car driver simply compensates by providing an offset at the steering wheel that is necessary to overcome the misalignment. A closer examination of the system parameters that introduce the Phugoid response characteristics revealed that certain parameters could be neglected when operations are primarily directed at the pilot frequencies (i.e. pilot operations are directed at the short period dynamics). Applying these additional simplifications to the model of EQ(IV.A.3.-7) resulted in the low speed/powered-lift longitudinal model for pilot frequencies as given by:

$$\begin{bmatrix} \dot{V}_u \\ \dot{\theta} \\ \dot{q} \\ \dot{V}_w \end{bmatrix} = \begin{bmatrix} 0 & X_\theta & 0 & 0 \\ 0 & 0 & 1 & 0 \\ 0 & 0 & M_q & 0 \\ 0 & 0 & 0 & Z_w \end{bmatrix} \begin{bmatrix} V_u \\ \theta \\ q \\ V_w \end{bmatrix} + \begin{bmatrix} 0 & X_j & 0 \\ 0 & 0 & 0 \\ M_e & 0 & 0 \\ 0 & 0 & Z_T \end{bmatrix} \begin{bmatrix} \delta_e \\ \delta_j \\ \delta_T \end{bmatrix} \quad \text{(IV.A.3.-8)}$$

This model represents the core longitudinal dynamics that were incorporated in the OCM's internal reference model.

Lateral-Directional Dynamics Model

A generalized linear representation of the core lateral-directional dynamics is given by:

$$\begin{bmatrix} \dot{\phi} \\ \dot{p} \\ \dot{r} \\ \dot{V}_v \end{bmatrix} = \begin{bmatrix} 0 & 1 & 0 & 0 \\ 0 & L_p & L_r & L_v \\ 0 & N_p & N_r & N_v \\ Y_\phi & Y_p & Y_r & Y_v \end{bmatrix} \begin{bmatrix} \phi \\ p \\ r \\ V_v \end{bmatrix} + \begin{bmatrix} 0 & 0 \\ L_a & L_{\pi} \\ N_a & N_{\pi} \\ Y_a & Y_{\pi} \end{bmatrix} \begin{bmatrix} \delta_a \\ \delta_r \end{bmatrix} \quad \text{(IV.A.3.-9)}$$

Applying the low speed assumptions of Appendix B, a variety of simplifications were obtained, which resulted in the following low speed/powered-lift lateral-directional model.

$$\begin{bmatrix} \dot{\phi} \\ \dot{p} \\ \dot{r} \\ \dot{V}_v \end{bmatrix} = \begin{bmatrix} 0 & 1 & 0 & 0 \\ 0 & L_p & L_r & 0 \\ 0 & N_p & N_r & 0 \\ Y_\phi & 0 & 0 & Y_v \end{bmatrix} \begin{bmatrix} \phi \\ p \\ r \\ V_v \end{bmatrix} + \begin{bmatrix} 0 & 0 \\ L_a & L_{\pi} \\ N_a & N_{\pi} \\ 0 & Y_{\pi} \end{bmatrix} \begin{bmatrix} \delta_a \\ \delta_r \end{bmatrix} \quad \text{(IV.A.3.-10)}$$

The response characteristics of this model were examined and compared against the non-linear simulation program and the classical V/STOL responses (see Appendix B). As in the longitudinal case, many of the low frequency lateral modes could be neglected (e.g. spiral and dutch role modes). Applying these further simplifications to the model of EQ(IV.A.3.-10), a low speed/powered-lift lateral-directional model for pilot frequencies is given by:

$$\begin{bmatrix} \dot{\phi} \\ \dot{p} \\ \dot{r} \\ \dot{V}_v \end{bmatrix} = \begin{bmatrix} 0 & 1 & 0 & 0 \\ 0 & L_p & 0 & 0 \\ 0 & 0 & N_r & 0 \\ Y_\phi & 0 & 0 & 0 \end{bmatrix} \begin{bmatrix} \phi \\ p \\ r \\ V_v \end{bmatrix} + \begin{bmatrix} 0 & 0 \\ L_a & L_{rr} \\ N_a & N_{rr} \\ 0 & 0 \end{bmatrix} \begin{bmatrix} \delta_a \\ \delta_r \end{bmatrix} \qquad \text{(IV.A.3.-11)}$$

This model represents the core longitudinal dynamics that were incorporated in the OCM's internal reference model.

IV.B. Black Hawk UH-60A: A High Performance Helicopter

The primary focus of the research on pilot models for the Black Hawk helicopter was directed at developing a group of McRuer-Krendel pilots that spanned the flight envelope. This section discusses the development of a set of low order linear transfer function models that where obtained by an analysis of the nonlinear simulation model responses due to cockpit control mechanism operations. To simplify and limit this discussion, only a few transfer function models will be examined. The full set of vehicle models obtained are presented in [19].

During the initial stages of the pilot model development a linear point mass, small perturbation, state space model [24] of Black Hawk dynamics was utilized. This model was linearized about trimmed flight conditions and considered only the pure body dynamics. Augmenting this model with actuation and automated systems created a model whose complexity approached that of the nonlinear simulation model. The high order of this model created significant difficulties in the design and evaluation of the low order pilot models. For this reason, low order transfer functions where utilized to create more understandable vehicle models. As suggested above, these transfer function models where developed and used in a manner similar to the low order Harrier models.

Simulation model response tests where conducted while in trimmed flight at forward velocities of 20, 40, 60, 80, and 100 knots. The initial test scenarios where carried out with all onboard automatic control systems disabled and showed low frequency divergence. To improve the overall response characteristics, the pitch bias actuator, automatic tail stabilator control, and stability augmentation systems (both digital and analog) where enabled. The results showed substantial improvement.

IV.B.1. - Control Structure and Low Order Transfer Function Models

The cockpit control mechanisms and their associated vehicle responses where decoupled into the longitudinal control set (Longitudinal cyclic stick (δ_{lo_c}), Main rotor collective stick (δ_{mr_c}) and the lateral control set (Lateral cyclic stick (δ_{la_c}), Tail rotor collective pedals (δ_{tr_c})). A more detailed analysis of the control sets and their associated response characteristics is presented in [19]. The following model identification examples illustrate the fundamental approach utilized.

Pitch Angle/Longitudinal Cyclic Stick

Consider the pitch angle dynamics associated with the manipulation of the longitudinal cyclic stick. Plot IV.B.1-1 and Plot IV.B.1-2 show the pitch rate responses due to an impulse on the longitudinal cyclic stick while flying at 60 and 100 knots, respectively. Both plots show a damped sinusoidal response characteristic whose damping ratio decreases with increasing forward velocity. This type of response can be approximated by the transfer function shown below.

$$\frac{q}{\delta_{lo\_c}} \sim \frac{K_{TD}}{S^2+2\delta_\theta w_\theta S+w_\theta{}^2} \qquad \text{(IV.B.1.-1)}$$

The pitch angle response is given by:

$$\frac{\theta}{\delta_{lo\_c}} \sim \frac{K_T}{S(S^2+2\delta_\theta w_\theta S+w_\theta{}^2)} \qquad \text{(IV.B.1.-2)}$$

Where the pitch rate is measured in radians/second and the pitch angle is measured in degrees. Evaluating the pitch rate response throughout the flight envelope resulted in the parameter values listed in Table IV.B.1.-1.

Roll Angle/Lateral Cyclic Stick

Helicopter roll dynamics are dominated by the operation of the lateral cyclic stick. An analysis of the response characteristics of the simulation model program indicated slightly different roll reactions, one for low speeds (20 to 40 kn) and one for high speeds (60 to

100 kn). This type of behavior has been attributed to the low/high speed mode switching of the on-board yaw SAS near 60 kn. The low speed model is given by the transfer function:

$$\frac{\phi}{\delta_{la\_c}}(20,40) \sim \frac{820}{S(S^2+2\delta_p w_p S+w_p{}^2)^2} \qquad \text{(IV.B.1.-3)}$$

where $\delta_p \sim 0.15$ and $w_p \sim 9.0$ rads/sec.

The high speed model is given by:

$$\frac{\phi}{\delta_{la\_c}}(60,80,100) \sim \frac{210(S+3)}{S(S^2+2\delta_p w_p S+w_p{}^2)^2} \qquad \text{(IV.B.1.-4)}$$

These models do not indicate the resonant behavior that can be seen in the time and frequency responses. Figure IV.B.1.-3 shows the frequency response of the roll rate at 80 kn. A relatively large peak-notch type characteristic can be seen near 2 and 22 rads/sec. The high frequency resonance is attributed to the main rotor. The low frequency resonance is associated with aerodynamic phenomena. The low frequency peak is, however, troublesome because the pilot will attempt to close the control loop near this frequency.

Altitude/Main Rotor Collective

The altitude components of the helicopter's flight dynamics are dominated by the main rotor collective. Figure IV.B.1.-4 shows the altitude rate response due to the injection of a 1 inch step on the main rotor collective stick while at a traveling at 60 kn. This type of first order response suggests the transfer function model given by:

$$\frac{ALTDT}{\delta_{mr\_c}} \sim \frac{K_{ALT}}{S+a_{ALT}} \qquad \text{(IV.B.1.-5)}$$

The altitude response is therefore given by:

$$\frac{ALT}{\delta_{mr\_c}} \sim \frac{K_{ALT}}{S(S+a_{ALT})} \qquad \text{(IV.B.1.-6)}$$

Evaluating the altitude rate response throughout the flight envelope resulted in the parameter values listed in Table IV.B.1.-2.

V. PILOT DEVELOPMENT AND INSERTION

This chapter will illustrate the development and insertion of a variety of pilot models within the control loop of the non-linear simulation programs. First, a set of McRuer-Krendel pilot mechanisms will be developed for the Harrier and the Black Hawk. A group of flight control maneuvers is defined and insertion set configurations are organized. Results of multi-variable pilot insertions are illustrated by examining several examples of Harrier and Black Hawk flight control maneuvers. Finally, the OCM is developed for use in the Harrier. Control tasks and display configurations are discussed. Task and pilot parameters are chosen. Results of OCM insertion are examined and compared to actual human pilot flight data.

V.A. - Static McRuer-Krendel Pilots

The concepts involved in the selection and insertion of the McRuer-Krendel model are based on the selection of a set of single variable pilot mechanisms (SVPM), to provide a variety of control functions associated with each of the cockpit control mechanisms. From this set/pool of SVPMs, a group (insertion set) is chosen, one SVPM for each cockpit control mechanism. The insertion set is chosen from an analysis of the control functions associated with the expected flight maneuvers. This section will illustrate the design of some example single variable pilot mechanisms and the selection of various insertion sets based on the flight control objectives. Examples of insertion set operation within the simulation environment of the non-linear program are presented and discussed.

V.A.1. - Design of the Single Variable Pilot Mechanisms

This section presents some examples of the design of the single variable pilot mechanisms (SVPM). The objective is to develop a set of SVPMs, where each pilot mechanism is selected to perform a specific control function. The elements of the multi-variable configurations will ultimately be chosen from this pool of SVPMs.

During the design of the individual pilot's, attempts were made to maximize the system TYPE. This simulates the pilot's ability to choose the control parameters that will tend to improve his error tracking ability. The ability to obtain the desired closed loop response characteristics was at times hampered by control mechanism restrictions and difficult vehicle response modes (e.g. high frequency complex poles near the right half plane, resonant behavior near the closed loop frequencies). Gain limitation and reduced closed loop bandwidths were required, in some cases, to keep pilot responses within limits.

Harrier Pitch Control Pilot

This pilot provides the position control of the pitch angle by considering visual assessment of the pitch angle and manipulating the longitudinal stick. Typically the human pilot would derive this feedback from the artificial horizon or from some type of external target. This individual SVPM will be used to maintain level flight or to perform specific pitch angle positioning. In addition, the pitch angle control can be applied to velocity control when performing fixed nozzle angle maneuvers.

Returning to the pitch angle response model of EQ(IV.A.2.-3), one can see that the integrating pole of the pitch angle response provides an intrinsic TYPE I system

characteristic. Attempts at introducing the pilot's equalization pole as a second integrating pole (to achieve a TYPE II system characteristic) did not provide adequate response characteristics due to the positioning restrictions of the equalization zero ($a \geq 0.8$). The pilot's equalization profile was relaxed and the equalization pole was removed to S = 8. The equalization zero was placed at S = 3 to maximize the Root-Locus dominant pole placement characteristics and provide the necessary phase considerations. This configured the equalization as a lead network which in-turn improved the low frequency response characteristics and oriented the pilot to be error rate sensitive. The resulting pilot transfer function is given by:

$$G^{HARRIER}_{THETA}(s) = \frac{4.3\,(S + 3)\,e^{-0.2S}}{(S + 8)(S + 10)} \qquad \text{(V.A.1.-1)}$$

The Root-Locus for this configuration is shown in Figure V.A.1.-1. The dominant poles were placed near the desired locations ($w_n = 3.1$ rads/sec, $\zeta = 0.74$).

Additional Pilot Mechanisms for the Harrier

Table V.A.1.-1 lists the remaining single variable pilot mechanisms for the Harrier, that were developed in [20]. The models are based on the form:

$$G^{HARRIER}_{PILOTS}(s) = \frac{K\,(S + A)\,e^{-0.2S}}{(S + B)(S + 10)} \qquad \text{(V.A.1.-2)}$$

Black Hawk Pitch Control Pilot

As in the Harrier pitch control pilot, this pilot also controls the pitch angle position by visually assessing the pitch angle and operating the longitudinal cyclic stick. The different response characteristics of the Black Hawk required a significantly different pilot configuration. The transfer function model of the Black Hawk's pitch dynamics, EQ(IV.B.1.-2), permits the construction of a TYPE II system. The problems associated with the pitch control pilot development stemmed from the presence of the high frequency complex poles (see EQ(IV.B.1.-2). These poles are quite close to the imaginary axis and due to the destabilizing distortions of the delay Root-Locus, can be easily shifted into unstable conditions. Closing the loop near w_n = 3 rads/sec introduced large resonant reactions in the vehicle's lateral-directional body plane (X-Y body plane), due to torque reactive disturbances. To reduce this type of behavior, the closed loop dominant poles were placed near w_n = 1.8 rads/sec and ζ = 0.65. The pitch control pilot transfer function was given by:

$$G_{THETA}^{PILOT}(s) = \frac{K_{PT}\,(S + 0.8)\,e^{-0.2S}}{S(S + 10)} \qquad \text{(V.A.1.-3)}$$

The gain profile is listed in Table V.A.1.-2.

Additional Pilot Mechanisms for the Black Hawk

Tables V.A.1.-3 through V.A.1.-7 list the remaining single variable pilot mechanisms for the Black Hawk, that were developed in [18,19]. The models are based on the form:

$$G^{BHAWK}_{PILOTS}(s) = \frac{K\,(S + A)\,e^{-0.2S}}{(S + B)(S + 10)} \qquad \text{(V.A.1.-4)}$$

V.A.2. - Selection of Multi-Variable Configurations

The maneuvering characteristics associated with flight control objectives will determine the configuration of the insertion set. The insertion set configuration is based on the multi-variable control structure shown in Figure III.B.3.-1 (for the Harrier, the Black Hawk provides only four cockpit control mechanisms [18]). Some typical flight control maneuvers that are considered in [18,20] are listed below.

1. Pitch Reorientation
2. Velocity Translation
3. Altitude Translation
4. Small Scale Heading Modification
5. Altitude Rate Maneuver
6. Flat Turn
7. Coordinated Turn

These maneuvers can be executed by the control configuration shown in Figure III.B.3.-2. The application of this method to this class of control maneuvers is straight forward. The insertion sets and their associated configurations for the above maneuvers are discussed in [18,20], and are summarized in Tables V.A.2.-1 and V.A.2.-2.

V.A.3. - Results of Static Pilot Insertion

The results of pilot insertion can be best illustrated by considering several examples of multi-variable McRuer-Krendel pilot configurations actively participating in the control structure of the non-linear simulation program. Further results of static pilot insertion can be seen in [18,19,20].

Harrier : Pitch Reorientation

The pitch reorientation maneuver is designed to provide pitch angle translation while maintaining level flight characteristics in the lateral, altitude, and velocity components. The multi-variable pilot configuration, for this maneuver, is given in Table V.A.2.-1. The pitch angle rotation will cause a redirection of the primary thrust vector, which will directly influence the altitude and velocity components. The velocity and altitude component pilot mechanisms will therefore be called upon to provide the necessary compensation. The command sequence issued to the pilot is of the form of a step in pitch angle while the remaining variables are held at their trimmed values. A 10 degree step maneuver in pitch from a 10 knot trimmed flight at 100 feet is driven by the control sequence shown in Table V.A.3.-1.

The command sequence was injected at 1 second into the simulation run. Plot V.A.3.-1 shows the execution of the 10 degree set in vehicle pitch angle. This closed loop pitch angle response indicates a reasonably close match to the closed loop poles placed in the Root-Locus design. Plot V.A.3.-2 shows the pitch control pilots manipulation of the longitudinal stick. The change in pitch angle causes the primary thrust vector to be reoriented, creating a decelerating disturbance in the forward velocity. Plot V.A.3.-3 shows the forward velocity

response due to the pitch maneuver. Plot V.A.3.-4 shows the velocity pilot's compensative reactions to the velocity disturbance. Plot V.A.3.-3 shows that the pilot successfully reoriented the thrust vector and restored the commanded forward velocity. It is interesting to note that the final, steady state nozzle redirection is approximately 10 degrees (the commanded pitch angle). Plot V.A.3.-5 shows the altitude reaction due to the pitch maneuver. Plot V.A.3.-6 shows the pilot's manipulation of the throttle to handle the altitude disturbance. These plots indicate that the velocity pilot's reactions were fast enough to maintain proper thrust vector orientation with respect to the inertial frame (i.e. the velocity pilot was able to keep the thrust vector pointed towards the ground and therefore suffered little lift component degradation). The symmetry associated with this maneuver created insignificant disturbances in the lateral-direction modes.

Harrier : Velocity Translation

The velocity translations maneuver is designed to modify the forward velocity while maintaining level flight at a constant altitude. The multi-variable pilot configuration, for this maneuver, is given in Table V.A.2.-1. This maneuver uses the redirection of the primary thrust vector to modify the forward thrust. Reorienting the primary thrust vector tends to disturb the flight characteristics of the pitch and lift components. The command sequence issued to the pilot is of the form of a step in forward velocity while the remaining variables are held at their trimmed values. A 5 knot step reduction in forward velocity from a 25 knot trimmed flight at 100 feet is commanded by the control sequence shown in Table V.A.3.-2.

This command sequence was injected at 1 second into the simulation run. Plot V.A.3.-7 shows the execution of the 5 knot reduction in velocity. Plot V.A.3.-8 shows the velocity control pilot's reaction to the application of the command. Plot V.A.3.-7 's response

characteristic is very sluggish. This is due to the reduction in closed loop bandwidth via forward path gain reduction to reduce the pilot's control deflection. The initial pilot parameter selection created a response characteristics that tended to overdrive the nozzle angle ($\theta_j > 98.5°$) during decelerating maneuvers. The velocity pilot parameters were adjusted to prevent the control mechanism overdrive, see Plot V.A.3.-8. Plot V.A.3.-9 shows the pitch angle reaction to the thrust vector redirection during the execution of the velocity control maneuver. Plot V.A.3.-10 shows the pitch control pilot's compensative response due to the "nose down" effects of the velocity translation. The steady state error of Plot V.A.3.-9 is typical for the TYPE I system characteristic of the piloted pitch control loop. Plot V.A.3.-11 shows a very small altitude response due to the velocity change. Plot V.A.3.-12 shows the small scale adjustments to the throttle by the pilot mechanism.

Black Hawk : Coordinated Turn

The coordinated turn maneuver provides a heading change through the execution of roll operations. The coordinated turn is executed be performing a roll maneuver while minimizing sideslip and maintaining level flight (pitch angle only) and constant altitude. The multi-variable pilot configuration, for this maneuver, is given in Table V.A.2.-2. It is interesting to note that the tail rotor collective pedal pilot mechanism has had it's visual feedback redirected from the heading to the sideslip indicator (slip ball). Heading control must therefore be supplied by the commanding process (i.e. the navigation/guidance process that is issuing the command). The roll angle modification will tend to cause a loss of the lift components due to the redirection of the main rotor thrust vector. The command sequence issued to the pilot is of the form of a step in roll angle, while the remaining variables are held at their trimmed values. A 20 degree bank turn from an 80 knot trimmed flight at 200 feet is driven by the control sequence shown in Table V.A.3.-3.

The command sequence was injected at the initiation of the simulation run. Plot V.A.3.-13 shows a smooth roll angle response to the command. The heading response, shown in Plot V.A.3.-14, indicates the execution of the turn. The transient heading response is due to the settling of the roll angle and the turn coordination operations. Plot V.A.3.-15 shows the suppression of the sideslip angle and indicates that turn coordination has been achieved. Plot V.A.3.-16 shows the altitude response during the bank turn and shows the compensatory effects of the altitude control pilot. Plot V.A.3.-17 shows the compensatory effects of the pilot mechanism on the pitch angle.

V.A.4. - Conclusions on the McRuer-Krendel Models

The McRuer-Krendel pilot models have shown their ability to operate the V/STOL aircraft over a wide range of flight control maneuvers. Control and regulation activities have been shown to adequately achieve the control objectives. The multi-variable configurations provide for a wide range of possible flight scenarios. The fixed structure of the multi-variable configurations does, however, create certain difficulties when the flight control objectives require the use of multiple configurations. The switch between configurations has been examined in [19]. Finally, the sluggish response characteristics due to the reduction of closed loop bandwidths to accommodate various vehicle constraints tends to limit successful prediction of human behavior.

V.B. - Optimal Control Model Pilots

The concepts involved in the insertion of the OCM are based on the selection of two parameter sets: 1) Control task related, 2) Pilot related. The control task parameters describe the vehicle under control and the control objectives associated with the flight maneuvers that the pilot is required to perform. The pilot parameters describe the basic human response characteristics and inherent limitations. This section will illustrate the design and insertion of the OCM within the control loops of the Harrier and will present the results of various flight control tasks along with a comparison of the response characteristics of the OCM to some actual pilot flight data.

V.B.1. - Description of the Control Tasks and Display Configurations

The flight control tasks that have been considered for the testing of the OCM are classical precision hovering maneuvers that are performed outside of the ground effects region. Two primary maneuvers have been utilized to analyze the OCM: 1) Vertical tracking maneuver, 2) Lateral tracking maneuver. Each maneuver is complex in nature and exploits various aspects of the pilots control characteristics. The vertical hover maneuver consists of traversing between and positioning/aligning the vehicle at two vertically spaced targets,as shown in Figure V.B.1.-1. The targets, described in [25], are placed at 40 feet and 80 feet above the runway surface, and thus are outside of the vehicles ground effects region. The control objective is to hold at one target for a period of time, traverse to the other target at a constant rate, hold at that target for a period of time and then return to the initial target. Alignment with the targets is considered to be a positioning/disturbance regulation operation, while motion between the target is considered to be a rate control/tracking maneuver [25]. The Lateral tracking maneuver is similar to the Vertical task with the

exception that the targets are separated horizontally, as shown in Figure V.B.1.-2. The targets are placed 40 feet apart at an altitude of 50 feet.

The vehicle that is used in this study is the Harrier II AV-8B. The cockpit controls available to the pilot, for the maneuvers in question, are: 1) Longitudinal stick (right hand), 2) Lateral stick (right hand), 3) Throttle (left hand), 4) Rudder pedals (feet). The complexity of the maneuvers and their basic control structure, requires that the pilot maintain a fixed nozzle angle, thus forward velocity and longitudinal positioning control are indirectly handled through pitch angle control.

The displays that the pilot monitors are assumed to be the targets (external visual cues). The targets have been designed [25] to supply the pilot with the following information: Pitch, Roll, and Yaw angles, Longitudinal, Lateral, and Vertical positions. The pilot can therefore derive the output vector shown in Table IV.A.3.-1. The state space model and the above output vector, derived in Appendix B, are based on this display assumption.

V.B.2. - Overview of the Piloted Flight Data and Analysis

The precision hover maneuvers, described above, where used in a simulation fidelity study by [25]. The time domain flight test data of the actual pilot activities and the vehicle responses from this study were supplied by NASA-Lewis. This information provided a valuable tool in the design and insertion of the OCM pilot. The flight data was reviewed and the basic flight maneuver trajectories were extracted. This trajectory information is the basis of the command sequences that are injected into the OCM.

V.B.3. - Description of Pilot and Task Parameter Selection

The OCM task parameters were selected from an analysis of the fundamental structure of the control tasks in the piloted flight data. The limited information available from the flight data required that most task parameters were selected subjectively. Thus, a simplified performance index was chosen to represent the task of minimizing the hover attitude and position errors indicated by the external target.

$$J = J_{long} + J_{lat}$$

$$J_{long} = \lim_{T \to \infty} \left\{ \frac{1}{T} \int_0^T \left[\left(\frac{XX_u}{XX_M}\right)^2 + \left(\frac{V_u}{V_M^u}\right)^2 + \left(\frac{\theta}{\theta_M}\right)^2 + \left(\frac{ZZ_w}{ZZ_M}\right)^2 + \left(\frac{\delta_e}{\delta_M^e}\right)^2 + \left(\frac{\delta_T}{\delta_M^T}\right)^2 \right] dt \right\} \tag{V.B.3.-1}$$

$$J_{lat} = \lim_{T \to \infty} \left\{ \frac{1}{T} \int_0^T \left[\left(\frac{YY_y}{YY_M}\right)^2 + \left(\frac{V_y}{V_M^y}\right)^2 + \left(\frac{\phi}{\phi_M}\right)^2 + \left(\frac{\psi}{\psi_M}\right)^2 + \left(\frac{\delta_a}{\delta_M^a}\right)^2 + \left(\frac{\delta_r}{\delta_M^r}\right)^2 \right] dt \right\} \tag{V.B.3.-2}$$

The maximum desirable values of the position errors (XX_M, YY_M, ZZ_M), were chosen to correspond to the relative target size and reflects the specifications associated with precision hovering. The values of the attitude angle cost parameters were chosen subjectively by considering a 10 degree deviation as being large. The maximum values of the cockpit control mechanisms were selected to be approximately 0.25 of the total control travel, as suggested in [26]. Table V.B.3.-1 and V.B.3.-2 list the values of the cost function weights associated with the vertical and lateral flight maneuvers, respectively.

The vertical maneuver parameters were originally designed for all maneuvers. During tests (discussed later sections), the lateral operations showed unstable response characteristics in the pitch and yaw (heading) components when using the values of Table V.B.3.-1. Tightening the allowable deviations in pitch and yaw (compare Tables V.B.3.-2 to V.B.3.-1), improved these response modes. The response characteristics in the yaw angle are expected because of the inherent couplings in the lateral-directional components. The responses of the pitch angle were more pronounced than were expected. These problems appear to stem from the limitations of the OCM's internal reference model, since the optimal control gains are based on the internal reference model (it's knowledge of the system under control). Another possible reason for the differences of Tables V.B.3.-1 and V.B.3.-2 can be reflection of the OCM's sensitivity to the inherent differences between the two maneuvers. This may be due to a reconfiguration of the manner in which the pilot must obtain information during the maneuvers.

The pilot parameters were chosen according to some typical values. The weightings of the control rates were selected to provide a neuro-muscular lag time constant, T_N, near 0.15 seconds for each control mechanism. The magnitude of the motor noise sources for each control is shown in Table V.B.3.-3. These correspond to an approximate -15dB signal to noise ratio (S/N). The magnitude of the observation noise was chosen to correspond to an approximate -10dB (S/N). These values create a remnant that is considered reasonable for a multi-axis hovering control task [10]. The pure time delay was selected to be 0.2 seconds.

V.C.4. - Results and Comparisons of OCM Pilot Insertion

The OCM pilot was inserted into the nonlinear simulation environment of the Harrier. The structure of the OCM required that the vehicle trajectory associated with the control

task be specified in position/attitude and velocity/rate. This type of trajectory is generated by the velocity/rate driven system shown in Figure V.B.4.-1, for the pitch angle components. This generator is replicated for the other state variables. The low pass filter provides bandwidth limiting of the forcing function as described in [2]. The time constant of this filter was selected to be 2.5 seconds.

An analysis of the vertical and lateral flight data showed a variety of pre-test procedures used by the pilot to approach and align the vehicle with the target. In both cases, the vehicle was at rest on the ground away from the targets. The approach and alignment operations consisted of a vertical takeoff, followed by a ground translation and a flat rotation (yawing maneuver). During initial attempts at constructing the command sequence for these maneuvers for the OCM, trim discrepancies in the non-linear simulation program created problems. These primarily stemmed from problems associated with simulating the vehicle on the ground. To overcome these problems, the OCM tests were initialized near the targets with the vehicle already airborne. This allowed closer matches of trimmed values and simplified the test command sequences.

Vertical Tracking Maneuver

The vertical tracking maneuver consisted of an initial yawing rotation (to simulate the final stages of the pilot's alignment with the targets), followed by a holding period and then by the cyclic execution of the vertical operations. The cost function weightings of Table V.B.3.-1 were used to select the control aspects of the OCM. The vehicle was trimmed to the values shown in Table V.B.4.-1. The vertical rate and yaw rate command sequences of Figure V.B.4.-2 were applied to the OCM pilot during a 125 second simulation run. This command sequence requires the pilot to rotate the vehicle (flat turn - approximately 60°) to

acquire the upper target. The pilot holds at the target (for approximately 10 seconds) then proceeds to the lower target at a constant rate (2.5 feet/sec). The pilot is then repeatedly commanded to proceed back and forth between targets.

Plot V.B.4.-1 shows a heading angle comparison of the OCM (solid line) and the piloted flight data (dashed line). This type of comparison strategy will be used throughout the following discussion. Transients associated with the target alignment phases are not present for times greater than 35 seconds (TIME>35 seconds). Plot V.B.4.-2 shows a comparison of the rudder pedal activity. The "fuzziness" of the OCM response is due to the noise model of the controller remnant. Rudder pedal operations differ significantly. This has been attributed to the limitations in the lateral dynamics of the OCM's internal reference model. The flight data tends to suggest that the heading angle regulation is not particularly critical to this maneuver. It appears that this type of activity may stem from a threshold regulation process where no corrective actions are taken until the error crests a certain level. The present version of the OCM does not account for this type of behavior.

Plots V.B.4.-3 and V.B.4.-4 compare the altitude and vertical rate responses, respectively. These plots show similar trends in command trajectory following. Target alignment operations can be seen during the initial phases of the run (TIME<35 sec). The vertical rate responses of Plot V.B.4.-4 show that the OCM has similar behavior during the execution of the vertical maneuvers (TIME>35 sec), but does not capture the higher frequency content of the pilot data. This has been attributed to the low order altitude component representation of the of OCM's internal reference model, and possibly the lack of auditory feedback.

Plot V.B.4.-5 shows a very dissimilar comparison of throttle operations. Plot V.B.4.-6 shows a comparison of the engine speeds. During the execution of the vertical maneuvers (TIME>35 sec), the engine speeds show strikingly similar response characteristics from very dissimilar throttle operations. This discrepancy may be due to infidelities in the simulation environment, particularly in the throttle linkages and servo-systems.

Plot V.B.4.-7 compares the pitch angle responses. This plot shows very similar vehicle orientations during the vertical maneuvering. This is an important response characteristic due to the fixed nozzle angle which couples the pitch angle to the forward velocity and position. Plot V.B.4.-8 shows the comparison of the longitudinal stick activity. The offset in stick operations is due to the trimmed value of the piloted data being ~-1.35 inches. As in the case of the rudder pedal, the OCM does not predict the higher frequency operations of the pilot.

Plot V.B.4.-9 shows a comparison of the airspeed responses. The OCM pilot shows very similar characteristics in both magnitude and frequency content during the vertical maneuvers (TIME>35 sec). Plot V.B.4.-10 compares the longitudinal position. The offset is due to the initial target approach operations by the pilot. This plot shows similar but out-of-phase positioning response.

Plots V.B.4.-11 and V.B.4.-12 show comparisons of the roll angle responses and lateral stick deflections, respectively. In both plots, the OCM fails to match the frequency content of the actual pilot.

Lateral Tracking Maneuver

The lateral tracking maneuver was simplified by not including the initial yawing operations of the target alignment. The vehicle was trimmed to the values shown in Table V.B.4.-2. The lateral velocity command sequence of Figure V.B.4.-3 was applied to the OCM pilot during a 100 second simulation run.

Plot V.B.4.-13 shows a comparison of the lateral position responses. This plot indicates a good trajectory following by the OCM. Plot V.B.4.-14 compares the lateral velocity responses. As in the vertical maneuvers, the OCM's response characteristics do not capture the higher frequency content of the pilot data. This is illustrated in the regulatory operations shown in Plots V.B.4.-15 - V.B.4.-20.

V.C.5. - Conclusions on the OCM pilots

The OCM pilots have shown their abilities of providing adequate multi-variable flight control of the V/STOL research aircraft. The OCM is not structurally limited in it's maneuvering characteristics and can therefore be applied to a wide range of flight control objectives. Differences between the cost function weightings of the vertical and lateral tracking maneuvers illustrate the pilot's alteration of his approach to the individual control problems (possible modification of feedback to handle the characteristics of a specific maneuver). The OCM showed an excellent match in the longitudinal components of the vertical maneuver. This appears to stem from a reasonable model of the aircraft's longitudinal dynamics (since lateral excitation is minimal) and subjective assumptions in the cost function weight selection.

The reasons behind the OCM's inability to predict the higher frequency components of the pilot data are not clear. A possible reason stems from the manner in which the pilot obtains information. The limited information available on the targets and actual flight control objectives of the piloted flight data required the use of an intuitive selection of displays. A close examination of the pilot's control activities showed a higher degree of sensitivity to the angular rates than to the angular position. Attempts at configuring the OCM to be more sensitive to angular rates did not resolve this issue. The addition of a display scanning algorithm induced a cyclic feature in the OCM's responses that was similar to that of the pilot data. The presence of scanning behavior in the pilot flight data can not be substantiated and thus the OCM scanning model is only marginally permissible. Another possible reason is the OCM's remnant models. In some regulation operations [10], the pilot tends to "battle" his own remnant more than the external disturbance. Modifying the OCM's remnant models did not significantly alter the frequency content. Finally, it is possible that the OCM's reliance on the internal reference model of the vehicle dynamics creates this phenomena. Limitations in the model may restrict the manner in which the OCM applies it's control efforts. The lack of deadband considerations in the model (i.e. the 0.1 inch deadband in the servo-channels of the longitudinal and lateral stick linkages) leads to the suppression of OCM control mechanism deflections that are based on small errors. Possible over-accuracy in the model may provide the OCM with such a good understanding of the vehicle under control that all compensative actions are near optimal. This would account for the OCM's limited control deflection activities in the regulation modes.

The OCM is very sensitive to changes in cost function weightings and muscular system time constants. In some cases (pitch and roll components), maximum deviation values of

20-30% larger produced unstable results. This may be due to the nonlinearities in the simulation environment. This tends to complicate the subjective selection of cost functions.

VI. - SUMMARY AND CONCLUSIONS

This report has illustrated the application of "Paper Pilots" within the flight control loops of V/STOL research aircraft. Two types of human dynamics models have been considered: 1) McRuer-Krendel - single variable transfer function, 2) Optimal Control Model - multi-variable approach based on optimal control and stochastic estimation theory. Descriptions of the models and discussions of their inherent limitations in predicting human behavior have been provided. Design strategies and methods of inserting the pilots within the control loops have been discussed and illustrated for two V/STOL research aircraft: 1) Sikorski Black Hawk UH-60A - a high performance helicopter, 2) McDonnell Douglas Harrier II AV-8B - a thrust vectored jet fighter. Results of simulated pilot insertion have been analyzed and compared to the control activities of actual human pilots performing similar control objectives.

The "Paper Pilots" have shown their abilities to successfully "fly" the V/STOL aircraft that have been considered in this research. The simulated pilots provide a stabilized control over the vehicle and respond to control objectives in a manner similar to human pilots. The response characteristics of the pilot models are, however, very general in nature. This appears to stem from the "Paper Pilots" inability to completely simulate the human's complex manner of obtaining and processing information, and applying the controls to the vehicle. In addition, it may be possible that the pilots have an over-detailed description of the vehicle under control and thus exert a nearly ideal control response.

Of the two human dynamics models that have been considered, the OCM appears to provide the better simulation of human activities. It's multi-variable structure and state variable framework provide a simple yet effective method for describing the pilot's abilities and the control objectives that the pilot is confronted with. The maneuvers that have been considered for the OCM are in the low speed/powered-lift region of the flight envelope. To maneuver in other regions of the flight envelope, the control objectives (i.e. the vehicle model and control strategies) must be altered because of the changes in vehicle dynamics. The use of envelope based gain tables provides a possible solution but the tables must be constructed in an off-line approach (not a simple task) and do not allow for alternative flight configurations. In addition, transition/interpolation between flight regions must be well defined to avoid control transients.

Improvements are needed to provide the OCM with a more complete description of pilot activities and to simplify the OCM pilot design process. Adaptive procedures have been successfully applied to the single variable McRuer-Krendel model. This strategy appears to have a good prospects for use in the OCM based pilots. The OCM is, however, a much more detailed and complex system. Adaptive procedures for the OCM will require a different parameter estimation scheme (because of it's high order) and will also need a different optimization scheme if muscular system time constants are to remain the same. Initial research on this subject (not discussed in this report) indicated favorable results. Due to time constraints, this work was not fully established. A further investigation in these areas is suggested as the focus of future research efforts.

In conclusion, the "paper pilot" provides a safe, convenient, and seemingly effective method for introducing human pilot response characteristics during the design process

without resorting to the use of manned, fixed-base simulators. Construction and application of the pilot models are relatively straight forward and the pilots can be configured to achieve a large number of flight configurations and control objectives.

APPENDIX A
DESCRIPTION OF THE OCM

This appendix presents a mathematical overview of the Optimal Control Model of Human Dynamics that is developed in [4]. A continuous time description of the OCM is discussed.and a discrete time representation is then developed for use in the computer simulation environment.

A.1. Mathematical Overview of the OCM

This section provides a general overview of the mathematical concepts involved with the OCM. Figure A.1.-1 shows a block diagram of the internal structure of the OCM. For the purpose of definition, the dynamics of the system under control will include the dynamics of the actuation, sensory subsystem, SAS, and any other on-board control systems. The overall system under control will be represented by a set of linearized equations of motion.

$$\dot{\bar{x}}(t) = A\,\bar{x}(t) + B\,\bar{u}(t) + \bar{w}(t) \qquad \text{(A.1.-1)}$$

$$\bar{y}(t) = C\,\bar{x}(t) \qquad \text{(A.1.-2)}$$

The system dimension is assumed to be "n", the number of inputs (i.e. cockpit control mechanisms) is assumed to be "m" and the number of outputs (i.e. visually and extracted displays) is assumed to be "l". The variables and parameters are defined as follows:

$\bar{x}(t)$ = "n" dimensional system state vector

$\bar{u}(t)$ = vector of "m" control inputs (in this case, the cockpit control mechanisms)

$\bar{y}(t)$ = vector of "l" system outputs (linear combination of the system states as perceived and deduced by the human from the displayed information)

$\bar{w}(t)$ = vector of "n" external disturbances that are independent, zero mean, white, gaussian noise sources, where:

$$E\{\bar{w}(t),\bar{w}^T(\sigma)\} = Q_w \delta(t-\sigma) \qquad \text{(A.1.-3)}$$

A = (n,n) system matrix

B = (n,m) input distribution matrix

C = (l,n) output measurement matrix

It is assumed that the human pilot/operator maintains an internal model of the system under control to base his control and estimates on.

$$\dot{\bar{x}}(t) = F\,\bar{x}(t) + G\,\bar{u}(t) \qquad \text{(A.1.-4)}$$

$$\bar{y}(t) = H\,\bar{x}(t) \qquad \text{(A.1.-5)}$$

The parameters are defined as follows:

F = Human's perception of the system matrix

G = Human's perception of the input distribution matrix

H = C

It is assumed that the control task is adequately reflected in the human's choice of the best control input, "$u^*(t)$". In addition, the human's choice is also based on his inherent knowledge of his neuro-muscular limitations. The optimal control input "$u^*(t)$" minimizes, in steady state, the cost function given by:

$$J(u) = \lim_{T \to \infty} E \left\{ \frac{1}{T} \int_0^T [\, \bar{x}(t)^T Q \bar{x}(t) + \bar{u}(t)^T R \bar{u}(t) + \dot{\bar{u}}(t)^T S \dot{\bar{u}}(t)]dt \right\}_{y_p(\sigma)} \quad \text{(A.1.-6)}$$

where

$\sigma \leq t$

Q and R are positive semi-definite

S is positive definite

The formulation of EQ(A.1.-6) does not directly include the neuro-muscular dynamics of EQ(II.-1), but instead provides a cost on the control rate in J(u). The inclusion of a control rate term results in a first-order lag being introduced in the optimal controller. This term is utilized to indirectly model the physiological limitations of the rate at which a human can perform a control action due to the neuro-muscular/motor dynamics.

The solution to this optimization problem is obtained by defining an augmented system.

$$\dot{\bar{X}}_0(t) = F_0 \bar{X}_0(t) + G_0 \dot{\bar{u}}(t) + W_0 \quad \text{(A.1.-7)}$$

where

$$\bar{X}_0(t) = \begin{bmatrix} \bar{x}(t) \\ \\ \bar{u}(t) \end{bmatrix} \tag{A.1.-8a}$$

$$F_0 = \begin{bmatrix} F & G \\ 0 & 0 \end{bmatrix} \qquad G_0 = \begin{bmatrix} 0 \\ I \end{bmatrix} \qquad W_0 = \begin{bmatrix} \bar{w}(t) \\ 0 \end{bmatrix} \tag{A.1.-8b}$$

An optimal control rate is generated by the linear feedback law:

$$\dot{\bar{u}}^*(t) = - K_0 \bar{X}_0(t) = - \begin{bmatrix} K_0^0 & K_0^1 \end{bmatrix} \begin{bmatrix} \bar{x}(t) \\ \\ \bar{u}(t) \end{bmatrix} \tag{A.1.-9}$$

From EQ(II.A.2.A.-3) and Figure II.A.2.A.-2 we have:

$$T_n \dot{\bar{u}}^*(t) + \bar{u}^*(t) = \bar{u}_c(t) + V_{uu}(t) \tag{A.1.-10a}$$

$$\bar{u}_c(t) = - K^* \bar{x}(t) \tag{A.1.-10b}$$

thus

$$\dot{\bar{u}}^*(t) = - T_n^{-1} \bar{u}^*(t) + T_n^{-1} \bar{u}_c(t) + T_n^{-1} V_{uu}(t) \tag{A.1.-10c}$$

or

$$\dot{\bar{u}}^*(t) = - T_n^{-1} \bar{u}^*(t) - T_n^{-1} K^* \bar{x}(t) + T_n^{-1} V_{uu}(t) \tag{A.1.-10d}$$

which results in

$$\dot{\bar{u}}^*(t) = - K_0 \bar{X}_0(t) = - \begin{bmatrix} K_0^0 & K_0^1 \end{bmatrix} \begin{bmatrix} \bar{x}(t) \\ \bar{u}^*(t) \end{bmatrix} + K_0^1 V_{uu}(t) \qquad \text{(A.1.-10e)}$$

where

$$K_0^0 = T_n^{-1} K^* \qquad \text{(A.1.-10f)}$$

$$K_0^1 = T_n^{-1} \qquad \text{(A.1.-10g)}$$

The feedback gain matrix, K_0, is obtained from:

$$K_0 = G_0^T S^{-1} P_0 \qquad \text{(A.1.-11)}$$

P_0 is the unique positive definite solution of the "n+m" dimensional matrix Ricatti Equation.

$$F_0^T P_0 + P_0 F_0 + Q_0 - P_0 G_0 S^{-1} G_0^T P_0 = 0 \qquad \text{(A.1.-12)}$$

where

$$Q_0 = \begin{bmatrix} Q & 0 \\ 0 & R \end{bmatrix} \qquad \text{(A.1.-13)}$$

The key to implementing this control strategy is in the selection of the control rate cost weightings, S, to obtain:

$$K_0 = \begin{bmatrix} K_0^0 & T_n^{-1} \end{bmatrix} \qquad \text{(A.1.-14)}$$

The Kalman Filter estimates the delayed system state from the observation of the delayed, noisy system outputs and an inherent knowledge of the delayed "command" control, $\bar{u}_c(t\text{-}d)$. The Kalman Filter uses an alternate augmented system to derive it's estimates.

$$\dot{\bar{X}}_1(t) = F_1 \bar{X}_1(t) + G_1 \bar{u}_c(t\text{-}d) + G_{11} W_1 \qquad \text{(A.1.-15)}$$

where

$$\bar{X}_1(t\text{-}d) = \begin{bmatrix} \bar{x}(t\text{-}d) \\ \bar{u}(t\text{-}d) \end{bmatrix} \qquad \bar{W}_1 = \begin{bmatrix} \bar{w}(t\text{-}d) \\ \bar{V}_{uu}(t\text{-}d) \end{bmatrix} \qquad \text{(A.1.-16a)}$$

$$F_1 = \begin{bmatrix} F & G \\ 0 & -T_n^{-1} \end{bmatrix} \qquad G_1 = \begin{bmatrix} 0 \\ T_n^{-1} \end{bmatrix} \qquad G_{11} = \begin{bmatrix} I & 0 \\ 0 & T_n^{-1} \end{bmatrix} \qquad \text{(A.1.-16b)}$$

$$H_1 = [\, H \quad 0 \,] \qquad \text{(A.1.-16c)}$$

It is important to note that the estimated state of EQ(A.1.-15) utilizes the delayed desired control input, $\bar{u}_c(t\text{-}d)$, as the driven deterministic input. The Kalman Filter generates the delayed estimate of the delayed state via:

$$\hat{\dot{\bar{X}}}_1(t\text{-}d) = F_1 \hat{\bar{X}}_1(t\text{-}d) + G_1 \bar{u}_c(t\text{-}d) + K_1 \left[\bar{y}_p(t) - H_1 \hat{\bar{X}}_1(t\text{-}d) \right] \qquad \text{(A.1.-17)}$$

The output error is weighted by the Kalman gains, K_1, that are generated by:

$$K_1 = P_1 H_1^T R_y^{-1} \qquad \text{(A.1.-18)}$$

where the error covarience matrix, P_1, satisfies

$$F_1^T P_1 + P_1 F_1 + Q_1 - P_1 H_1 R_y^{-1} H_1^T P_1 = 0 \qquad \text{(A.1.-19)}$$

$$Q_1 = \begin{bmatrix} Q_w & 0 \\ 0 & \hat{Q}_u \end{bmatrix} \qquad \text{(A.1.-20a)}$$

where

$$\hat{Q}_u = E\left\{ T_n^{-1} V_{uu}(t) \ , \ V_{uu}(t)^T T_n^{-1\,T} \right\} = T_n^{-1} Q_u T_n^{-1T} \qquad \text{(A.1.-20b)}$$

The least-squared error predictor generates a time advanced estimate of the present time state from the delayed estimated state of EQ(A.1.-17). The prediction is based on the internal reference model:

$$\dot{\bar{\zeta}}(t) = F_1 \bar{\zeta}(t) + G_1 \bar{u}_c(t) \qquad \text{(A.1.-21)}$$

where

$$\bar{\zeta}(t) = \begin{bmatrix} \hat{\bar{x}}(t) \\ \\ \bar{u}_c(t) \end{bmatrix} \qquad \text{(A.1.-22)}$$

The time update of the predicted state is generated by:

$$\hat{\bar{X}}_1(t) = \hat{\bar{\zeta}}(t) + K_2 \left[\hat{\bar{X}}_1(t\text{-}d) - \hat{\bar{\zeta}}(t\text{-}d) \right] \qquad \text{(A.1.-23)}$$

The delayed state error weighting, K_2, is given by:

$$K_2 = e^{F_1 d} \qquad \text{(A.1.-24)}$$

which is the state transition matrix for the time advancement.

The fundamental modules of the OCM, that have been defined above, are summarized by Figure II.B.-2.

A.2. Discrete Time Representation of the OCM

The continuous time OCM described above was transformed to a discrete time equivalence for insertion into the simulation environment. The following sections describe the transformation technique and the resulting discrete time model. It is important to note that the Kalman Filter and the Optimal Control gain calculations will be based on time varying solutions.

Discrete Time System Model

The discrete time representation of the system's involved in the OCM are based on the Zero-Order-Hold equivalence transform (ZOH) described in [27]. The difference equation representation of the perceived system's state equation, EQ(A.1.-4), is given by

$$\bar{x}_{k+1} = \Phi \bar{x}_k + \Gamma \bar{u}_k + \Gamma_w \bar{w}_k \qquad \text{(A.2.-1)}$$

and the measurement equation, EQ(A.1.-5), is given by

$$\bar{y}_k = H\,\bar{x}_k + H_y\,V_k^y \qquad \text{(A.2.-2)}$$

The discrete time "n" system states, "m" system inputs, and "l" system outputs are represented by

$$\bar{x}_k = [x_k^1, x_k^2, \ldots, x_k^n]^T \qquad \text{(A.2.-3)}$$

$$\bar{u}_k = [u_k^1, u_k^2, \ldots, u_k^m]^T \qquad \text{(A.2.-4)}$$

$$\bar{y}_k = [y_k^1, y_k^2, \ldots, y_k^l]^T \qquad \text{(A.2.-5)}$$

The discrete time process noise model and covarience matrix are given by

$$\bar{w}_k = [w_k^1, w_k^2, \ldots, w_k^n]^T \qquad \text{(A.2.-6)}$$

$$Q_k^w = E[\,\bar{w}_k\,,\,\bar{w}_k^T\,] = \Gamma_w\,Q_w\,\Gamma_w^T \qquad \text{(A.2.-7)}$$

The discrete time observation noise model and covarience matrix are given by

$$V_k^y = [v_y^1, v_y^2, \ldots, v_y^m]^T \qquad \text{(A.2.-8)}$$

$$R_k^y = E[\,V_k^y\,,\,V_k^{yT}\,] = R_y \qquad \text{(A.2.-9)}$$

The ZOH discrete time equivalence transformations are given by

$$\Phi = e^{F\,T_s} \qquad \text{(A.2.-10a)}$$

$$\Gamma = \int_0^{T_s} e^{F T_s} d\sigma \; G \qquad \text{(A.2.-10b)}$$

$$\Gamma_w = \int_0^{T_s} e^{F T_s} d\sigma \qquad \text{(A.2.-10c)}$$

where

T_s = Sampling period

Pure Delay Model

Information processing and neuro-motor signal delays are represented by the pure delays shown in Figure A.1.-1. The delays are implemented by a sliding window FIFO buffer of length D.

$$D = \text{MOD}\left(\frac{d}{T_s}\right) \qquad \text{(A.2.-11)}$$

where

D = Number of sampling periods

d = Continuous time delay

T_s = Sampling period

The FIFO buffer is driven by

DO I = D,1,-1

$$\bar{X}_{K-I} = \bar{X}_{K-I+1} \qquad \text{(A.2.-12)}$$

ENDDO

Neuro-muscular and Optimal Control Generator

A recursive time varying solution of the discretized optimal control/gain generator described in [27] is utilized. The optimal control rate is defined by EQ(A.1.-10e) and it's discrete time representation is given by

$$\bar{u}^{*}_{k+1} = \Phi_{K_0^1} \bar{u}^{*}_{k} + \Gamma_{K_0^0} \bar{x}_k + \Gamma_{K_0^1} \bar{v}^{u}_{k} \tag{A.2.-13}$$

where the motor noise and it's covarience matrix are given by

$$\bar{v}^{u}_{k} = \left[\bar{v}^{u_1}_{k}, \bar{v}^{u_2}_{k}, , , \bar{v}^{u_m}_{k} \right] \tag{A.2.-14a}$$

$$Q^{u}_{k} = E\left[\bar{v}^{u}_{k}, \bar{v}^{u^T}_{k} \right] = \Gamma_{K_0^1} Q_u \Gamma_{K_0^1}^{T} \tag{A.2.-14b}$$

The optimal state feedback gains can be rewritten into the form of the recursive solution

$$\bar{u}^{*}_{k+1} = - K^{0}_{k} \begin{bmatrix} \bar{x}_k \\ \bar{u}^{*}_{k} \end{bmatrix} + \Gamma_{K_0^1} \bar{v}^{u}_{k} \tag{A.2.-15a}$$

where

$$K^{0}_{k} = \left[K^{0}_{0_k} \; \Phi_{K_0^1} \right] \tag{A.2.-15b}$$

The feedback gain matrix is obtained from the recursive relations in terms of the augmented system

$$\Phi_0 = \begin{bmatrix} \Phi & \Gamma \\ 0 & 0 \end{bmatrix} \qquad \Gamma_0 = \begin{bmatrix} 0 \\ I \end{bmatrix} \tag{A.2.-16}$$

The recursive solution of the optimal control gains is given by:

$$K_k^0 = \left(S_k + \Gamma_0^T \bar{P}_k^0 \Gamma_0 \right)^{-1} \Gamma_0^T \bar{P}_k^0 \Phi_0 \tag{A.2.-17a}$$

$$P_k^0 = \bar{P}_k^0 - \bar{P}_k^0 \Gamma_0 \left(S_k + \Gamma_0^T \bar{P}_k^0 \Gamma_0 \right)^{-1} \Gamma_0^T \bar{P}_k^0 \tag{A.2.-17b}$$

$$\bar{P}_k^0 = \Phi_0^T P_k^0 \Phi_0 + Q_k^0 \tag{A.2.-17c}$$

The cost weightings on the states, controls, and control rates (Q,R,S) respectively, are introduced in the manner used in the continuous problem

$$Q_k^0 = \begin{bmatrix} Q & 0 \\ 0 & R \end{bmatrix} \qquad S_k = S \tag{A.2.-18}$$

The control rate weightings, S_k, are chosen such that, in steady state, the set of equations EQ(A.1.-17) result in

$$\Phi_{K_0^1} = e^{-K_0^1 T_s} = e^{-T_s T_n^{-1}} = \begin{bmatrix} e^{-\frac{T_s}{T_n^1}} & & & & \\ & e^{-\frac{T_s}{T_n^2}} & & & \\ & & \ddots & & \\ & & & & e^{-\frac{T_s}{T_n^m}} \end{bmatrix} \tag{A.2.-19}$$

The state feedback matrix directly results from the solutions of EQ(A.1.-17). The diagonal elements represent the time constants of the individual neuro-muscular systems associated

with the separated cockpit control mechanisms. The motor noise gain matrix is obtained from

$$\Gamma_{K_0^1} = I - \Phi_{K_0^1} \tag{A.2.-20}$$

The finalized state feedback matrix results from

$$\Gamma_{K_0^0} = \Gamma_{K_0^1} K^0_{0_k} \tag{A.2.-21a}$$

Discrete Time Kalman Filter

A recursive time varying solution of the discrete time Kalman Filter described in [28] is utilized. The Kalman Filter is used to estimate the delayed system state from the observation of the delayed noisy system outputs

$$y^p_k = \bar{y}_{k-D} + V^y_{k-D} \tag{A.2.-22}$$

from a knowledge of the desired delayed control command

$$\bar{u}^c_{k-D} = [u^c_1, u^c_2, \ldots, u^c_m]^T_{k-D} = - K_0^{0^*} \hat{\bar{x}}_k = - \Phi_{K_0^1} \Gamma_{K_0^0} \hat{\bar{x}}_k \tag{A.2.-23}$$

and an understanding of the motor and process noises and their respective covariences. The Kalman Filter bases it's estimates on the augmented system given by

$$\hat{\bar{X}}^{1}_{k\text{-}D} = \begin{bmatrix} \hat{\bar{x}}_{k\text{-}D} \\ \hat{\bar{u}}_{k\text{-}D} \end{bmatrix} \qquad \bar{W}^{1}_{k\text{-}D} = \begin{bmatrix} \hat{\bar{w}}_{k\text{-}D} \\ \hat{\bar{V}}^{u}_{k\text{-}D} \end{bmatrix} \tag{A.2.-24a}$$

$$\Phi_1 = \begin{bmatrix} \Phi & \Gamma \\ 0 & \Phi_{K_0^1} \end{bmatrix} \qquad \Gamma_1 = \begin{bmatrix} 0 \\ \Phi_{K_0^1}^{-1} \end{bmatrix} \tag{A.2.-24b}$$

The measurement update equations are

$$\hat{\bar{X}}^{1}_{k\text{-}D} = \hat{\bar{X}}^{\bar{1}}_{k\text{-}D} + K^1_k \left[y^p_k - H \hat{\bar{X}}^{\bar{1}}_{k\text{-}D} \right] \tag{A.2.-25a}$$

$$P^1_k = \bar{P}^1_k - K^1_k H \bar{P}^1_k \tag{A.2.-25b}$$

and the time updates are given by

$$\hat{\bar{X}}^{\bar{1}}_{k\text{-}D} = \Phi_1 \hat{\bar{X}}^{1}_{k\text{-}D} + \Gamma_1 \bar{u}^c_{k\text{-}D} \tag{A.2.-26a}$$

$$\bar{P}^1_k = \Phi_1 P^1_k \Phi_1^T + Q^1_k \tag{A.2.-26b}$$

where

$$Q^1_k = \begin{bmatrix} Q^w_k & 0 \\ 0 & \hat{Q}^u_k \end{bmatrix} \qquad \hat{Q}^u_k = \Gamma_{K_0^1} Q^u_k \Gamma_{K_0^1}^T \tag{A.2.-26c}$$

The time varying Kalman gains are generated by

$$K^1_k = \bar{P}^1_k H^T \left(H \bar{P}^1_k H^T + R^y_k \right)^{-1} \tag{A.2.-27}$$

with the initial conditions

$$\bar{P}_k^1 = 0 \qquad \text{(A.2.-28a)}$$

$$\hat{\bar{X}}_{k\text{-}D}^{\bar{1}} = \bar{x}_k \qquad \text{(A.2.-29b)}$$

Discrete Time Predictor

The discrete time, time advance predictor uses the internal reference model given by

$$\bar{\zeta}_{k+1} = \Phi_1 \bar{\zeta}_k + \Gamma_1 \bar{u}_k^c \qquad \text{(A.2.-30a)}$$

$$\bar{\zeta}_k = \begin{bmatrix} \hat{\bar{x}}_{k\text{-}D} \\ \hat{\bar{u}}_{k\text{-}D} \end{bmatrix} \qquad \text{(A.2.-30b)}$$

The prediction matrix is given by

$$\hat{\bar{X}}_k^1 = \bar{\zeta}_k + K_k^2 \left[\hat{\bar{X}}_{k\text{-}D}^{\,1} - \bar{\zeta}_{k\text{-}D} \right] \qquad \text{(A.2.-31)}$$

where the state projection matrix is given by

$$K_k^2 = e^{F_1 D} \qquad \text{(A.2.-32)}$$

APPENDIX B

A LINEAR STATE SPACE MODEL

This appendix presents a linear state space model of the Harrier AV-8B dynamics from trim, while operating in the low speed/powered lift region of the flight envelope. This model is directly utilized as the internal reference model in the OCM implementations. This appendix is separated into two sections: 1) Assumptions, simplifications and general derivation of the model, 2) Identification of model parameters from an analysis of the response characteristics of the non-linear simulation program.

B.1. - Harrier AV-8B Model Development

A generalized linear representation of the core longitudinal dynamics is given by:

$$\begin{bmatrix} \dot{V}_u \\ \dot{\theta} \\ \dot{q} \\ \dot{V}_w \end{bmatrix} = \begin{bmatrix} X_u & X_\theta & X_q & X_w \\ 0 & 0 & 1 & 0 \\ M_u & 0 & M_q & M_w \\ Z_u & Z_\theta & Z_q & Z_w \end{bmatrix} \begin{bmatrix} V_u \\ \theta \\ q \\ V_w \end{bmatrix} + \begin{bmatrix} X_e & X_j & X_T \\ 0 & 0 & 0 \\ M_e & M_j & M_T \\ Z_e & Z_j & Z_T \end{bmatrix} \begin{bmatrix} \delta_e \\ \delta_j \\ \delta_T \end{bmatrix} \quad \text{(B.1.-6)}$$

Due to the low speed assumption, a variety of simplifications can be made and verified by an analysis of the responses of the simulation model program. The first series of assumptions are directed at the forward velocity components. A very general assumption that can be made is: $X_q \sim 0$. This assumption is based on the relative unimportance of the angular rate on the forward velocity through the entire flight envelope [21,22]. The next simplification is: $X_w \sim 0$. This assumption is based on aerodynamic symmetry and an analysis of the vehicle's forward velocity response characteristic due to an positive impulse

of the throttle while in a near hover as shown in Plot B.1.-1. An additional simplification of $X_T \sim 0$, can be derived from Plot B.1.-1 and an intuitive analysis of the low speed/powered-lift thrust vector's effect on the forward velocity as shown in Figure IV.A.1.-2. The final forward velocity component assumption is: $X_e \sim 0$. This simplification is based on the longitudinal stick's dominant effect on vehicle pitching motions, shown in Figure IV.A.1.-3. Plot B.1.-2 backs-up this assumption by illustrating that the longitudinal stick's effect on forward velocity is coupled to the redirection of the thrust vector associated with the pitching motion and is therefore not direct. Thus as shown in the thrust diagram of Figure IV.A.1.-1, the nozzle angle control, X_j, will dominate the control of the vehicle's forward velocity. It is important to note that this model does take into account the pitch angle's effect on the forward velocity, where typically, $X_\theta = g$, the gravitational acceleration.

The effects of the lateral system components on the response characteristics of the forward velocity where considered insignificant from a analysis of the responses of the simulation model program. Plot B.1.-3 shows the forward velocity response due to an impulse on the lateral stick. Plot B.1.-4 shows the response of the same state variable due to an impulse on the rudder pedals. The forward velocity reactions to the lateral stick and rudder pedal operations are similar in magnitude to those of the longitudinal stick and throttle. For this reason, the lateral components of the forward velocity are ignored.

The next series of assumptions are directed at the rotational modes of the longitudinal dynamics. The first assumption is based on aerodynamic symmetry and the negligible pitching reactions due to vertical motion, thus $M_w \sim 0$. Plot B.1.-5 illustrates the relatively small pitch rate response due to an impulse of the throttle. Although M_w does have a small

effect on the pitching rate, it will not effect the hovering characteristics. An additional assumption that can be derived from Plot B.1.-5 is $M_T \sim 0$. This term primarily describes the moment arm of the thrust vector on the vehicle's center of gravity. A final rotational component assumption is $M_j \sim 0$. This term describes the rotational effects of the nozzle angle due to the thrust vector's moment arm on the vehicle center of gravity. Plot B.1.-6 shows pitch rate reaction due to an impulse of the nozzle angle. Again, this response characteristic will not have a significant effect on the low speed flight dynamics. The control mechanism assumptions of $M_T \sim M_j \sim 0$, indicate that the longitudinal stick will dominate the control of the rotational dynamics due to the relatively large moment arm associated with the physical locations of the forward and aft RCS jet vents, as shown in Figure IV.A.1.-3. The term M_u is retained to provide a coupling between the forward velocity and longitudinal rotations. Although, low speeds are assumed, it will be shown later that this term and the forward velocity terms, X_θ and X_u, provide the couplings that tend to generate the long term Phugoid responses.

The pitch rate responses due to impulses of the lateral stick and rudder pedals are shown in Plot B.1.-7 and Plot B.1.-8, respectively. These reactions are similar in magnitude to those of the throttle component, M_T, and are therefore neglected.

The final series of assumptions in the longitudinal dynamics are directed at the vertical velocity components. The first assumption is based on the relatively small contribution of the pitch rate on the vertical components [21,22], thus, $Z_q \sim 0$. Plot B.1.-9 illustrates the vertical rate response due to an impulse on the longitudinal stick. This response characteristics reveals that the longitudinal stick's component, $Z_e \sim 0$, is also a realistic assumption. The pitch angle component is small due to the small angle and low speed

assumptions, thus, $Z_\theta \sim 0$. Another simplification due to the low speed assumption is $Z_u \sim 0$. This assumption would not hold true if the Harrier was a tilt-wing V/STOL aircraft. For those types of vehicles, Z_u approaches Z_w. The final simplification is directed at the relation between the nozzle angle and the vertical components. Plot B.1.-10 shows the response of the vertical rate due to an impulse of the nozzle angle. An examination of Plot B.1.-10 and Figure IV.A.1.-1 shows that perturbations about the large nozzle angle has only a small effect on the lift components, thus $Z_j \sim 0$. The control mechanism assumptions of $Z_j \sim Z_e \sim 0$, indicate that the throttle control will tend to dominate the vertical dynamics due to the large nozzle angle associated with low speed/powered-lift flight.

The vertical rate reactions due to operations of the lateral stick and rudder pedals can be seen in Plot B.1.-11 and Plot B.1.-12, respectively. These responses are on the order of those associated with the longitudinal stick and nozzle angle. This suggests that the lateral components can be neglected.

Incorporating the above assumptions within the longitudinal system model of EQ(B.1.-6) results in the following low speed/powered-lift longitudinal model.

$$\begin{bmatrix} \dot{V}_u \\ \dot{\theta} \\ \dot{q} \\ \dot{V}_w \end{bmatrix} = \begin{bmatrix} X_u & X_\theta & 0 & 0 \\ 0 & 0 & 1 & 0 \\ M_u & 0 & M_q & 0 \\ 0 & 0 & 0 & Z_w \end{bmatrix} \begin{bmatrix} V_u \\ \theta \\ q \\ V_w \end{bmatrix} + \begin{bmatrix} 0 & X_j & 0 \\ 0 & 0 & 0 \\ M_e & 0 & 0 \\ 0 & 0 & Z_T \end{bmatrix} \begin{bmatrix} \delta_e \\ \delta_j \\ \delta_T \end{bmatrix} \quad \text{(B.1.-7)}$$

To better understand the longitudinal responses of the low speed/powered-lift region of the flight envelope and the correspondence of the vehicle model that has been developed, an

analysis of the vehicle's longitudinal dynamics will now be conducted. This analysis is based on the Laplacian approach used in [22]. An additional objective of this analysis is to obtain an understanding of the transfer function relationships to the above system model. This will be helpful in implementing parameter identification techniques. Before initiating the analysis it should be observed that the vertical components are strongly decoupled from the translational and rotational components. This is primarily due to the dominance of the powered-lift assumptions associated with the vertical components and Z_u being negligibly small while in low speed flight.

The rotational and translational components of the longitudinal dynamics can be approximated by the following system.

$$\begin{bmatrix} \dot{V}_u \\ \dot{\theta} \\ \dot{q} \end{bmatrix} = \begin{bmatrix} X_u & X_\theta & 0 \\ 0 & 0 & 1 \\ M_u & 0 & M_q \end{bmatrix} \begin{bmatrix} V_u \\ \theta \\ q \end{bmatrix} + \begin{bmatrix} 0 & X_j \\ 0 & 0 \\ M_e & 0 \end{bmatrix} \begin{bmatrix} \delta_e \\ \delta_j \end{bmatrix} \qquad \text{(B.1.-8)}$$

The characteristic equation of this reduced system is given by:

$$\Delta_{LONG} = \det(SI - A) = \det \begin{bmatrix} S - X_u & -X_\theta & 0 \\ 0 & S & -1 \\ -M_u & 0 & S - M_q \end{bmatrix} \qquad \text{(B.1.-9)}$$

which results in

$$\Delta_{LONG} = S(S - M_q)(S - X_u) - X_\theta M_u \qquad \text{(B.1.-10a)}$$

or

$$\Delta_{LONG} = S^3 - (X_u + M_q)S^2 + M_q X_u S - X_\theta M_u \qquad \text{(B.1.-10b)}$$

EQ(B.1.-10b) is the classical longitudinal hovering cubic [22]. From Plot B.1.-13, one can observe both the short period and long period dynamics of the pitch rate's response. This type of response supports a characteristic equation of the form:

$$\Delta_{LONG} \sim (S + T_{sp})(S^2 + 2w_{lp}\delta_{lp}S + w_{lp}^2) \qquad \text{(B.1.-11)}$$

where the parameters are given by:

T_{sp} = The pole associated with the time constant of the short period response

w_{lp} = The natural frequency of the long period response

δ_{lp} = The damping ratio of the long period response

Expanding EQ(B.1.-11) to the form of EQ(B.1.-10b) results in:

$$S^3 + S^2(2w_{lp}\delta_{lp} + T_{sp}) + S(w_{lp}^2 + 2w_{lp}\delta_{lp}T_{sp}) + T_{sp}w_{lp}^2 \qquad \text{(B.1.-12)}$$

Relating the terms of EQ(B.1.-10b) and EQ(B.1.-12) we have:

$$-(X_u + M_q) = 2w_{lp}\delta_{lp} + T_{sp} \qquad \text{(B.1.-13a)}$$

$$M_q X_u = w_{lp}^2 + 2w_{lp}\delta_{lp}T_{sp} \qquad \text{(B.1.-13b)}$$

$$-X_\theta M_u = T_{sp}w_{lp}^2 \qquad \text{(B.1.-13c)}$$

From [16,17,19], we can assume:

$$T_{sp} >> w_{lp} \tag{B.1.-14a}$$

$$w_{lp}^2 \text{ is small} \tag{B.1.-14b}$$

Applying these assumptions to EQ(B.1.-13) results in:

$$M_q \sim -T_{sp} \tag{B.1.-15a}$$

$$X_u \sim -2w_{lp}\delta_{lp} \tag{B.1.-15b}$$

Thus we can see that the long period modes are due to the coupling between the translational and rotational components. The short period modes are purely due to the rotation of the vehicle about it's center of gravity. X_θ transmits the short and long period rotational perturbations to the translational motion. M_u primarily couples the long term translational perturbations to the rotational dynamics. It can be shown, through a more detailed analysis [23], that $M_u < 0$ causes divergence in the phugoid modes. This may be the case for the Harrier configuration that is used in this study. Plot B.1.-14 shows a diverging phugoid mode in the pitch rate. This type of unstable phugoid oscillation appears to be typical for hovering vehicles when out of ground effect [22].

The resulting low speed/powered-lift longitudinal model for pilot frequencies is given by:

$$\begin{bmatrix} \dot{V}_u \\ \dot{\theta} \\ \dot{q} \\ \dot{V}_w \end{bmatrix} = \begin{bmatrix} 0 & X_\theta & 0 & 0 \\ 0 & 0 & 1 & 0 \\ 0 & 0 & M_q & 0 \\ 0 & 0 & 0 & Z_w \end{bmatrix} \begin{bmatrix} V_u \\ \theta \\ q \\ V_w \end{bmatrix} + \begin{bmatrix} 0 & X_j & 0 \\ 0 & 0 & 0 \\ M_e & 0 & 0 \\ 0 & 0 & Z_T \end{bmatrix} \begin{bmatrix} \delta_e \\ \delta_j \\ \delta_T \end{bmatrix} \tag{B.1.-16}$$

The characteristic equation of this system is given by:

$$\Delta'_{LONG} = S^2(S - M_q)(S - Z_w) \qquad \text{(B.1.-17a)}$$

or

$$\Delta'_{LONG} = S^4 - S^3(M_q+Z_w) + S^2M_qZ_w \qquad \text{(B.1.-17b)}$$

A generalized representation of the lateral-directional dynamics is given by:

$$\begin{bmatrix} \dot{\phi} \\ \dot{p} \\ \dot{r} \\ \dot{V}_v \end{bmatrix} = \begin{bmatrix} 0 & 1 & 0 & 0 \\ 0 & L_p & L_r & L_v \\ 0 & N_p & N_r & N_v \\ Y_\phi & Y_p & Y_r & Y_v \end{bmatrix} \begin{bmatrix} \phi \\ p \\ r \\ V_v \end{bmatrix} + \begin{bmatrix} 0 & 0 \\ L_a & L_{\pi} \\ N_a & N_{\pi} \\ Y_a & Y_{\pi} \end{bmatrix} \begin{bmatrix} \delta_a \\ \delta_r \end{bmatrix} \qquad \text{(B.1.-18)}$$

In a manner similar to the longitudinal model, a variety of simplifications can be made and verified by an analysis of the simulation model responses. The first series of assumptions are directed at the lateral velocity components. The coupling of the roll rate to the lateral velocity, Y_p, can be neglected due to it's general unimportance throughout the flight envelope [21,22]. The primary coupling of the roll rotational dynamics is provided by the roll angle component, Y_ϕ. This is because of the thrust vector redirection due to roll angle perturbations, as shown in Figure IV.A.1.-4. A comparison of Plots B.1.-15, B.1.-16 shows the direct relationship of roll angle to the lateral acceleration. In the low speed region of the flight envelope, the yaw rate component, $Y_r \sim 0$, due to the lack of forward velocity. This component tends to translate the forward velocity into the lateral velocity. As the

forward velocity increases this term directly increases in the form $Y_r \sim -V_u$. The geometry of the wing-tip RCS jets, as shown in Figure IV.A.1.-4, relates the operations of the lateral stick to purely rolling motions. Assuming symmetry and the wing-tip RCS jet's lack of a direct effect on the lateral velocity, results in $Y_a \sim 0$. The primary coupling of the yaw rotational motions to the lateral translations is provided by the tail-end RCS jets via rudder pedal control, Y_{rr}. Plot B.1.-17 shows the direct relation of the rudder pedals to the lateral acceleration. This is due to the relatively large moment arm of the tail-end jet's physical configuration.

The next group of simplifications are directed at the yaw/directional components. Using the geometry and symmetry arguments of above, the low speed characteristics of the couplings of the roll rate to the yaw rate is threw N_p. The lateral velocity effects on the yaw rate are primarily due to the non-symmetric vehicle body configuration along the x axis (i.e. cross sectional area of the vertical stabilizer/rudder when compared to that of the forward/nose section). During low speed flight the yaw rate is not very sensitive to lateral translations and thus $N_v \sim 0$. It is interesting to note that this term is important when dealing with a single main rotor helicopter with a tail rotor. This is due to the tail rotor's sensitivity to local sideslip and it's generally high main rotor disk loading [22].

The final area of simplification is directed at the roll dynamics. During low speed flight, the effects of small perturbations in lateral velocity on the roll rate, L_v, can be neglected. This, however, is not the case for larger lateral velocities due to the size and orientation of the Harrier II AV-8B's critical wing.

Incorporating the above assumptions within the lateral-directional model of EQ(B.1.-18) results in the following low speed/powered-lift lateral model.

$$\begin{bmatrix} \dot{\phi} \\ \dot{p} \\ \dot{r} \\ \dot{V}_v \end{bmatrix} = \begin{bmatrix} 0 & 1 & 0 & 0 \\ 0 & L_p & L_r & 0 \\ 0 & N_p & N_r & 0 \\ Y_\phi & 0 & 0 & Y_v \end{bmatrix} \begin{bmatrix} \phi \\ p \\ r \\ V_v \end{bmatrix} + \begin{bmatrix} 0 & 0 \\ L_a & L_{\pi} \\ N_a & N_{\pi} \\ 0 & Y_{\pi} \end{bmatrix} \begin{bmatrix} \delta_a \\ \delta_r \end{bmatrix} \qquad \text{(B.1.-19)}$$

An analysis will now be conducted to better understand the lateral responses of the low speed region of the flight envelope. This analysis will also provide some insight to further simplifications of the system model. The characteristic equation of the simplified system of EQ(B.1.-19) is given by:

$$\Delta_{LAT} = \det \begin{bmatrix} S(S - L_p) & -L_r & 0 \\ -SN_p & S - N_r & 0 \\ -Y_\phi & 0 & S - Y_v \end{bmatrix} \qquad \text{(B.1.-20)}$$

which results in

$$\Delta_{LAT} = S(S - L_p)(S - N_r)(S - Y_v) - SL_rN_p(S - Y_v) \qquad \text{(B.1.-21a)}$$

or

$$\Delta_{LAT} = S^4 - (L_p+N_r+Y_v)S^3 + (L_pN_r+Y_vL_p+Y_vN_r-L_rN_p)S^2 + Y_v(L_rN_p-L_pN_r)S$$

(B.1.-21b)

The classical lateral dynamics can be described by the characteristics equation:

$$\Delta_{LAT} = (S + T_s)(S + T_r)(S^2 + 2w_d\delta_d S + w_d{}^2) \qquad \text{(B.1.-22)}$$

where

T_s = The pole associated with the time constant of the spiral mode

T_r = The pole associated with the time constant of the roll subsidence mode

w_d = Natural frequency of the dutch role mode

δ_d = Damping ratio of the dutch role mode

In general the time constant of the spiral mode is very long. For this reason and the fact that only the pilot frequencies are considered, the spiral mode can be reduced to an integrator model, thus:

$$\Delta'_{LAT} = S(S + T_r)(S^2 + 2w_d\delta_d S + w_d{}^2) \qquad \text{(B.1.-23a)}$$

or

$$\Delta'_{LAT} = S^4 + S^3(T_r + 2w_d\delta_d) + S^2(2w_d\delta_d T_r + w_d{}^2) + ST_r w_d{}^2 \qquad \text{(B.1.-23b)}$$

The terms of EQ(B.1.-23b) can be related to those of EQ(IV.a.1.b.-21b) as follows:

$$-L_p - N_r - Y_v = T_r + 2w_d\delta_d \qquad \text{(B.1.-24a)}$$

$$L_pN_r+Y_vL_p+Y_vN_r-L_rN_p = 2w_d\delta_dT_r + w_d^2 \quad \text{(B.1.-24b)}$$

$$Y_v(L_rN_p-L_pN_r) = T_rw_d^2 \quad \text{(B.1.-24c)}$$

Plot B.1.-18 shows both the long and short period modes of the yaw rate response due to an impulse on the rudder pedals. This plot shows a divergent dutch roll mode that maintains a relatively long period. From this, one can assume:

$$w_d^2 \text{ is small} \quad \text{(B.1.-25)}$$

Including this assumption within EQ(B.1.-24c) we have:

$$Y_v \sim 0 \quad \text{(B.1.-26a)}$$

$$L_rN_p \sim 0 \quad \text{(B.1.-26b)}$$

The resulting low speed/powered-lift lateral dynamics model for pilot frequencies is given by:

$$\begin{bmatrix} \dot{\phi} \\ \dot{p} \\ \dot{r} \\ \dot{V}_v \end{bmatrix} = \begin{bmatrix} 0 & 1 & 0 & 0 \\ 0 & L_p & 0 & 0 \\ 0 & 0 & N_r & 0 \\ Y_\phi & 0 & 0 & 0 \end{bmatrix} \begin{bmatrix} \phi \\ p \\ r \\ V_v \end{bmatrix} + \begin{bmatrix} 0 & 0 \\ L_a & L_{\pi r} \\ N_a & N_{\pi r} \\ 0 & Y_{\pi r} \end{bmatrix} \begin{bmatrix} \delta_a \\ \delta_r \end{bmatrix} \quad \text{(B.1.-27)}$$

The characteristic equation of this system is given by:

$$\Delta''_{LAT} = S^4 - S^3(L_p+N_r) + S^2L_pN_r \quad \text{(B.1.-28)}$$

B.2. - Identification of Vehicle Model

The high order state space models have been developed to facilitate direct parameter identification techniques. This section will derive the relationships that are used to identify the model parameters and finally obtain a parameter set from an analysis of the responses of the simulation program. The parameter identification techniques that are considered, rely on transfer function representations. To interface with these identification approaches, a set of transfer functions will be derived from the system models developed above. The transfer function representations are obtained by applying the Laplacian techniques used in the previous sections. The key to this approach is the development of a set of coupling numerators. These numerators will provide the transmission path characteristics from the cockpit control mechanisms to a specific state variable. The transfer function of a specific control function is obtained by introducing the appropriate characteristic equation as the denominator. To simplify this analysis, the longitudinal and lateral dynamics will again be decoupled to the forms of EQ(B.1.-16) and EQ(B.1.-27).

The longitudinal transfer functions are based on the state system of EQ(B.1.-16) and the characteristics equation of EQ(B.1.-17a). The parameters that require identification within the longitudinal model are: M_e, M_q, X_θ, X_j, Z_T, and Z_w. The coupling numerator of the longitudinal stick to the pitch angle is given by:

$$\frac{\theta(S)}{\delta_e(S)}\Delta'_{LONG}(S) = \det\begin{bmatrix} S & 0 & 0 \\ 0 & M_e & 0 \\ 0 & 0 & S-Z_w \end{bmatrix} = M_eS(S - Z_w) \qquad \text{(B.2.-1)}$$

The resulting transfer function is:

$$\frac{\theta(S)}{\delta_e(S)} = \frac{M_e S}{\Delta'_{LONG}(S)} = \frac{M_e}{S(S - M_q)} \qquad \text{(B.2.-2)}$$

The pitch rate transfer function is therefore:

$$\frac{p(S)}{\delta_e(S)} = \frac{M_e}{(S - M_q)} \qquad \text{(B.2.-3)}$$

This transfer function is a reasonably accurate model of the short period response characteristics of the pitch rate in Plot B.2.-1. The the parameters M_e and M_q are directly identifiable from EQ(B.2.-3) and Plot B.2.-1.

$$M_e \sim 0.71 \qquad \text{(B.2.-4a)}$$

$$M_q \sim -1.56 \qquad \text{(B.2.-4b)}$$

The coupling numerator of the nozzle angle to the forward velocity is given by:

$$\frac{V_x(S)}{\delta_j(S)}\Delta'_{LONG}(S) = \det\begin{bmatrix} X_j & 0 & 0 \\ 0 & S(S-M_q) & 0 \\ 0 & 0 & S-Z_w \end{bmatrix} = X_j S(S-M_q)(S - Z_w) \qquad \text{(B.2.-5)}$$

The resulting transfer function is given by:

$$\frac{V_x(S)}{\delta_j(S)} = \frac{X_j S(S-M_q)(S - Z_w)}{\Delta'_{LONG}(S)} = \frac{X_j}{S} \qquad \text{(B.2.-6)}$$

This provides a fairly accurate approximation to the initial time response of Plot B.2.-2. The parameter X_j is obtained from the step height and is given by:

$$X_j \sim -0.017 \qquad \text{(B.2.-7)}$$

The pitch angle coupling term, X_θ, can be directly obtained from gravitational components. Due to the low speed assumption, the pitching component will tend to follow the response characteristics of the nozzle angle, which results in:

$$X_\theta = -0.017 \qquad \text{(B.2.-8)}$$

This is a good assumption if fixed nozzle angles are considered.

The coupling numerator for the throttle to the vertical rate is given by:

$$\frac{V_z(S)}{\delta_T(S)}\Delta'_{LONG}(S) = \det\begin{bmatrix} S & 0 & 0 \\ 0 & S(S-M_q) & 0 \\ 0 & 0 & Z_T \end{bmatrix} = Z_T S^2(S-M_q) \qquad \text{(B.2.-10)}$$

The resulting transfer function is given by:

$$\frac{V_z(S)}{\delta_T(S)} = \frac{Z_T S^2(S-M_q)}{\Delta'_{LONG}(S)} = \frac{Z_T}{(S - Z_w)} \qquad \text{(B.2.-11)}$$

Plot B.2.-3 shows a damped sinusoidal response instead of the first order response. This is due to the engine response characteristics as shown in Plot B.2.-4. Comparing these plots, the terms Z_T and Z_w can be extracted and result in:

$$Z_T \sim 0.024 \qquad \text{(B.2.-12a)}$$

$$Z_w \sim -0.83 \qquad \text{(B.2.-12b)}$$

The lateral transfer functions are based on the state system of EQ(B.1.-27) and the characteristics equation of EQ(B.1.-28). The parameters that require identification in the lateral-directional model are: L_p, N_p, N_r, Y_ϕ, L_a, L_r, N_π, and Y_π. The coupling numerator of the lateral stick to the pitch angle is given by:

$$\frac{\phi(S)}{\delta_a(S)}\Delta'_{LAT}(S) = \det\begin{bmatrix} L_a & 0 & 0 \\ 0 & (S-N_r) & 0 \\ 0 & 0 & S \end{bmatrix} = L_aS(S-N_r) \qquad \text{(B.2.-13)}$$

The resulting transfer function is given by:

$$\frac{\phi(S)}{\delta_a(S)} = \frac{L_aS(S-N_r)}{\Delta'_{LAT}(S)} = \frac{L_a}{S(S-L_p)} \qquad \text{(B.2.-14)}$$

The roll rate transfer function is therefore:

$$\frac{p(S)}{\delta_a(S)} = \frac{L_a}{(S-L_p)} \qquad \text{(B.2.-15)}$$

This transfer function is a reasonable approximation to the short period response of Plot B.2.-5. The parameters L_a and L_p can be directly obtained from Plot B.2.-5 and EQ(B.2.-15):

$$L_a \sim 1.89 \qquad \text{(B.2.-16a)}$$

$$L_p \sim -3.45 \qquad \text{(B.2.-16b)}$$

The coupling numerator for the lateral stick to the yaw rate is given by:

$$\frac{r(S)}{\delta_a(S)}\Delta'_{LAT}(S) = \det\begin{bmatrix} S(S - L_p) & L_a & 0 \\ 0 & N_a & 0 \\ -Y_\phi & 0 & S \end{bmatrix} = N_a S^2(S - L_p) \qquad \text{(B.2.-17)}$$

The resulting transfer function is given by:

$$\frac{r(S)}{\delta_a(S)} = \frac{N_a S^2(S - L_p)}{\Delta'_{LAT}(S)} = \frac{N_a}{(S - N_r)} \qquad \text{(B.2.-18)}$$

The parameter N_a can be obtained by comparing the short term response of Plot B.2.-6 to EQ(B.2.-18).

$$N_a \sim 0.2 \qquad \text{(B.2.-19)}$$

The term N_r is not easily derived from the relation of EQ(B.2.-18) ot Plot B.2.-7. Plot B.2.-7 will be utilized to determine N_r in a later examination.

The coupling numerator for the lateral stick to the lateral velocity is given by:

$$\frac{V_y(S)}{\delta_a(S)}\Delta'_{LAT}(S) = \det\begin{bmatrix} S(S - L_p) & 0 & L_a \\ 0 & (S-N_r) & 0 \\ -Y_\phi & 0 & 0 \end{bmatrix} = L_a Y_\phi (S-N_r) \qquad \text{(B.2.-21)}$$

The resulting transfer function is given by:

$$\frac{V_y(S)}{\delta_a(S)} = \frac{L_a Y_\phi}{\Delta'_{LAT}(S)} = \frac{L_a Y_\phi}{S^2(S-L_p)} \qquad \text{(B.2.-22)}$$

The above transfer function provides a manner in which the pitch coupling term, Y_ϕ, can be obtained. The difficulty with this approach is the presence of the double integrator. A more straight forward approach is to directly obtain Y_ϕ from a comparison of Plots B.1.-15 and B.1.-16 which yields:

$$Y_\phi \sim 0.56 \tag{B.2.-23}$$

The coupling numerator of rudder pedals to the yaw rate is given by:

$$\frac{r(S)}{\delta_r(S)}\Delta'_{LAT}(S) = \det\begin{bmatrix} S(S - L_p) & L_\pi & 0 \\ 0 & N_\pi & 0 \\ -Y_\phi & Y_\pi & S \end{bmatrix} = N_\pi S^2(S - L_p) \tag{B.2.-24}$$

The resulting transfer function is given by:

$$\frac{r(S)}{\delta_r(S)} = \frac{N_\pi S^2(S - L_p)}{\Delta'_{LAT}(S)} = \frac{N_\pi}{(S-N_r)} \tag{B.2.-25}$$

A comparison of EQ(B.2.-25) and Plot B.2.-7 shows a much more direct access to the parameter N_r. The parameters, N_r and N_π are given by:

$$N_r \sim -0.83 \tag{B.2.-26a}$$

$$N_\pi \sim 0.5 \tag{B.2.-26b}$$

The coupling numerator for the rudder pedals to the roll angle is given by:

$$\frac{\phi(S)}{\delta_r(S)}\Delta'_{LAT}(S) = \det\begin{bmatrix} L_{\pi} & 0 & 0 \\ N_{\pi} & (S-N_r) & 0 \\ Y_{\pi} & 0 & S \end{bmatrix} = L_{\pi}S(S-N_r) \qquad \text{(B.2.-27)}$$

The resulting transfer function is given by:

$$\frac{\phi(S)}{\delta_r(S)} = \frac{L_{\pi}S(S-N_r)}{\Delta'_{LAT}(S)} = \frac{L_{\pi}}{S(S-L_p)} \qquad \text{(B.2.-28)}$$

The roll rate transfer function is therefore:

$$\frac{p(S)}{\delta_r(S)} = \frac{L_{\pi}}{(S-L_p)} \qquad \text{(B.2.-29)}$$

The parameter L_{π} can be obtained from Plot B.2.-8 and the use of the result of EQ(B.2.-29).

$$L_{\pi} \sim -0.25 \qquad \text{(B.2.-30)}$$

The full rank linearized state model used in the development of the OCM pilot can be seen in Figure B.2.-1. The identified parameters are listed below.

$$M_e = 0.71$$

$$M_q = -1.56$$

$$X_j = -0.017$$

$$X_\theta = -0.017$$

$$Z_T = 0.024$$

$$Z_w = -0.83$$

$$L_a = 1.89 \qquad \text{(B.2.-31)}$$

$$L_p = -3.45$$

$$L_r = -0.25$$

$$N_r = -0.83$$

$$N_p = 0.21$$

$$N_{\pi\pi} = 0.5$$

$$Y_\phi = 0.56$$

$$Y_{\pi\pi} = 0.0$$

APPENDIX C

A USERS GUIDE TO THE OCM SOFTWARE

This appendix serves as a user's guide for the OCM pilot software. An overview of the OCM software implementation is presented. The algorithm for configuring the OCM is illustrated. The procedure for operating the OCM within the VSRA environment is illustrated and examples are provided.

C.1. - Overview of the OCM Software

The OCM software is designed to be utilized as an active element of the NASA-VSRA simulation environment. The OCM software system consists of four software modules and a configuration file, as shown in the block diagram of Figure C.1.-1. The modules and file are defined as follows:

1. OCM_LIST.NML - This file serves as the configuration file for the OCM. The continuous time internal reference model (F,G,H matrices), pilot delay (T_D), noise parameters (Q_u, R_y), system initial conditions, forcing function time constant, and OCM cost function weightings (Q,R,S) are contained in this file. The file is arranged in a "namelist" format.

2. OCM_SETUP - This module initializes and configures the OCM environment. OCM initial condition, internal reference model, pilot data, and cost function weights are read from the OCM_LIST file. A discrete time representation of the internal reference model is generated. Optimal control gains are calculated by solving the steady state matrix Ricatti equation. Steady state Kalman gains are computed and covariance matrices are

initialized. The state transition matrix of the predictor is generated. All necessary information is loaded into specific COMMON regions for use by other OCM functions.

3. OCM_TRAJ - This module generates the time based trajectory that the OCM_PILOT is to follow. The time referenced command sequence is integrated and bandlimited to provide a full rank command. The command sequence is independent of the sampling rate of the simulation environment. The integration computations require sample period information.

4. OCM_PILOT - This module performs the active computations involved in the closed loop participation of the OCM within the VSRA simulation environment. These include measurements of the VSRA state, obtaining the command trajectory from the OCM_TRAJ module, noise model generation (via Box-Meuller approach), delay progression, measurement and update of the Kalman filter estimates, time advance predictions, and control input calculations. The control inputs are then applied to the VSRA through the cockpit control mechanism variables.

5. OCM_SUBS - This module contains a pool of utilities that simplify the organization and implementation of the other OCM modules. Some of the utility functions include: matrix and linear algebra operations, Kalman filter gain and covariance progression generators, optimal control solver and gain generator, and a continuous time to discrete time converter.

To interface the OCM software to the VSRA simulation environment, the main VSRA driver program (VSRA_DRIVER) was modified to accommodate the OCM system. The

modifications involved that allocation of various common areas to support OCM operations, and the implantation of the OCM_SETUP and OCM_PILOT modules at specific points within the simulation initialization and primary execution loops. In addition, two new VSRA commands were introduced to handle the OCM initialization phases and the flight simulation operations involving the participating OCM. The use of these commands will be explained in greater detail in later sections. To accommodate the output of the OCM, the file writing code of the PLOTDATA.FOR subroutine was modified to include OCM variables within the unformatted output data file VSRA_POLY.PLT.

C.2. - Installing the OCM

The OCM software is contained on a VAX Files-11 formatted tape labeled "PITT". The following files must be recovered from the tape:

1) OCM_SETUP.FOR
2) OCM_PILOT.FOR
3) OCM_SUBS.FOR
4) OCM_TRAJ.FOR
5) PLOTDATA.FOR
6) VSRA_OCM.FOR
7) OCM_PLOT.FOR
8) VSRA_OCM.OPT
9) FTP.OLB
10) *.OBJ
11)NAMELIST.NML
12) OCM_LIST.VRT
13) OCM_LIST.LAT
14) P00A.VRT
15) P00A.LAT
16) OCM_PLT.VRT
17) OCM_PLT.LAT
18) PITT151.DAT
19) PITT210.DAT

Files 1-6 correspond to the primary OCM software modules. File 7 is the modified plotting routine for the OCM. File 8 is the special linking configuration for the OCM. File 9 is the

VSRA library supplied by NASA-LEWIS. The file set *.OBJ (10) corresponds to the pool of pre-compiled VSRA modules used during the linking procedures by VSRA_OCM.OPT. File 11 is the VSRA configuration file. Files 12 and 13 are the OCM configuration files for vertical and lateral maneuvers, respectively. Files 14 and 15 are the VSRA setup command files for vertical and lateral maneuvers, respectively. Files 16 and 17 are the plotting configuration files for the vertical and lateral maneuvers, respectively. Files 18 and 19 are the unformatted data files of the pilot flight operations for the lateral and vertical maneuvers, respectively.

Files 1-6 should be compiled with the VAX Debug function enabled (to be consistent with the VSRA format). The VMS command string for compiling is as follows:

$ FORTRAN/DEBUG/NOOPT/CROSS_REF/CONT=99 filename.FOR

where "filename.FOR" is the appropriate Fortran file from the above list. Linking operations are controlled by a modified version of VSRA_DRIVER.OPT (VSRA_OCM.OPT). The modifications incorporate the OCM software modules during the link process. The linking command string is given by:

$ LINK/DEBUG VSRA_OCM/OPT,LIB:FTP/LIB

where the device LIB: contains the library FTP.OLB.

A previous version of the OCM software utilized three external libraries: 1) SLATECH, 2) IMSL, 3) DISPLA. These libraries offer many routines (particularly the SLATECH routine RICSOL, that solves various versions of the matrix Ricatti equation) that simplify the generation of the optimal control gains, muscular system time constants, Kalman filter gains and covariance matrices. To comply with the requirements that the software generated

in this research be completely self-supporting, the IMSL and SLATECH libraries were removed and the OCM was fitted with comparable algorithms. The algorithms utilized by the present version of the OCM are based primarily on iterative/time-varying solutions and are therefore rather sluggish. The DISPLA library was, however, retained because the plotting packages supplied by NASA-LEWIS were supported by DISPLA.

C.3. - Configuring the OCM

The configuration of the OCM defines the vehicle under control, control objectives, and the pilot description. The principle operations involved in the configuration of the OCM pilot are summarized in the following:

1. - Develop and insert the continuous time internal reference model of the vehicle under control into the OCM configuration file, OCM_LIST.NML. Appendix B illustrates the construction of the Harrier II AV-8B low speed/powered-lift, pilot frequency model that is supplied. Within the OCM_LIST.NML, the two dimensional arrays (FM,GM,HM) correspond to the state space representation matrices (A,B,C) or (F,G,H). Section C.7 of this appendix provides a listing of the primary variables used in the OCM. The model is dimensioned by the variables (NOCM,MOCM,LOCM) which correspond to the system order, number of inputs and outputs, respectively. The arrays, FM and GM, describe the vehicle dynamics while the measurement array, HM, is primarily dependent on the display configuration. The two dimensional array, WM, corresponds to the disturbance distribution matrix. The sampling period of the OCM execution (typically the sampling period of the simulation program) is selected and specified by the variable T1. This variable is primarily

for use in OCM applications that require execution at rates other that the fundamental frequency of the simulation environment.

2. - Determine and code the time based command sequence of the desired trajectory. The trajectory generating code resides in OCM_TRAJ. The version of OCM_TRAJ that has been supplied provides a simple implementation of the rate driven command sequencer and the rate integrating/bandlimiting full rank command generator. To use this strategy, a rate driven trajectory must be defined in the form of pulse trains on the appropriate rate commands. The pulse trains, in this case. are implemented by a sequence of "IF" statements creating a string of step functions that are overridden by the step occupying the present interval. With the trajectory specified, the time constant of the forcing function bandlimiting filter is selected and specified by the variable AFORCE in the configuration file OCM_LIST.NML. This time constant typically ranges between 1.5 and 4.5 seconds [2]. A value of 2,5 seconds has been utilized in the implementation supplied. The user may wish to insert his own trajectory defining code or route the trajectory information to the OCM from some external process via this routine. It is important to note that modifications to the OCM_TRAJ routine will require that the OCM_TRAJ.FOR file be re-compiled and the total software system be re-linked.

3. - The control objectives of the pilot's task is defined in the form of cost function weightings. The values utilized reflect the manner in which the pilot will respond to the given situation. The values will typically vary from task-to-task and from vehicle-to-vehicle. The cost function weights are loaded into the two dimensional arrays QOPT, ROPT, GOPT within OCM_LIST.NML. The array QOPT corresponds to the definition of the acceptable maximum deviations of the errors in vehicle attitude and orientation from that

of the trajectory. ROPT defines the maximum deflection of the cockpit control mechanisms and is usually a function of the vehicle (see section V.B.3.). The array GOPT is adjusted to obtain the desired muscular system time constants. This typically requires a degree of iterative adjustment. The values supplied in this version reflect a subjective analysis of the piloted flight data and a limited knowledge of the target configuration and control objectives.

4. - The final step is the selection of the pilot's inherent parameters. The discrete nature of the OCM and the VSRA simulation environment requires that the pilot delay be implemented as a chain of sample delay periods arranged in a FIFO buffer. The length of the buffer is determined by the number of sample periods needed to achieve the delay. The variable NDEL of the OCM_LIST.NML file, specifies the number of sample periods/elements of the buffer, that the pilot delay occupies. The remnant model noise sources, observation and motor, are selected according to the control objectives, vehicle under control, and the display configurations. The arrays STVU and STVY correspond to the noise model variances, Q_u and R_y, of the motor and observation noises respectively.

C.4. - Executing the OCM within the VSRA Simulation Environment

Executing the OCM software within the VSRA is relatively simple. The OCM operations are broken into two separate functions: 1) Initialization and preparation of the OCM environment, 2) Execution of the VSRA with the OCM actively participating in the flight control loops. These operations are provided by two VSRA commands:

/SOCM - This command executes the software module OCM_SETUP. The OCM environment is configured and loaded into specific common regions. This operation is typically performed after the vehicle has been trimmed with the TRIM command. The user may wish to modify the OCM_SETUP routine to create an external file of the pilot configurations instead of loading the common regions. The user will, however, have to provide the necessary file reading and common region loading facilities (possibly by an additional VSRA command). Upon the completion of this command, the pilot's parameters are displayed to the user. Again, the user may wish to modify the OCM_SETUP to have the pilot's parameters loaded into an external file.

/ROCM - This command executes the primary simulation of the VSRA and enables the OCM operations. This command is tailored after the DYNC command with the exception that is utilizes the cockpit control mechanism deflections of the OCM instead of the dynamic check tests. This command can only be executed after the use of the TRIM and SOCM commands. It is important to note that the OCM is designed to operate with ONLY the AV-8B aircraft dynamics and not those of the YAV-8B.

As mentioned previously, the algorithms utilized by the present version of the OCM software are based on iterative/time-varying solutions of the matrix Ricatti equation [27,28] (instead of the SLATECH RICSOL routine). This causes some complications in the techniques utilized to generate the optimal control gains, muscular system time constants. These are typically in the form of trial-and-error iterations of the OCM_SETUP operations

by using the command SOCM until the desired muscular system time constants are obtained.

The overall operation of the OCM within the VSRA can be summarized as follows:

1. - Configure the OCM environment by preparing the OCM_LIST file according to procedures of section C.3 of this appendix. The VSRA simulation environment is configured by preparing the NAMELIST.NML file.

2. - Enter the VSRA simulation environment and issue the command SOCM. This will generate the OCM control and estimation gains and loads the specific common areas. The values of the pilot parameters are displayed upon completion. The user should examine the pilot parameters to determine if a satisfactory pilot profile has been obtained. If so, proceed to step 3, if not, exit the VSRA and modify the OCM_LIST file, then repeat step 2.

3. - With the proper pilot parameters resident within the VSRA environment, the flight simulation may begin. The user issues the command ROCM and the VSRA proceeds to execute the simulation according to the NAMELIST.NML file. The output of the VSRA is deposited in the unformatted data file VSRA_POLY.PLT.

C.5. - Output Generated by the OCM

The time based output sequence of the VSRA simulation is deposited in the unformatted data file VSRA_POLY.PLY. This file is generated by a modified version of the subroutine PLOTDATA.FOR. The modifications were made to accommodate the output of the OCM.

In addition to the OCM software that has been provided, a pair of unformatted data files containing the human piloted flight data (PITT151.DAT [lateral tracking maneuver] and PITT210.DAT [vertical tracking maneuver]) are also included.

The data of the unformatted files can be plotted with the routine OCM_PLT.FOR. This routine is a modified version of the plotting package supplied by NASA-LEWIS and is based on the DISPLA library. This routine relies on the configuration file OCM_PLT.SRC to provide the necessary default plotting information. OCM_PLT.FOR permits the user to: 1) plot the OCM output, 2) plot the piloted flight data (either lateral or vertical maneuvers), or 3) plot a comparison of both (as shown in OCM comparison plots). This routine can also be utilized to plot data from strictly DYNC runs.

The plotting activities are arranged according to the cockpit control mechanisms and the dominant aircraft responses of those controls. These break-downs are given below:

1) Longitudinal Stick	Pitch angle	Pitch rate	Longitudinal stick
2) Lateral Stick	Roll angle	Roll rate	Lateral stick
	Lateral position	Lateral velocity	
3) Rudder Pedals	Yaw angle	Yaw rate	Rudder pedals
	Sideslip		

4) Throttle	Altitude	Vertical rate	Throttle
	Engine speed		
5) Nozzle Angle	Forward velocity	Nozzle angle	
	Forward position		

To execute the OCM plotting routine issue the following VMS commands:

```
$ FOR OCM_PLT.FOR
$ LINK OCM_PLT,LIB:DISPLA/LIB
$ RUN OCM_PLT
```

The term LIB:DISPLA/LIB corresponds to the link search of the DISPLA library residing on device LIB:. This command will depend on the VMS configuration and file structure being used. The routine will respond with the following question:

```
PLOTS?? (Flight:0, OCM:1, Both:2) >
```

The user should select the appropriate data set to plot and give a numerical answer. If the user selects either 0 or 2, the routine will request the desired flight maneuver.

```
Task??(Vert:0, Lat:1)>
```

The routine will then request the control mechanism group to be plotted by:

What kind of control input?

1 = Longitudinal Stick

2 = Lateral Stick

3 = Rudder Pedals

4 = Throttle

5 = Nozzle

Enter the appropriate number : >

The routine will then read in the VSRA_POLY.PLT, PITT151.DAT, or PITT210.DAT files and proceed to generate the appropriate plots. The plotted output of this routine will be a set of plot files that are in the Tektronix 4010 graphics format.

C.6. - Examples of VSRA/OCM Execution

As a conclusion to this overview of the OCM software, an example will now be presented. This example illustrates the configuration and execution of the OCM within the VSRA environment. The listings of the this interactive session was captured via terminal monitoring facilities. The maneuver in question is the vertical tracking maneuver.

Vertical Tracking Maneuver Example

The OCM_LIST.NML file for this maneuver is provided in the file OCM_LIST.VRT. The VSRA setup file is P00A.VRT. Both of these files must be copied to their operational names of OCM_LIST.NML and P00A.COM, respectively.

```
$ COPY OCM_LIST.VRT OCM_LIST.NML

 Copying USR5:[02350.MZVSTOL.HARRIER.SPOOL]OCM_LIST.VRT;6 to USR5:[02350.MZVSTOL
.HARRIER.SPOOL]OCM_LIST.NML;131  3 blocks
$ COPY POOA.VRT POOA.COM

 Copying USR5:[02350.MZVSTOL.HARRIER.SPOOL]POOA.VRT;3 to USR5:[02350.MZVSTOL.HAR
RIER.SPOOL]POOA.COM;25  2 blocks
$ RUN VSRA_OCM

        VAX DEBUG Version V5.0-00 MP

DEBUG-I-INITIAL, language is FORTRAN, module set to VSRA_OCM
DBG> @POOA


WELCOME TO THE VSRA VAX SIMULATIÓN PROGRAM




     Which aerodynamics would you like to use ?

1 = AV-8B aerodynamics
2 = YAV-8B aerodynamics

   Enter the appropriate number: 1


ENTER ?? FOR COMMAND LIST


VSRA> ??


VSRA SIMULATION INTERACTIVE COMMAND LIST:

/TRIM      RUN TRIM PROGRAM
/TRIM XX   RUN TRIM PROGRAM FOR XX CYCLES
/PRNT X    TO PRINT COMMON BLOCKS:  X=2 FOR XFLOAT COMMON BLOCK
                                    X=3 FOR USER COMMON BLOCKS
                                    X=4 FOR IFIXED COMMON BLOCK
/DATA      INPUT DATA TO XFLOAT AND IFLOAT FROM DATA FILE
/UDAT      INPUT DATA TO USER COMMON BLOCKS FROM DATA FILE
/ICRN XX   EXECUTE I.C. RUN FOR XX CYCLES
/DYNC X    RUN DYNAMIC CHECK - X>0  PRINT HEADER AND DATA FOR X SECS
/OPRN XX   TO EXECUTE RUN FOR XX SECONDS
/MESS      SEND MESSAGE TO PRINT OUTPUT FILE
/CHNG      TO CHANGE COMMON BLOCK VARIABLE INTERACTIVELY
/STAB      TO COMPUTE STABILITY DERIVATIVES
/FGTB      TO WRITE F & G MATRICES
/SAVT      TO SAVE TRIM VALUES
/REST      TO RESTORE TRIM VALUES
/CHGC      TO CHANGE CONFIGURATION ID
/SOCM      TO INITIALIZE AND SETUP THE OCM
/ROCM      TO EXECUTE THE OCM WITHIN THE VSRA
/END       TO TERMINATE THE PROGRAM
??         TO PRINT THIS LIST
```

```
VSRA> /SOCM

                    ******************************
                    *                            *
                    *          OCM SETUP         *
                    *                            *
                    ******************************


DISCRETE TIME REPRESENTATION COMPLETED
OPTIMAL CONTROL GENERATED
KALMAN FILTER GENERATED
TIME ADVANCE PREDICTOR GENERATED


OCM SETUP COMPLETED



PILOT PARAMETERS

PILOT DELAY  0.20

FORCING FUNCTION TIME CONSTANT  2.500

MUSCULAR SYSTEM TIME CONSTANTS
   CONTROL MECHANISM  1    0.15929
   CONTROL MECHANISM  2    0.00000
   CONTROL MECHANISM  3    0.15389
   CONTROL MECHANISM  4    0.15397
   CONTROL MECHANISM  5    0.13471

MOTOR NOISE VARIANCES
   CONTROL MECHANISM  1    1.00000
   CONTROL MECHANISM  2    1.00000
   CONTROL MECHANISM  3   20.00000
   CONTROL MECHANISM  4    0.50000
   CONTROL MECHANISM  5    0.50000

OBSERVATION NOISE VARIANCES
   DISPLAYED VARIABLE  1    0.85000
   DISPLAYED VARIABLE  2    0.60000
   DISPLAYED VARIABLE  3    1.00000
   DISPLAYED VARIABLE  4    0.71000
   DISPLAYED VARIABLE  5    0.85000
   DISPLAYED VARIABLE  6    0.60000
   DISPLAYED VARIABLE  7    1.00000
   DISPLAYED VARIABLE  8    0.71000
   DISPLAYED VARIABLE  9    1.00000
   DISPLAYED VARIABLE 10    0.71000
   DISPLAYED VARIABLE 11    0.85000
   DISPLAYED VARIABLE 12    0.60000
```

```
VSRA> /TRIM

                    ******************************
                    *                            *
                    *          TRIM MODE         *
                    *                            *
                    ******************************


        TRIM IS SUCCESSFUL AFTER 205 CYCLES
VSRA> /ROCM


                    ******************************
                    *                            *
                    *        OCM EXECUTION       *
                    *                            *
                    ******************************
VSRA> /END
VSRA SIMULATION COMPLETED SUCCESSFULLY
%DEBUG-I-EXITSTATUS, is '%SYSTEM-S-NORMAL, normal successful completion'
DBG> EXIT
$ DIR *.PLT
Directory USR5:[02350.MZVSTOL.HARRIER.SPOOL]

SMARTHIS.PLT;1      TRIMHIS.PLT;1       VSRA_POLY.PLT;1

Total of 3 files.
$
```

C.7. - Listing of the OCM variables

The OCM data structure has been implemented with the user in mind. No high performance array declaration or common area structures have been constructed. This will allow the user to best tailor the OCM environment to his application. The following list defines the primary variables utilized within the OCM.

INTEGERS

NOCM - Dimension of the OCM's internal reference model of the system under control.

MOCM - Number of cockpit control mechanisms (inputs).

LOCM - Number of displayed variables (system displays).

NDEL - Number of simulation sample periods per pilot delay

REAL*8

T1 - Sampling period of the OCM execution in seconds.

X(*) - System state vector.

U(*) - Vector of cockpit control mechanisms

FM(*,*) - System matrix of the internal reference model.

GM(*,*) - Input distribution matrix of the internal reference model.

HM(*,*) - Measurement matrix of the internal reference model

WM(*,*) - Disturbance distribution matrix

PHIM(*,*) - Discrete time system matrix

GMA(*,*) - Discrete time input distribution matrix

U0(*) - Initial conditions of the cockpit control mechanisms.

UC(*) - Desired control vector.

UCKDZ(*,*) - FIFO buffer for the control input delay.

YKDZ(*,*) - FIFO buffer for the system output delay.

QOPT(*,*) - Cost function weights for the system states

ROPT(*,*) - Cost function weights for the control inputs

GOPT(*,*) - Cost function weights for the control rates.

KOPT(*,*) - Optimal control gain state feedback matrix

POPT(*,*) - Update matrix of the optimal control gain generator

PMOPT(*,*) - Measurement update matrix of the optimal control gain generator

PHI0(*,*) - Augmented system matrix for the solution of the optimal control gains.

GMA0(*,*) - Augmented input distribution matrix for the solution of the optimal control gains.

Q1OPT(*,*) - Augmented cost function state weighting matrix for the solution of the optimal control gains.

STVU(*) - Variances of the motor noise sources.

STVY(*) - Variances of the observation noise sources.

VUM(*,*) - Covariance matrix of the motor noises.

VYM(*,*) - Covariance matrix of the motor noises.

PKAL(*,*) - Covariance matrix of the time-varying Kalman filter solution

PMKAL(*,*) - Measurement covariance matrix of the time-varying Kalman filter solution

PHIK10(*,*) - Full rank optimal control gain matrix

GMAK00(*,*) - State feedback optimal control gains

GMAK10(*,*) - Muscular system optimal control gains (time constants)

K1(*,*) - Kalman filter output error correction gain matrix

H1(*,*) - Augmented measurement matrix for the solution of the Kalman filter gains.

PHI1(*,*) - Augmented system matrix for the solution of the Kalman filter gains.

GMA1(*,*) - Augmented input distribution matrix for the solution of the Kalman filter gains.

Q1(*,*) - Augmented noise model covariance matrix for the solution of the Kalman filter gains.

X1(*) - Augmented estimate of the state vector from the Kalman filter.

X1MINUS(*) - Update estimate of the augmented state vector of the Kalman filter.

FM1(*,*) - Augmented continuous time system matrix for the generation of the state transition matrix of the least-squared predictor.

K2(*,*) - State transition matrix of the least-squared predictor.

ZKDZ(*,*) - FIFO buffer for the state estimate delay.

X2(*) - Time advanced prediction of the system augmented state

ZETA(*) - Predicted state estimate

XR(*) - Trajectory reference state vector.

XRKD(*) - Delayed trajectory reference state vector

XR1(*) - State vector of the bandlimiting filters of the trajectory generators

AR1(*,*) - System matrix of the bandlimiting filters

BR1(*,*) - Input distribution matrix of the bandlimiting filters

AFORCE - Time constant of the forcing function bandlimiting filter

XR2(*,*) - State vector of the integrated and distributed command sequence

AR2(*,*) - System matrix of the command sequence integrator

BR2(*,*) - Input distribution matrix of the command sequence integrator

XR3(*,*) - State vector of the rate command sequence

IDNT(*,*) - Utility identity matrix

NULL(*,*) - Utility zero matrix.

W(*,*) - Working array

W1(*,*) - Working array

W2(*,*) - Working array

WINV(*,*) - Working inversion array

REFERENCES

1. - "Dynamic Response of Human Operators", D.T. McRuer and E.S. Krendel, Wright Air Development Center, WDAC TR-56-524, October 1957.

2. - "Human Dynamics in Compensatory Systems", D.T. McRuer, D. Graham, E. Krendel, and W. Reisner, Jr., Air Force Dynamics Laboratory, AFFDL-TR-65-15, 1965.

3. - "Human Operator as a Servo System Element", D.T. McRuer and E.S. Krendel, Journal of the Franklin Institute, Vol. 267,pp 381-403, May 1959.

4. - "An Optimal Control Model of Human Response, Part I: Theory and Validation", D.L. Kleinman, S. Baron, and W.H. Levison, Automatica, Vol. 6, pp. 357-369, 1970.

5. - "An Optimal Control Model of Human Response, Part II: Prediction of Human Performance in a Complex Task", S. Baron, D.L. Kleinman, and W.H. Levison, Automatica, Vol. 6, pp. 371-383, 1970.

6. - "Human Dynamics in Man-Machine Systems", D.T. McRuer, presented at the 7th IFAC World Congress on a Link between Science and Applications of Automatic Control, Helsinki, Finland, June 1978.

7. - "Handbook of Human Factors", Salvendy Gavriel (editor), pp 1216, John Wiley and Sons, New York, 1977.

8. - "A Model of Human Controller Remnant", William H. Levison, Sheldon Baron, David L. Kleinman, IEEE Transactions on Man-Machine Systems, Vol. MMS-10, No. 4, December 1969.

9. - "The Relationship Between Saccadic and Smooth Tracking Eye Movements", C. Rashbass, Journal of Physiology, Vol. 159, pp. 326-388, 1961.

10. - "Model-Based Analysis of Control/Display Interaction in the Hover Task", Sanjay Garg and David K. Schmidt, presented at the AIAA Atmospheric Flight Mechanics Conference, Montery, CA., August 1987.

11. - "Model-Based Evaluation of Display-Dynamics Effects in Pursuit Tracking", Sanjay Garg and David K. Schmidt, presented at the 22nd Annual Conference on Manual Control, Dayton, OH., July 1986.

12. - "An Analysis of Pilot Adaption on a Simulated Multiloop VTOL Hovering Task", E.W. Vinje, IEEE Transactions on Man-Machine Systems, MMS-9, No. 4, December 1968.

13. - "Optimum Systems Control", A.P. Sage and C.C. White, Prentice-Hall Inc., Englewood Cliffs, NJ., 1977.

14. - "UH-60A Black Hawk Engineering Simulation Program, Vol. 1, Mathematical Model.", (ISER-70452, Sikorsky Aircraft; NASA Contract NAS2-10626), NASA CR-166309, 1981.

15. - "AV-8B Simulation Software", John W. Bunnell, Laurence C. Anderson, Naval Air Test Center, N00421-8-R-0289, May 1985.

16. - "AV-8B Simulation Model", John W. Bunnell, Laurence C. Anderson, Naval Air Test Center, N00421-81-C-0289, November 1985.

17. - "AV-8B Model Identification Results: Low and High Speed Longitudinal Model", Laurence C. Anderson, (SCT Report No. 5504-2), Systems Control Technology Inc., Palo Alto, CA., 1984.

18. - "Computer Simulation of Multiple Pilots Flying a Modern High Performance Helicopter", M.E. Zipf, W.G. Vogt, M.H. Mickle, R.G. Hoelzeman, Fei Kai, J.R. Mihaloew, NASA Technical Memorandum TM-100182, July 1988.

19. - Computer Simulation of a Single Pilots Flying a Modern High Performance Helicopter", M.E. Zipf, W.G. Vogt, M.H. Mickle, R.G. Hoelzeman, Fei Kai, J.R. Mihaloew, NASA Technical Memorandum TM-100183, July 1988.

20. - "A Computer Simulation of Low Order Pilot Models Flying a Thrust Vectored V/STOL Research Aircraft", M.E. Zipf, W.G. Vogt, M.H. Mickle, S. Kucuk, J.R. Mihaloew, To be published in the Proceedings of the Nineteenth Modeling and Simulation Conference, (Instrument Society of America, Durham, NC., 1988), Vol. 19.

21. - "Dynamics of Atmospheric Flight", Bernard Etkin, John Wiley and Sons, Inc. 1972.

22. - "Aircraft Dynamics and Automatic Control", Duane T. McRuer, Irving Ashkenas, Dunstan Graham, Princeton University Press, Princeton, New Jersey, 1973.

23. - "Flight Control of Manned Booster", F.D. Hauser and J.H. Bigelow, (T-70-48901-004), Martin Marietta Co., Denver, CO., 1971.

24. - "Multivariable Digital Control Laws For The UH-60A Black Hawk Helicopter", B.H. Mayhew, M.S. Thesis, Air Force Institue of Technology, 1984. (Available as NTIS AD-A141046)

25. - "Simulation Evaluation of the Control System Command Monitoring Concept for the NASA V/STOL Research Aircraft (VSRA)", J.A. Schroeder, AIAA Guidance, Navigation and Control Conference, AIAA-87-2255-CP, Moneray, CA., August 1987.

26. - "Prediction of Pilot Opinion Ratings Using an Optimal Pilot Model",R.A. Hess, Human Factors, Vol 19, No. 5, 1977, pp 459-475.

27. - "Digital Control of Dynamic Systems", G.F. Franklin and J.D. Powell, Addison-Wesley Publishing Co., Reading, MA., 1980.

28. - "Introduction to Random Signal Analysis and Kalman Filtering", R.G. Brown, John Wiley and Sons, New York, NY., 1983.

FIGURE GROUP

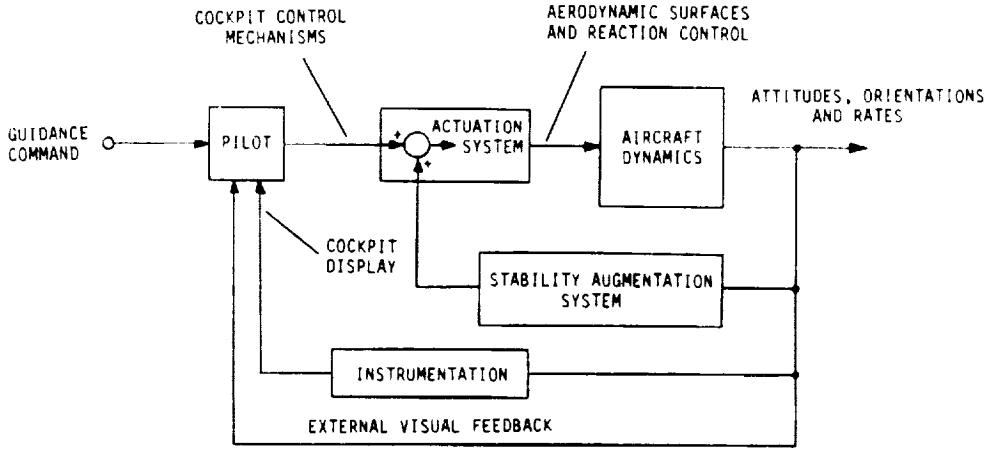

Figure I.A.-1 - Block Diagram of the closed loop piloted control structure

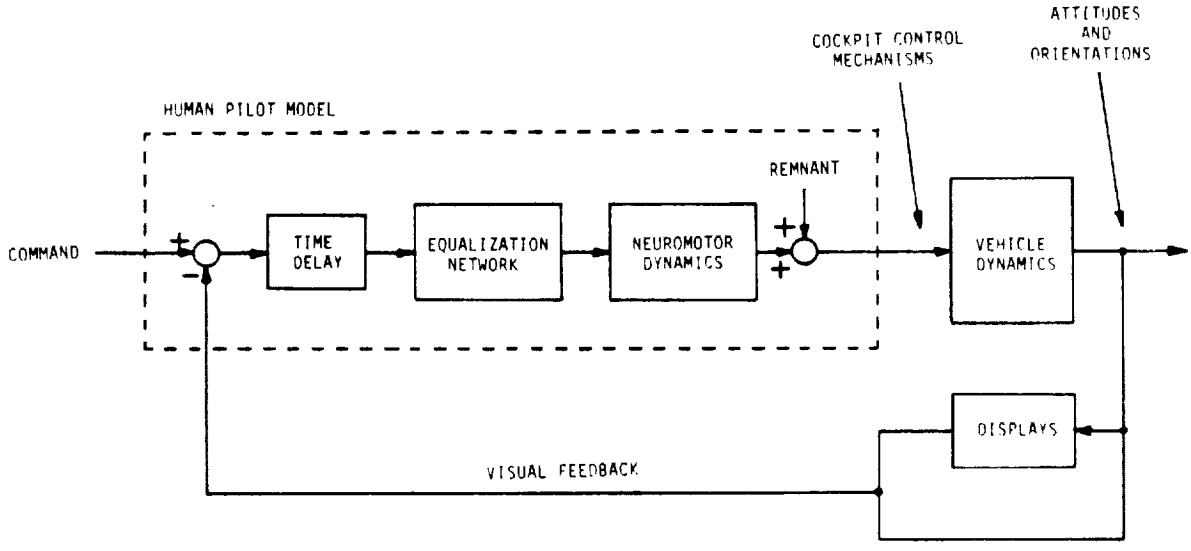

Figure II.-1. - Block diagram of the basic human controller characteristics

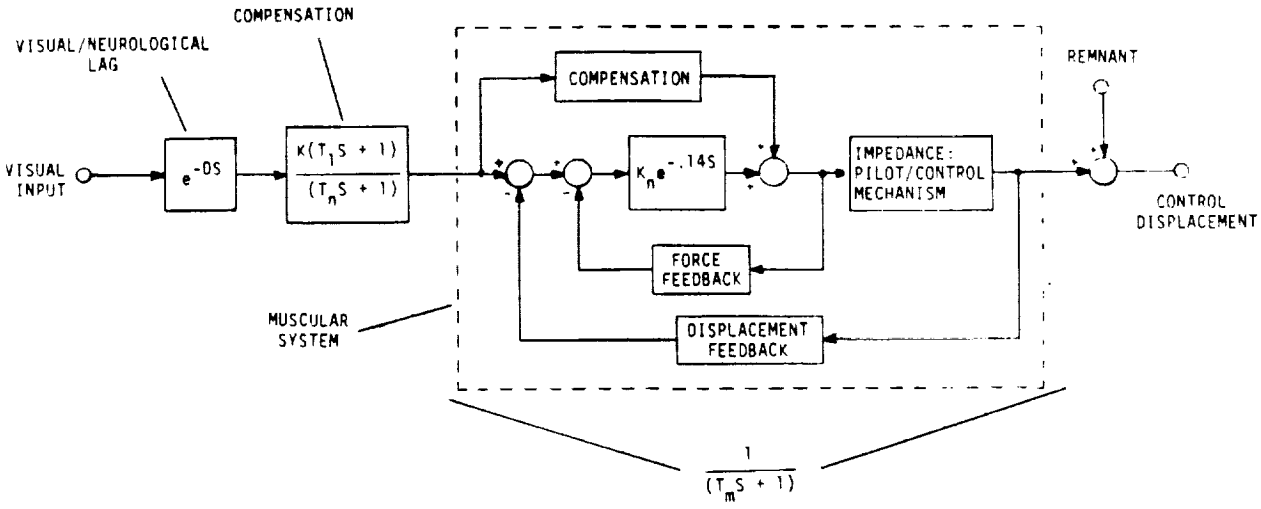

Figure II.A.-1. - Block diagram of the internal structure of the McRuer-Krendel model

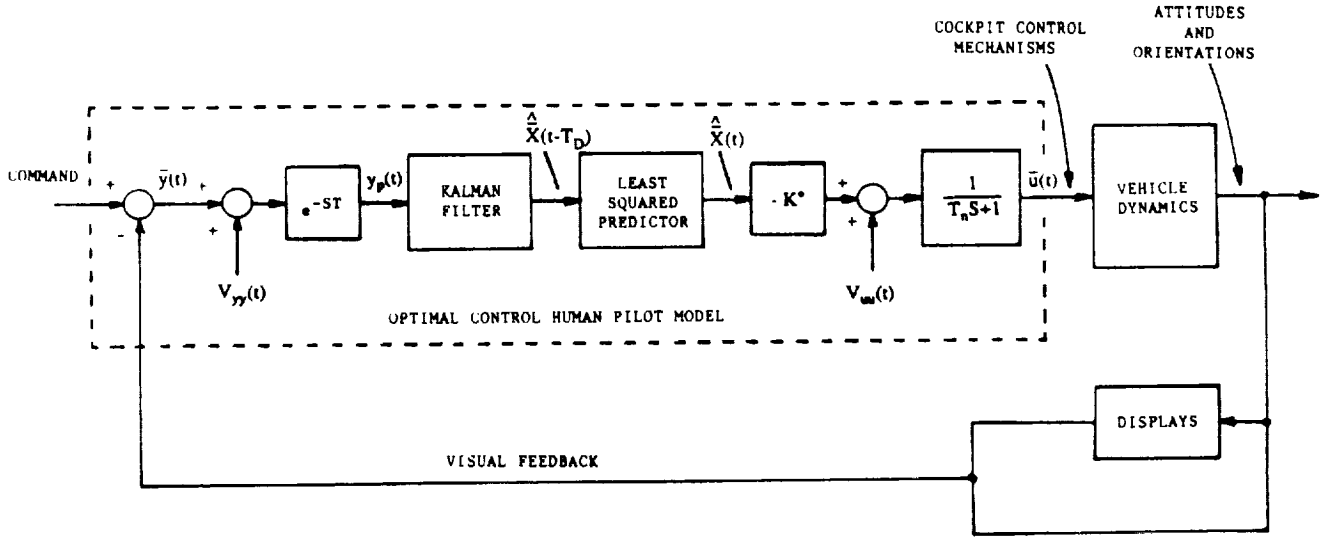

Figure II.B.-1. - Simple block diagram of the OCM within a control environment.

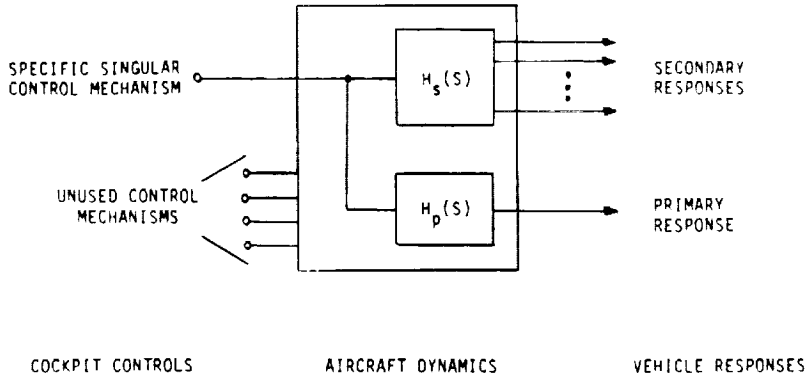

Figure III.B.1.-1. - A block diagram of the separation of the primary and secondary response characteristics associated with the decoupled transfer function models.

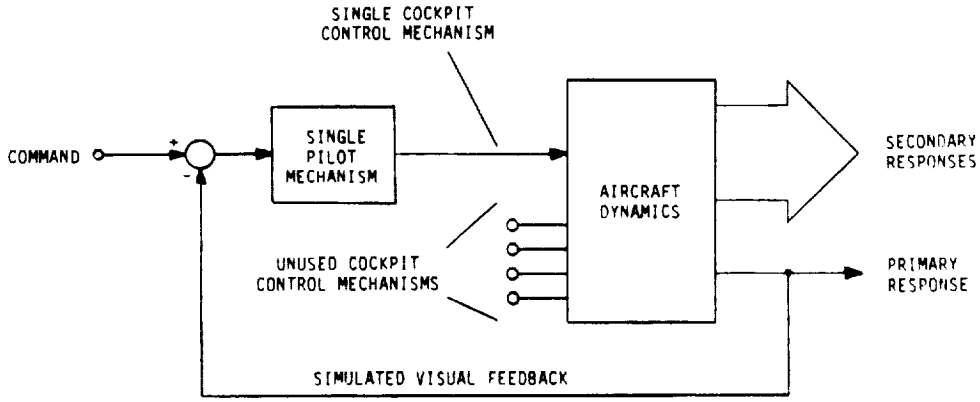

Figure III.B.2.-1. - Control loop closing strategy for the design of single variable pilot mechanisms

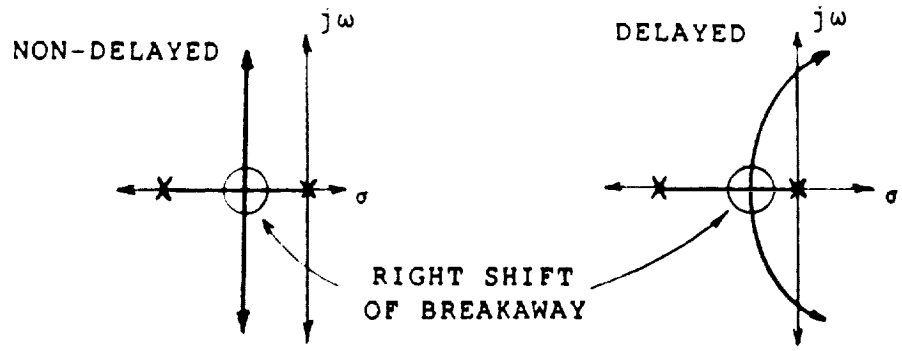

Figure III.B.2.-2. - Illustration of the destabilizing distortions associated with a delay Root-Locus

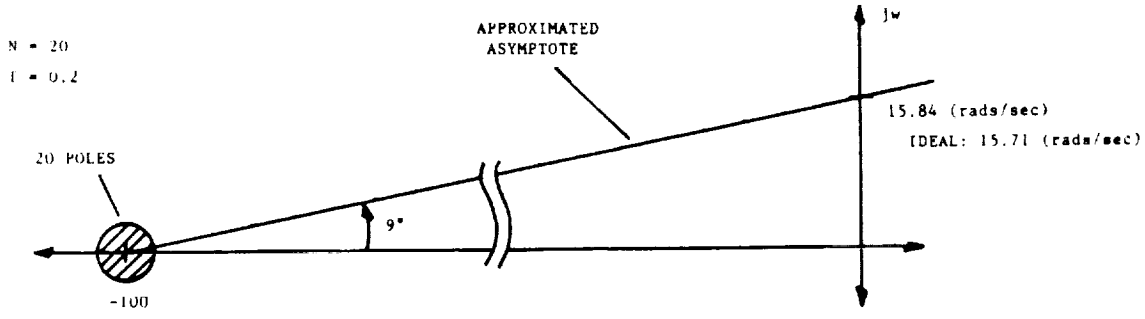

Figure III.B.2.-3. - Illustration of a delay approximation using a large pole set

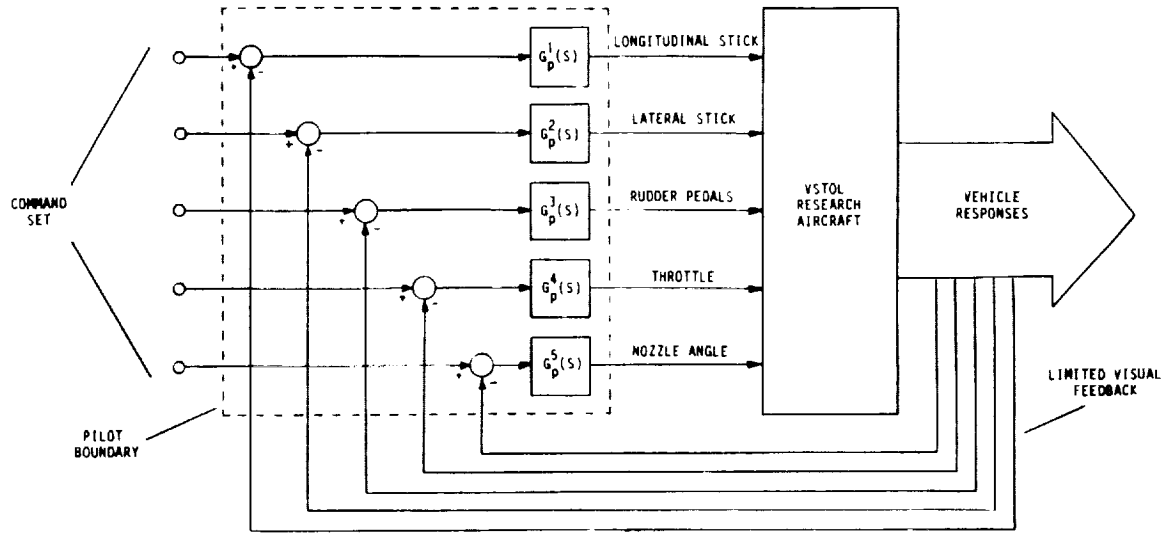

Figure III.B.3.-1. - Multi-variable control structure for the insertion of the McRuer-Krendel pilot models

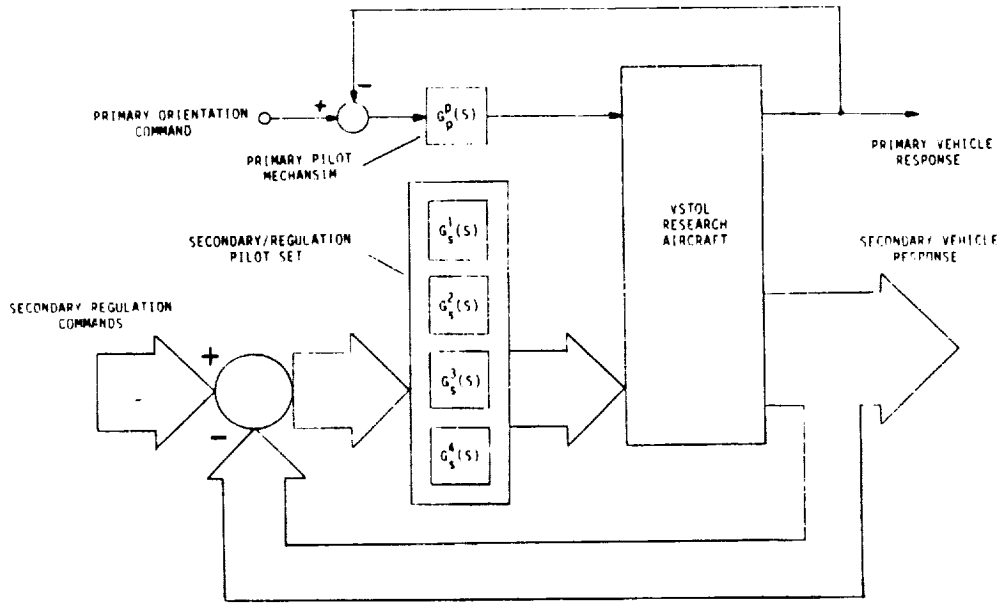

Figure III.B.3.-2. - Multi-variable control structure for executing simple flight control maneuvers.

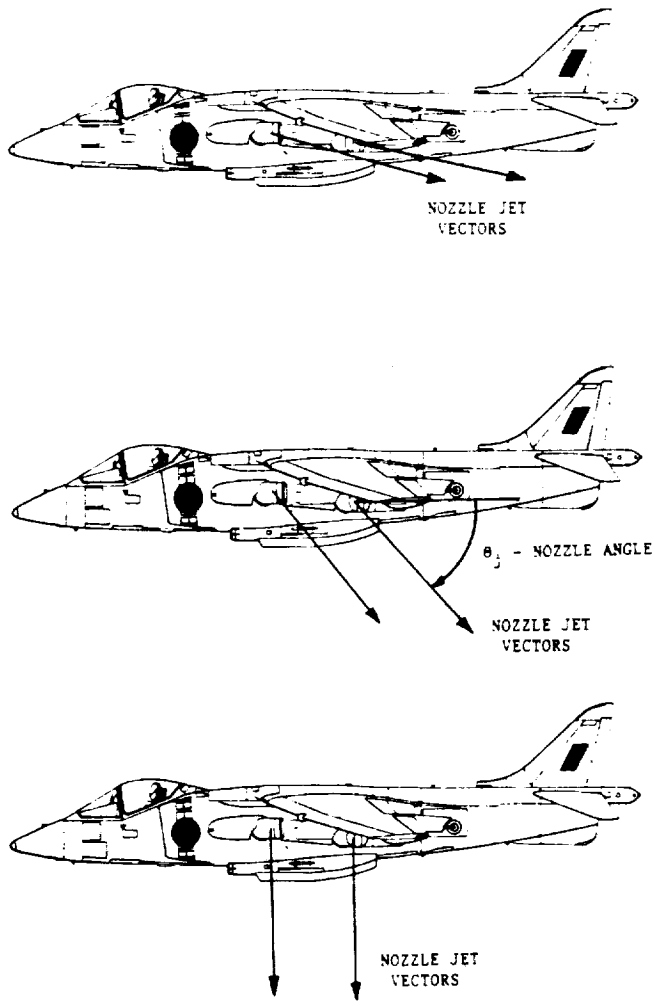

Figure IV.A.-1. - Flight envelope of the Harrier II AV-8B.

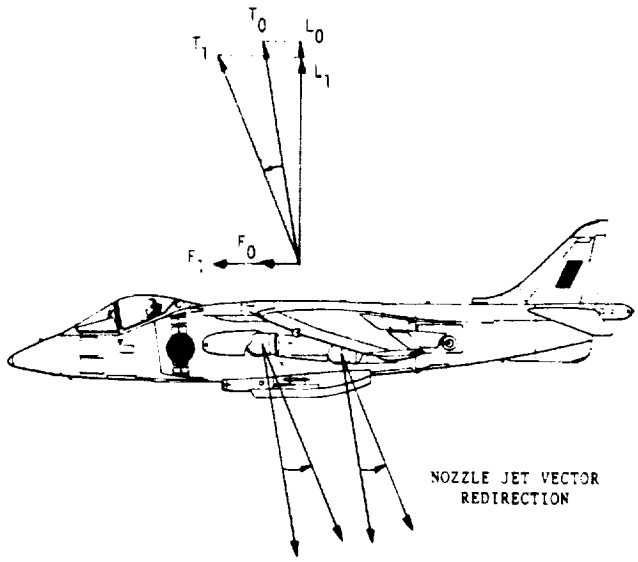

Figure IV.A.1.-1. - Illustration of the modification of the engine thrust vector due to a reduction in nozzle angle during low speed/powered-lift activities

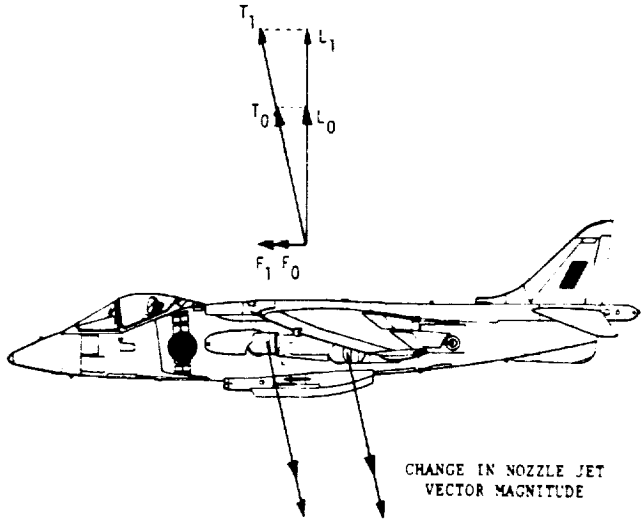

Figure IV.A.1.-2. - Illustration of the modification of the engine thrust vector due to an increase in engine speed during low speed/powered-lift activities

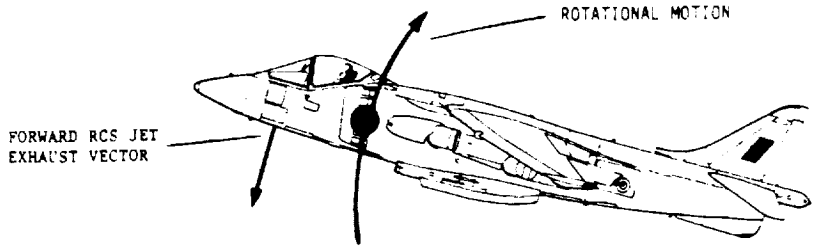

Figure IV.A.1.-3 - Illustration of the rotational motion due to the operation of the forward RCS jet from the backward deflection of the longitudinal stick during low speed/powered-lift activities.

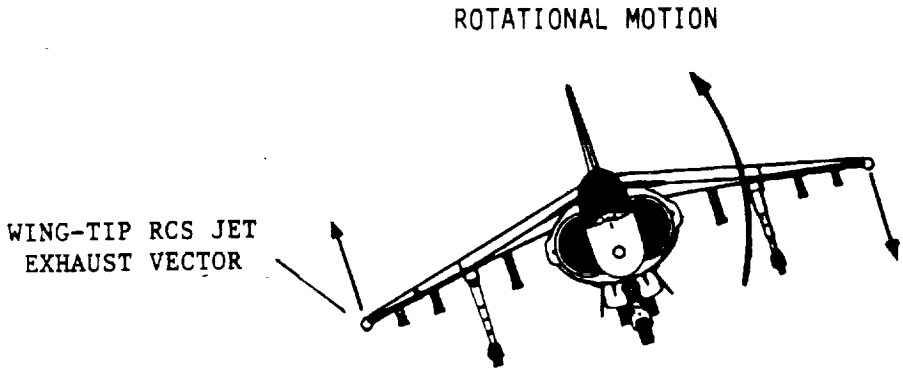

Figure IV.A.1.-4. - Illustration of the rotational motion due to the operation of the wing-tip RCS jets from the deflection of the lateral stick during low speed/powered-lift activities

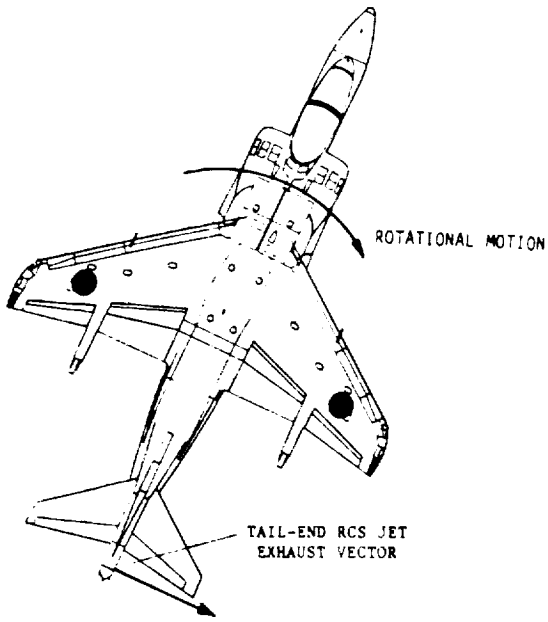

Figure IV.A.1.-5. - Illustration of the rotational motion due to the operation of the tail-end RCS jet from the deflection of the rudder pedals during low speed/powered-lift activities

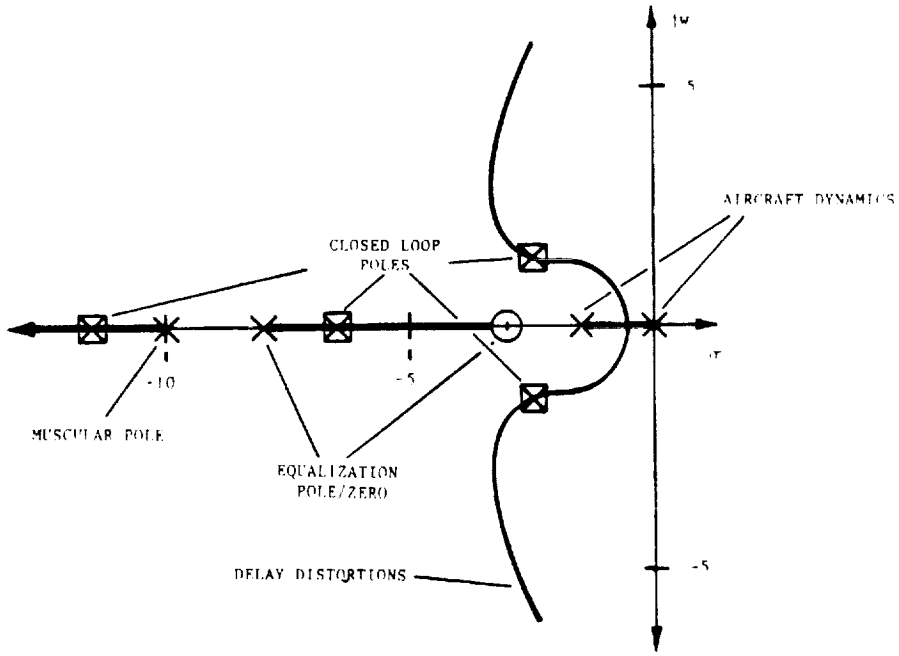

Figure V.A.1.-1. - Root-Locus of the pitch control pilot mechanism

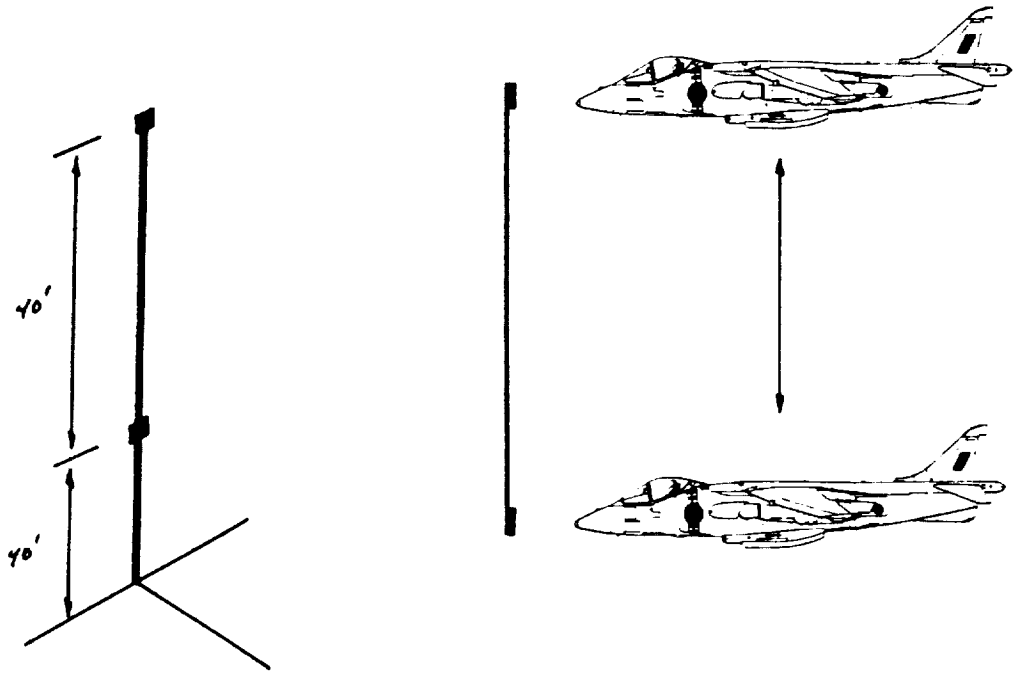

Figure V.B.1.-1. - Illustration of the target orientation and vehicle motion during the Vertical Tracking Hover maneuver

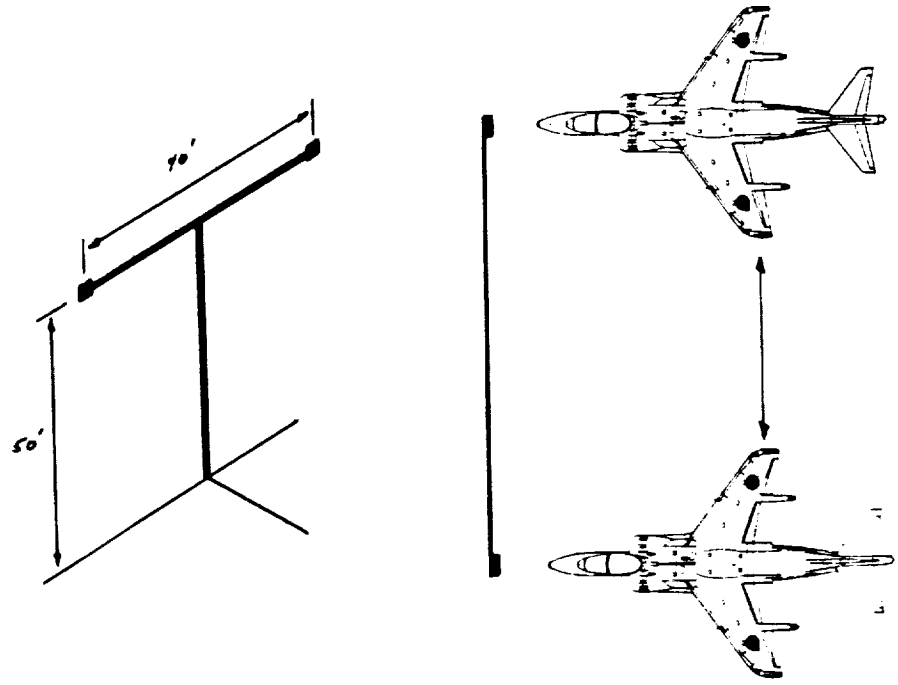

Figure V.B.1.-2. - Illustration of the target orientation and vehicle motion during the Lateral Tracking Hover maneuver

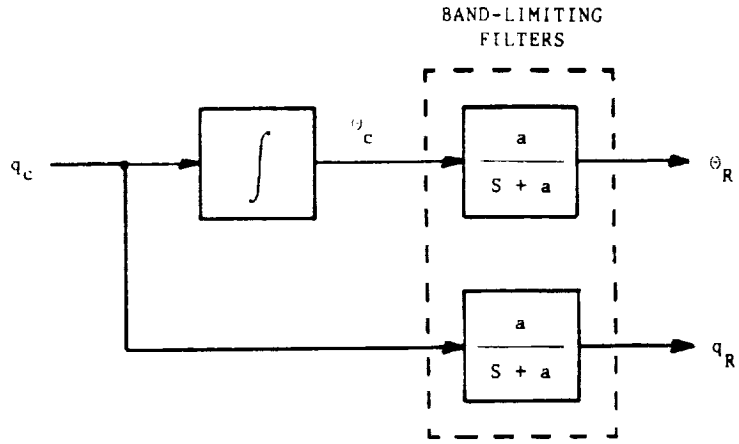

Figure V.B.4.-1. - Diagram of a trajectory reference generator for the pitch angle components driven by a pitch rate command sequence.

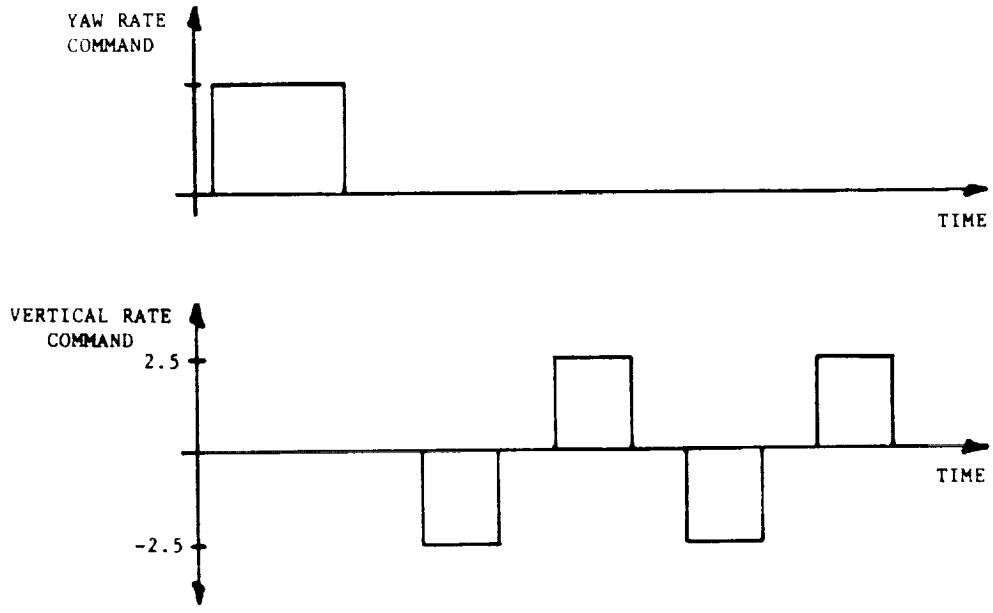

Figure V.B.4.-2. - Vertical rate and yaw rate command sequence for the vertical tracking maneuver.

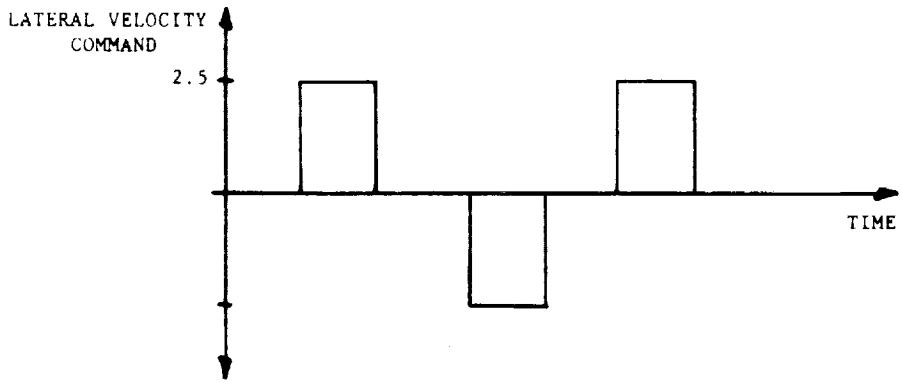

Figure V.B.4.-3. - Lateral velocity command sequence for the lateral tracking maneuver

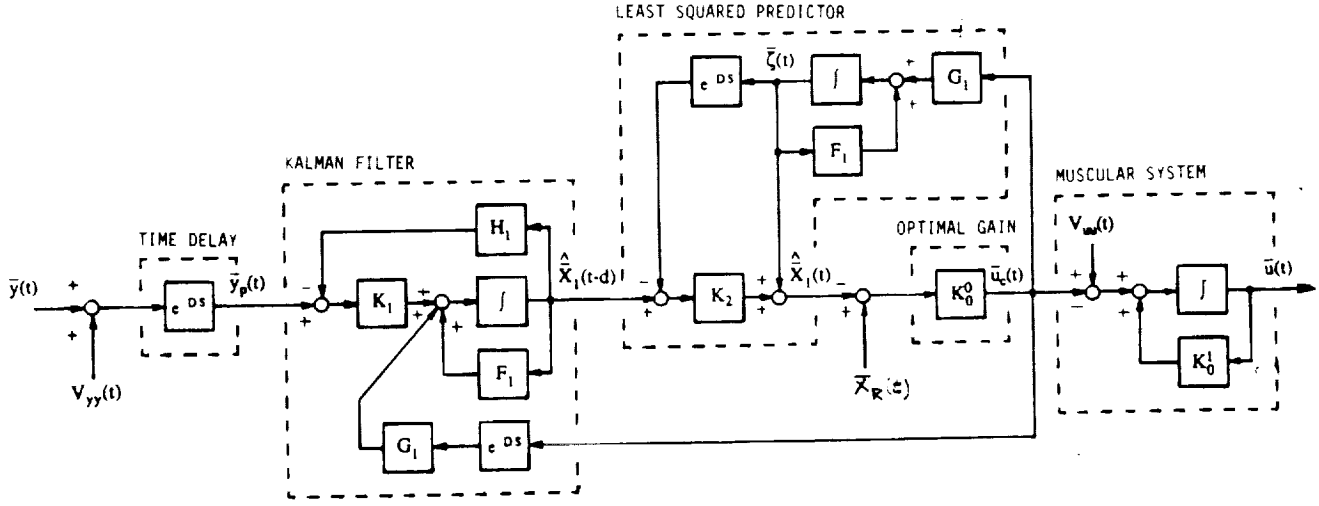

Figure A.1. -1. - Block diagram of the internal structure of the OCM

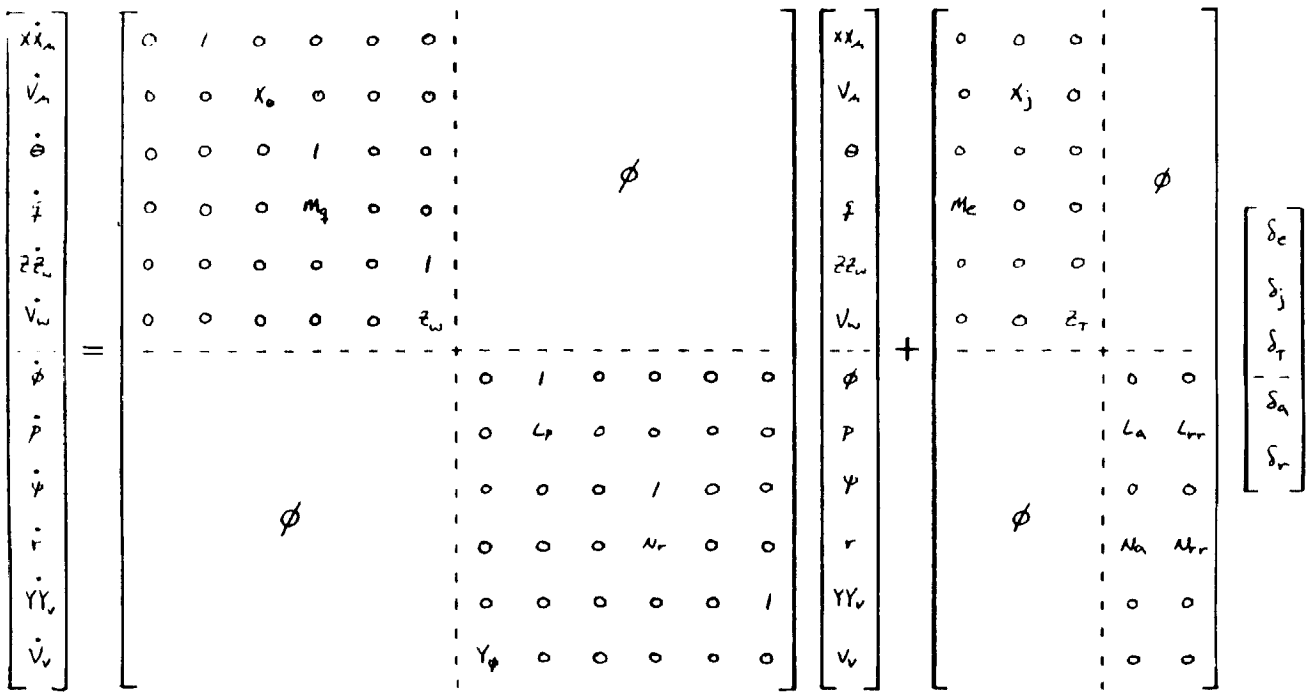

Figure B.2.-1. - Full rank linear state space model of the Harrier AV-8B flight dynamics from trimmed forward flight while in the low speed/powered-lift region of the flight envelope.

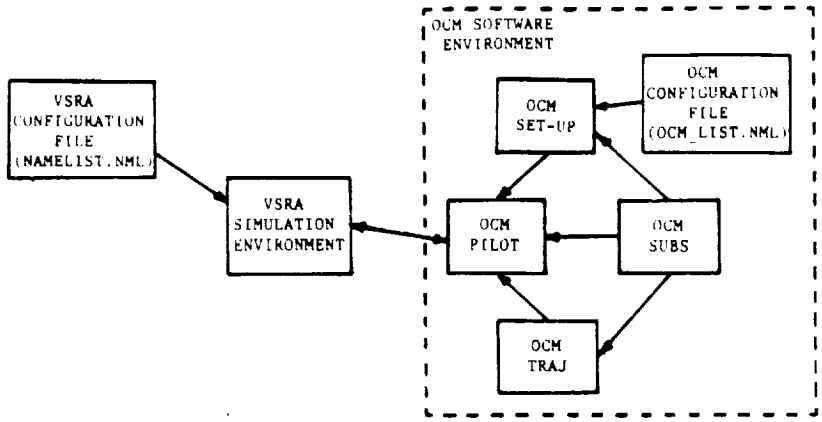

Figure C.1. - 1. - Block diagram of the software modules and configuration files of the OCM simulation environment.

TABLE GROUP

TABLE LISTING

XX_u		Longitudinal position
V_u		Forward velocity
θ		Pitch angle
q		Pitch rate
ZZ_w		Altitude
V_w	=	Vertical rate
ϕ		Roll angle
p		Roll rate
ψ		Yaw angle
r		Yaw rate
YY_v		Lateral position
V_v		Lateral velocity

Table IV.A.3.-1 - List of the state vector variables for the high order Harrier model.

$$\begin{bmatrix} \delta_e \\ \delta_j \\ \delta_T \\ \delta_a \\ \delta_r \end{bmatrix} = \begin{bmatrix} \text{Longitudinal stick position (inches)} \\ \text{Nozzle angle control position (degrees)} \\ \text{Power level/throttle position (percent)} \\ \text{Lateral stick position (inches)} \\ \text{Rudder pedal position (inches)} \end{bmatrix}$$

Table IV.A.3.-2. - List of the control vector variables for the high order Harrier model.

V (knots)	w_θ (rads/sec)	δ_θ	K_{TD} $(in\text{-}sec^3)^{-1}$	K_T $(in\text{-}sec^2)^{-1}$
20	4.7	0.28	0.041	2.32
40	4.9	0.19	0.045	2.59
60	5.1	0.14	0.051	2.91
80	5.4	0.10	0.049	2.83
100	5.7	0.07	0.048	2.77

Table IV.B.1.-1. - Transfer function parameters for the pitch response of the Black Hawk.

V (knots)	K_{ALT} ($\frac{feet}{in\text{-}sec^2}$)	a_{ALT} $(sec)^{-1}$
20	6.6	0.30
40	7.0	0.45
60	7.0	0.50
80	7.3	0.50
100	7.5	0.50

Table IV.B.1.-2. - Transfer function parameters for the altitude response components of the Black Hawk.

Pilot Mechanism	K	A $(sec)^{-1}$	B $(sec)^{-1}$
Altitude Control	52. $(\frac{in}{feet\text{-}sec})$	0.8	3.0
Vertical Rate Control	36. $(\frac{in}{feet})$	0.8	0.0
Velocity Control	-14. $(\frac{deg}{knot\text{-}sec})$	0.0	0.0
Roll Control	2.9 $(\frac{in}{deg\text{-}sec})$	3.6	8.0
Lateral Velocity Control	1.1 $(\frac{in}{feet})$	0.8	6.0
Heading Control	26. $(\frac{in}{deg\text{-}sec})$	0.8	20.
Yaw Rate Control	58. $(\frac{in}{deg})$	0.8	0.0
Sideslip Regulation	-32. $(\frac{in}{deg\text{-}sec})$	0.8	20.

Table V.A.1.-1. - Parameter list of the additional Harrier pilot mechanisms.

V (knots)	K_{PT} ($\frac{in}{deg\text{-}sec}$)
20	1.31
40	1.48
60	1.53
80	2.07
100	1.82

Table V.A.1.-2. - Parameters of the pitch control pilot of the Black Hawk

V (knots)	K ($\frac{in}{feet\text{-}sec}$)
20	5.77
40	5.68
60	4.97
80	5.07
100	5.19

$A = 0.8\ (sec)^{-1}$

$B = 5.5\ (sec)^{-1}$

Table V.A.1.-3. - Parameters of the altitude control pilot for the Black Hawk

V (knots)	K ($\frac{in}{feet}$)
20	1.82
40	1.74
60	1.43
80	1.51
100	1.57

$A = 0.8\ (sec)^{-1}$

$B = 0.0\ (sec)^{-1}$

Table V.A.1.-4. - Parameters of the altitude rate control pilot for the Black Hawk

V (knots)	K ($\frac{in}{deg\text{-}sec}$)
20	0.57
40	0.57
60	0.68
80	0.68
100	0.68

$A = 0.8\ (sec)^{-1}$

$B = 0.0\ (sec)^{-1}$

Table V.A.1.-5. - Parameters of the roll angle control pilot for the Black Hawk

V (knots)	K ($\frac{in}{deg\text{-}sec}$)	A $(sec)^{-1}$	B $(sec)^{-1}$
20	0.63	2.0	1.5
40	0.60	1.4	0.75
60	0.43	0.8	0.0
80	0.51	0.8	0.0
100	0.65	0.8	0.0

Table V.A.1.-6. - Parameters of the heading control pilot for the Black Hawk

V (knots)	K ($\frac{in}{deg\text{-}sec}$)
20	-0.25
40	-0.45
60	-0.55
80	-0.55
100	-0.55

$A = 0.8\ (sec)^{-1}$

$B = 0.0\ (sec)^{-1}$

Table V.A.1.-7. - Parameters of the Sideslip regulation pilot of the Black Hawk

cockpit control mechanism / maneuver	Longitudinal Stick	Lateral Stick	Rudder Pedals	Throttle	Nozzle Angle
Pitch Reorientation	Pitch Control Pilot	Roll Control Pilot	Heading Control Pilot	Altitude Control Pilot	Velocity Control Pilot
Velocity Translation	Pitch Control Pilot	Roll Control Pilot	Heading Control Pilot	Altitude Control Pilot	Velocity Control Pilot
Altitude Translation	Pitch Control Pilot	Roll Control Pilot	Heading Control Pilot	Altitude Control Pilot	Velocity Control Pilot
Heading Modification	Pitch Control Pilot	Roll Control Pilot	Heading Control Pilot	Altitude Control Pilot	Velocity Control Pilot
Altitude Rate Translation	Pitch Control Pilot	Roll Control Pilot	Heading Control Pilot	Altitude Rate Pilot	Velocity Control Pilot
Flat Turn	Pitch Control Pilot	Roll Control Pilot	Yaw Rate Control Pilot	Altitude Control Pilot	Velocity Control Pilot
Coordinated Turn	Pitch Control Pilot	Roll Control Pilot	Sideslip Regulation Pilot	Altitude Control Pilot	Velocity Control Pilot

Table V.A.2.-1. - Table of various flight control maneuvers and their associated configurations of Harrier SVPMs.

cockpit control mechanism / maneuver	Longitudinal Cyclic Stick	Lateral Cyclic Stick	Rudder Pedals	Collective Stick
Pitch Reorientation	Pitch Control Pilot	Roll Control Pilot	Heading Control Pilot	Altitude Control Pilot
Altitude Translation	Pitch Control Pilot	Roll Control Pilot	Heading Control Pilot	Altitude Control Pilot
Heading Modification	Pitch Control Pilot	Roll Control Pilot	Heading Control Pilot	Altitude Control Pilot
Altitude Rate Translation	Pitch Control Pilot	Roll Control Pilot	Heading Control Pilot	Altitude Rate Pilot
Coordinated Turn	Pitch Control Pilot	Roll Control Pilot	Sideslip Regulation Pilot	Altitude Control Pilot

Table V.A.2.-2. - Table of various flight control maneuvers and their associated configurations of Black Hawk SVPMs.

VARIABLE	TRIMMED	COMMAND
Pitch (θ_c)	7.3 degrees	17.3 degrees
Roll (ϕ_c)	0.0 degrees	0.0 degrees
Heading (ψ_c)	0.0 degrees	0.0 degrees
Altitude	100 feet	100 feet
Velocity	10 knots	10 knots

Table V.A.3.-1. - Pitch reorientation command sequence for the multi-variable Harrier pilot.

VARIABLE	TRIMMED	COMMAND
Pitch (θ_c)	6.5 degrees	6.5 degrees
Roll (ϕ_c)	0.0 degrees	0.0 degrees
Heading (ψ_c)	0.0 degrees	0.0 degrees
Altitude	100 feet	100 feet
Velocity	25 knots	20 knots

Table V.A.3.-2. - Velocity translation command sequence for the multi-variable Harrier pilot.

VARIABLE	TRIMMED	COMMAND
Pitch (θ_C)	2.8 degrees	2.8 degrees
Roll (ϕ_C)	0.0 degrees	20.0 degrees
Sideslip (β_C)	0.0 degrees	0.0 degrees
Altitude	200 feet	200 feet

Table V.A.3.-3. - Coordinated turn command sequence for the multi-variable Black Hawk pilot

XX_M	V_M^u	θ_M	ZZ_M	δ_M^e	δ_M^T
3.15	3.15	10.	5.	3.5	3.5

YY_M	V_M^y	ϕ_M	ψ_M	δ_M^a	δ_M^r
3.15	3.15	10.	7.0	3.5	1.25

Table V.B.3.-1. - Cost function weights of the OCM for the vertical tracking maneuver

XX_M	V_M^u	θ_M	ZZ_M	δ_M^e	δ_M^T
3.15	3.15	7.0	5.	3.5	3.5

YY_M	V_M^y	ϕ_M	ψ_M	δ_M^a	δ_M^r
3.15	3.15	10.	6.0	3.5	1.25

Table V.B.3.-2. - Cost function weights of the OCM for the lateral tracking maneuver

δ_e	δ_j	δ_T	δ_a	δ_r
1.0	1.0	0.22	1.4	1.4

Table V.B.3.-3. - Magnitudes of the OCM motor noise sources applied to each cockpit control mechanism

θ (degrees)	ϕ (degrees)	ψ (degrees)	ALT (feet)	Airspeed (knots)
6.5	0.0	0.0	80	1.0

Table V.B.4.-1. - Trimmed values of the Harrier simulation environment for the vertical tracking precision hover maneuver.

θ (degrees)	ϕ (degrees)	ψ (degrees)	ALT (feet)	Airspeed (knots)
6.5	0.0	0.0	55	1.0

Table V.B.4.-2. - Trimmed values of the Harrier simulation environment for the lateral tracking precision hover maneuver.

PLOT GROUP

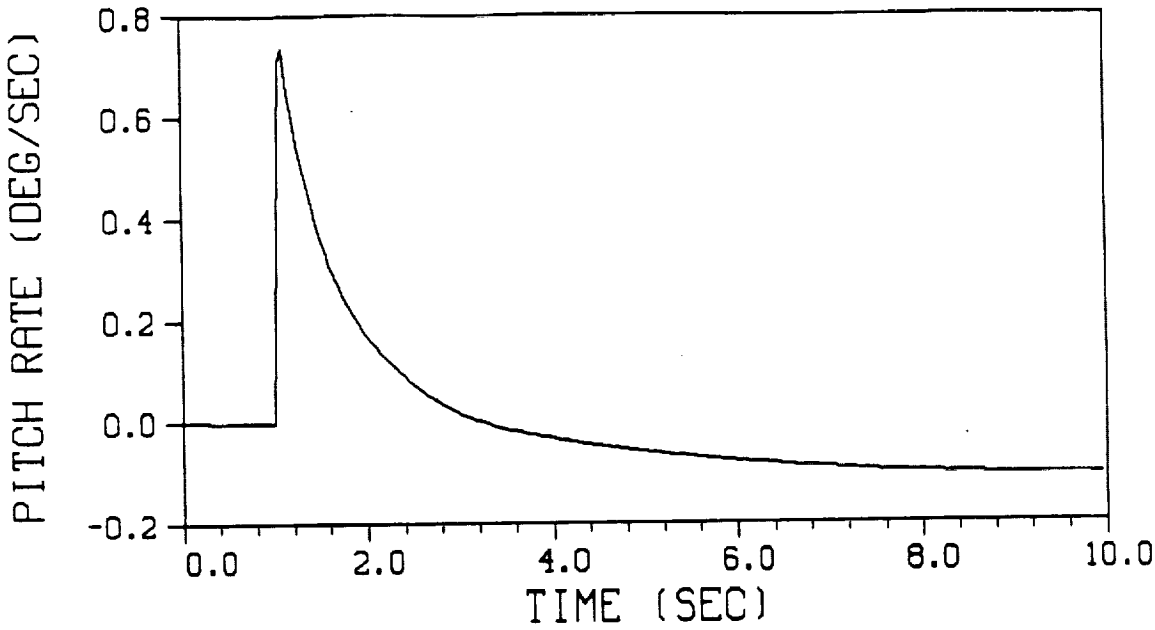

Plot IV.A.2.-1. - Pitch rate response of the Harrier AV-8B due to a unit impulse deflection of the longitudinal stick in a near hover

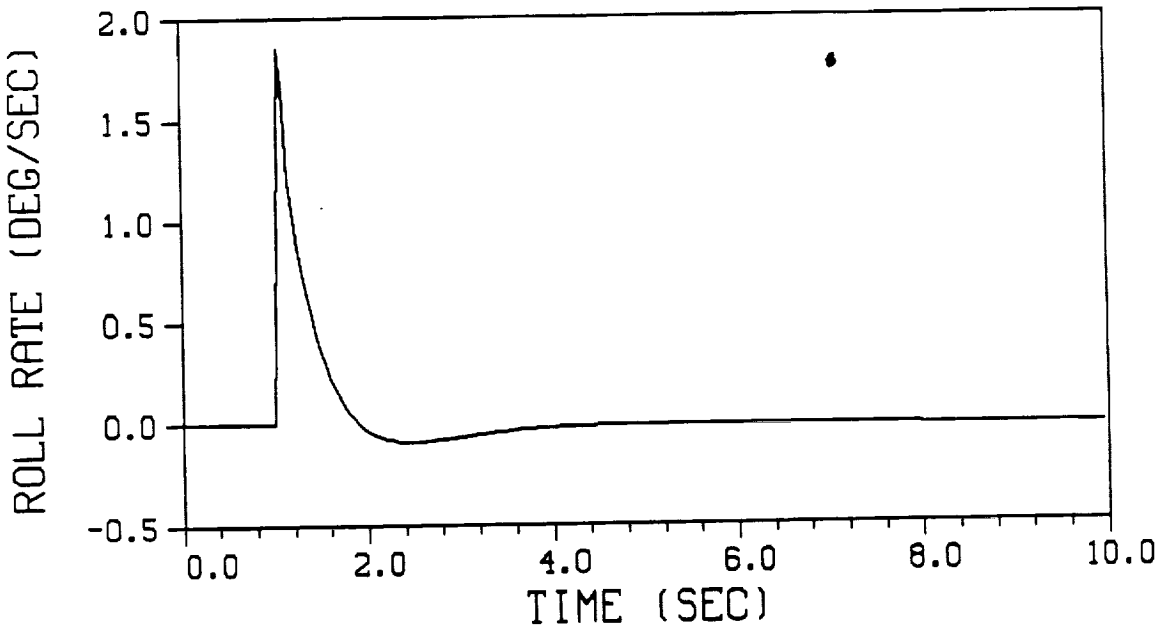

Plot IV.A.2.-2. - Roll rate response of the Harrier AV-8B due to a unit impulse deflection of the lateral stick in a near hover

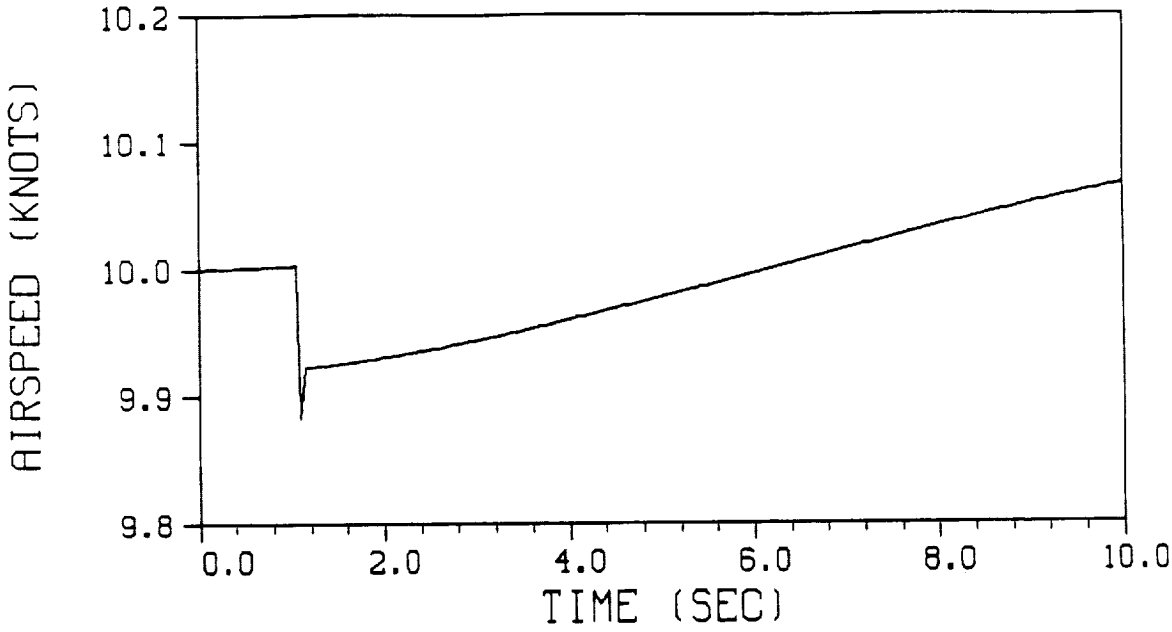

Plot IV.A.2.-3. - Forward velocity response of the Harrier AV-8B due to a 5 degree impulse deflection of the nozzle angle at 10 knots

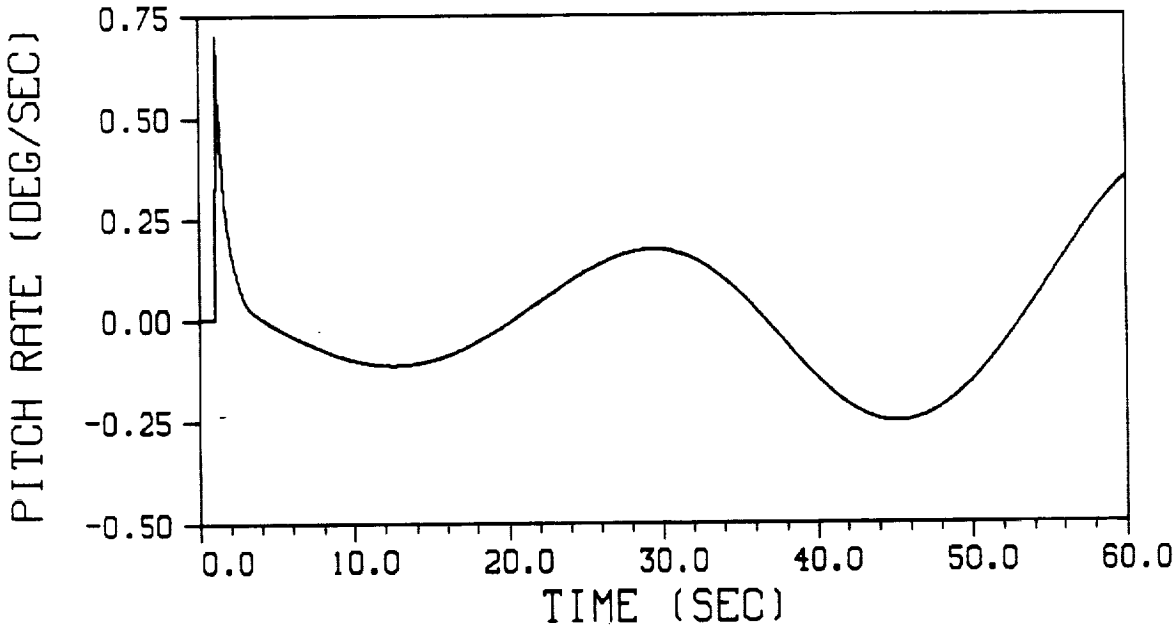

Plot IV.A.3.-1. - Long term pitch rate response of the Harrier AV-8B due to a unit impulse deflection of the longitudinal stick at 10 knots

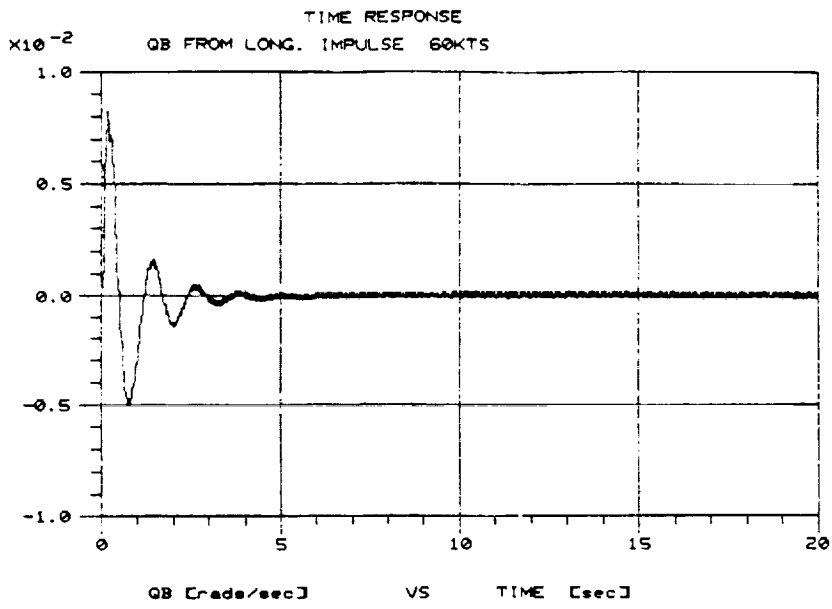

Plot IV.B.1.-1. - Pitch rate response of the Black Hawk UH-60A due to an impulse of the longitudinal cyclic stick at 60 knots.

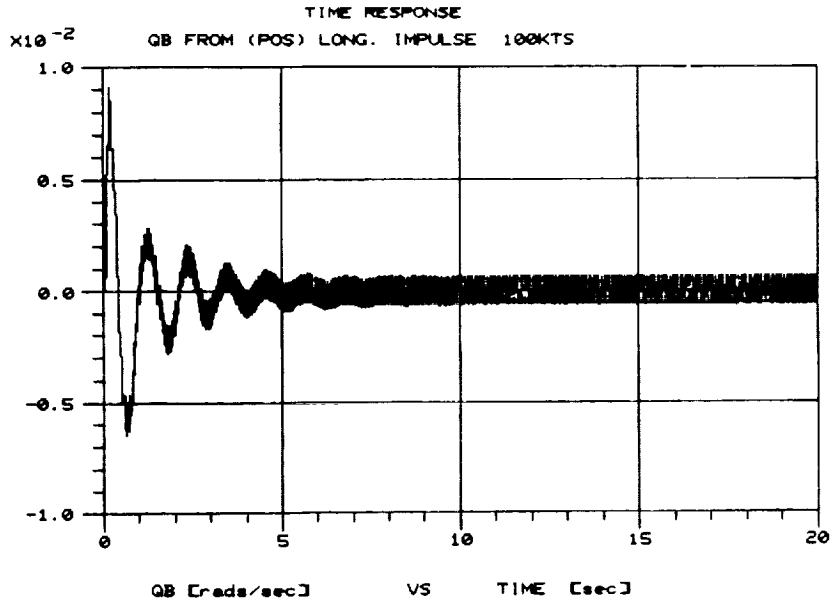

Plot IV.B.1.-2. - Pitch rate response of the Black Hawk UH-60A due to an impulse of the longitudinal cyclic stick at 100 knots.

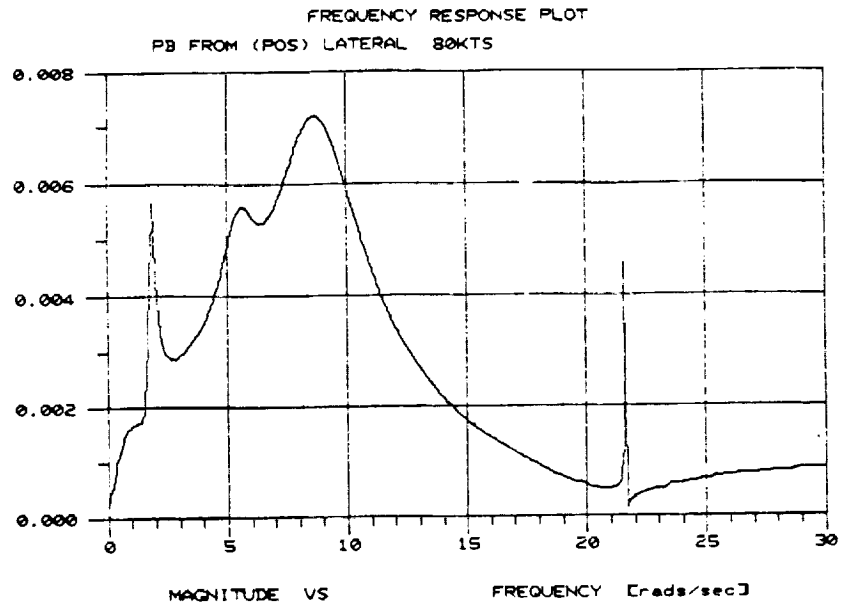

Plot IV.B.1.-3. - Roll rate frequency response of the Black Hawk UH-60A due to the operation of the lateral cyclic stick at 80 knots.

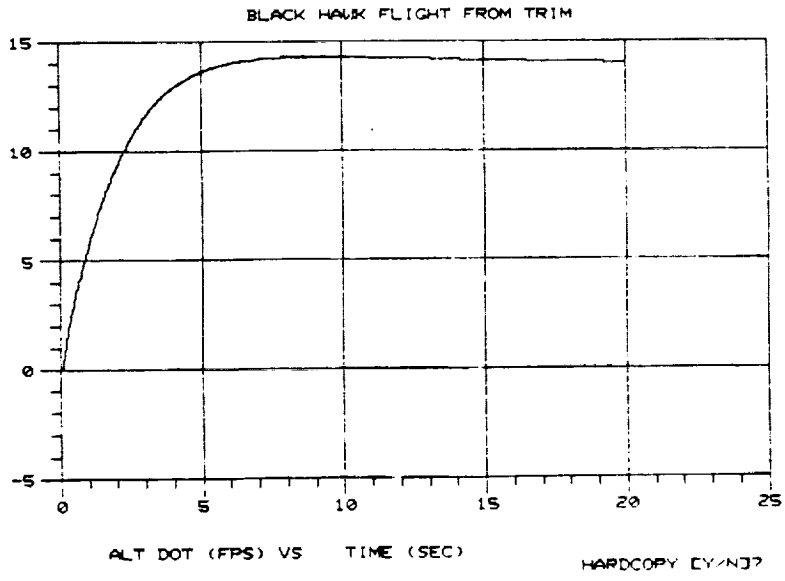

Plot IV.B.1.-4. - Altitude rate response of the Black Hawk UH-60A due to a step of the main rotor collective stick at 60 knots.

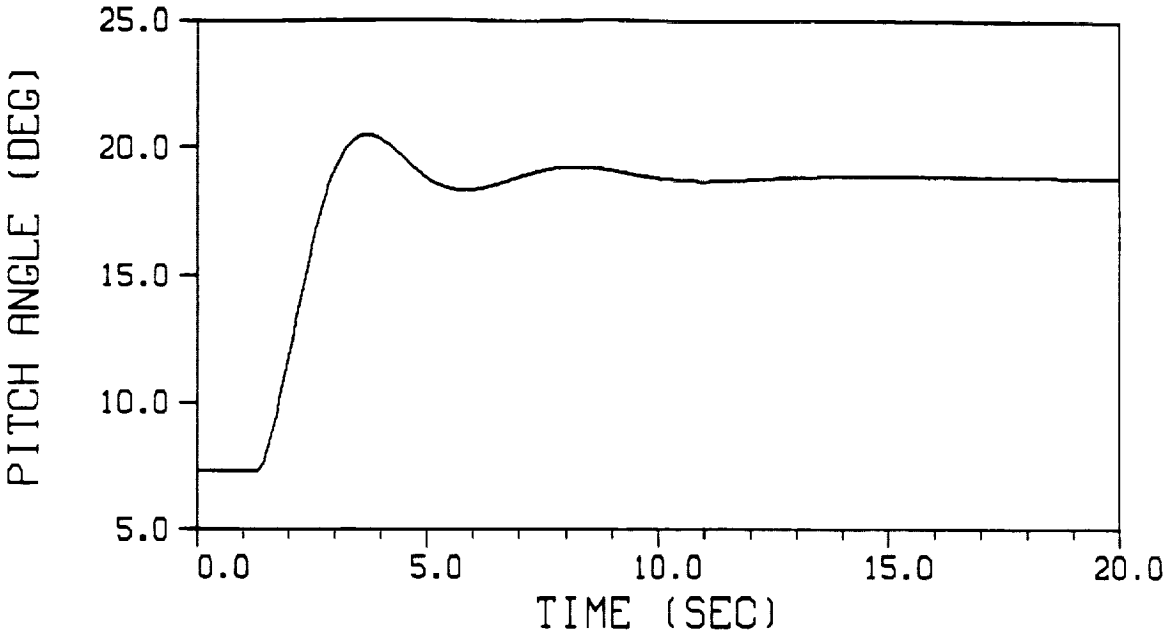

Plot V.A.3.-1. - Pitch angle response during a pitch reorientation maneuver by a multi-variable McRuer-Krendel pilot inserted in the Harrier AV-8B

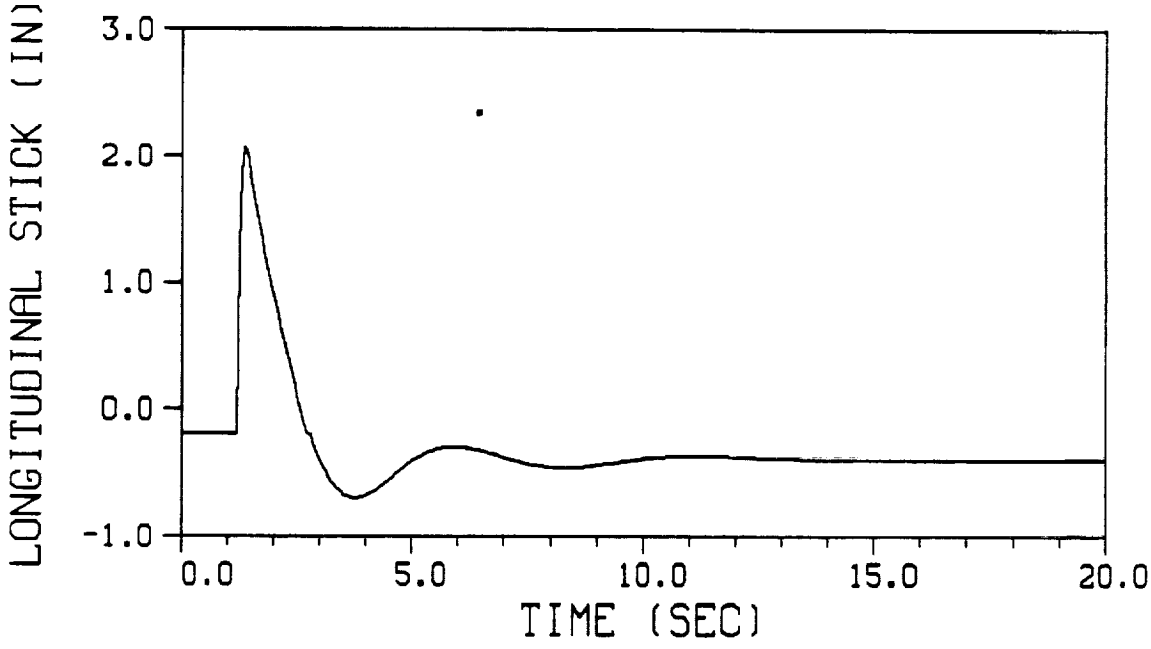

Plot V.A.3.-2. - Longitudinal stick response of a multi-variable McRuer-Krendel pilot during a pitch reorientation maneuver in the Harrier AV-8B

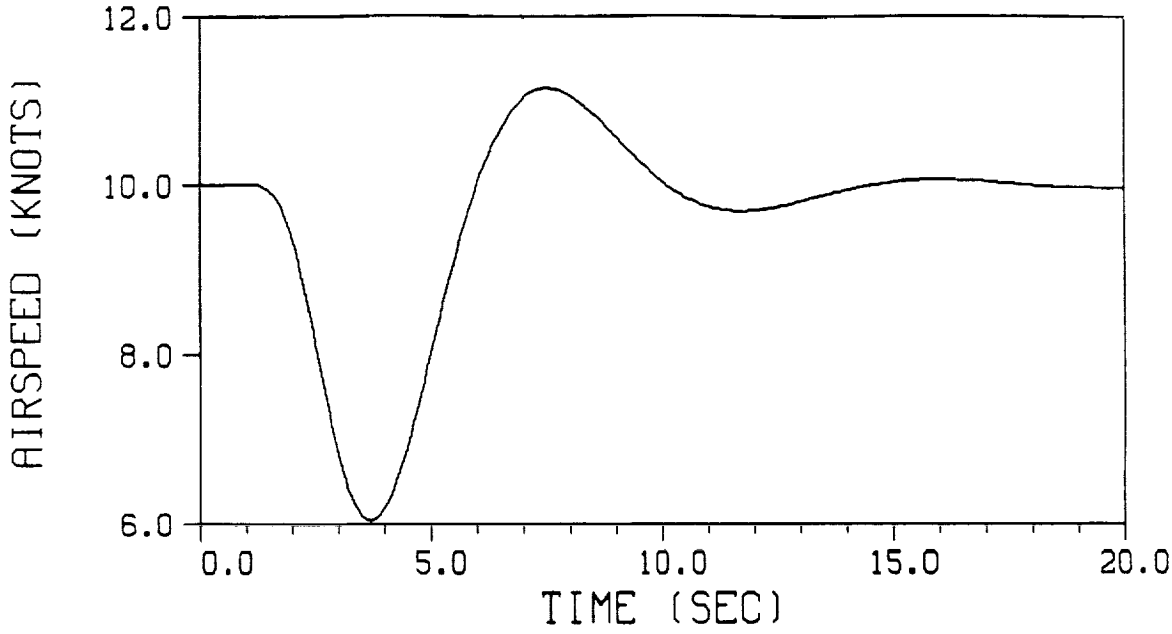

Plot V.A.3.-3. - Forward velocity response during a pitch reorientation maneuver by a multi-variable McRuer-Krendel pilot inserted in the Harrier AV-8B

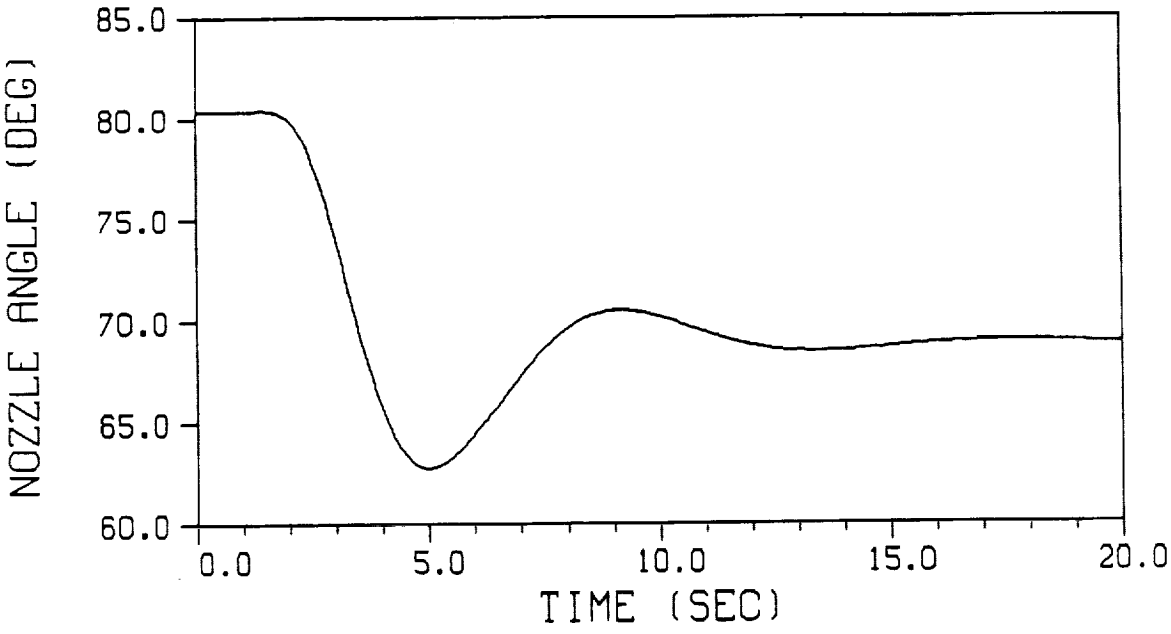

Plot V.A.3.-4. - Nozzle angle response of a multi-variable McRuer-Krendel pilot during a pitch reorientation maneuver in the Harrier AV-8B

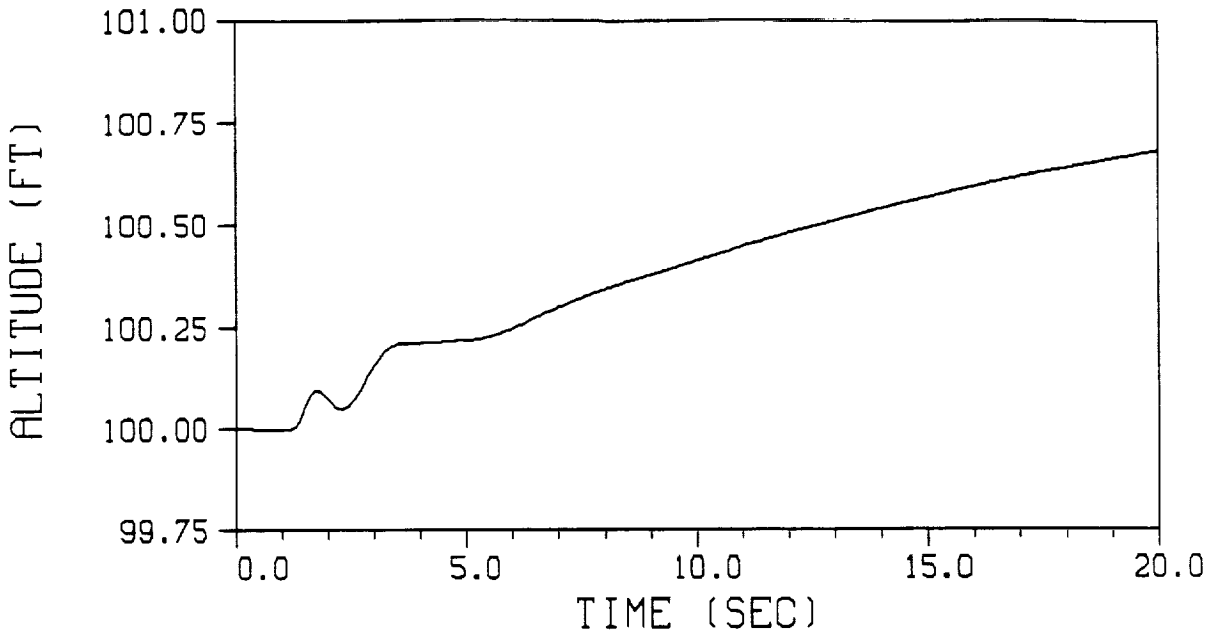

Plot V.A.3.-5. - Altitude response during a pitch reorientation maneuver by a multi-variable McRuer-Krendel pilot inserted in the Harrier AV-8B

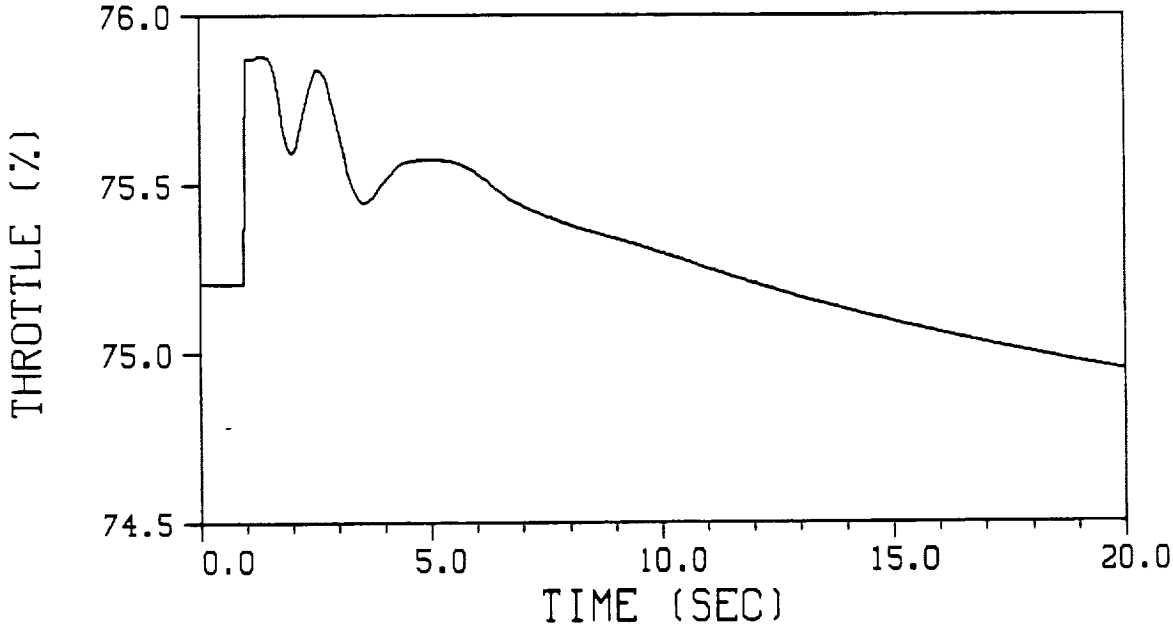

Plot V.A.3.-6. - Throttle response of a multi-variable McRuer-Krendel pilot during a pitch reorientation maneuver in the Harrier AV-8B

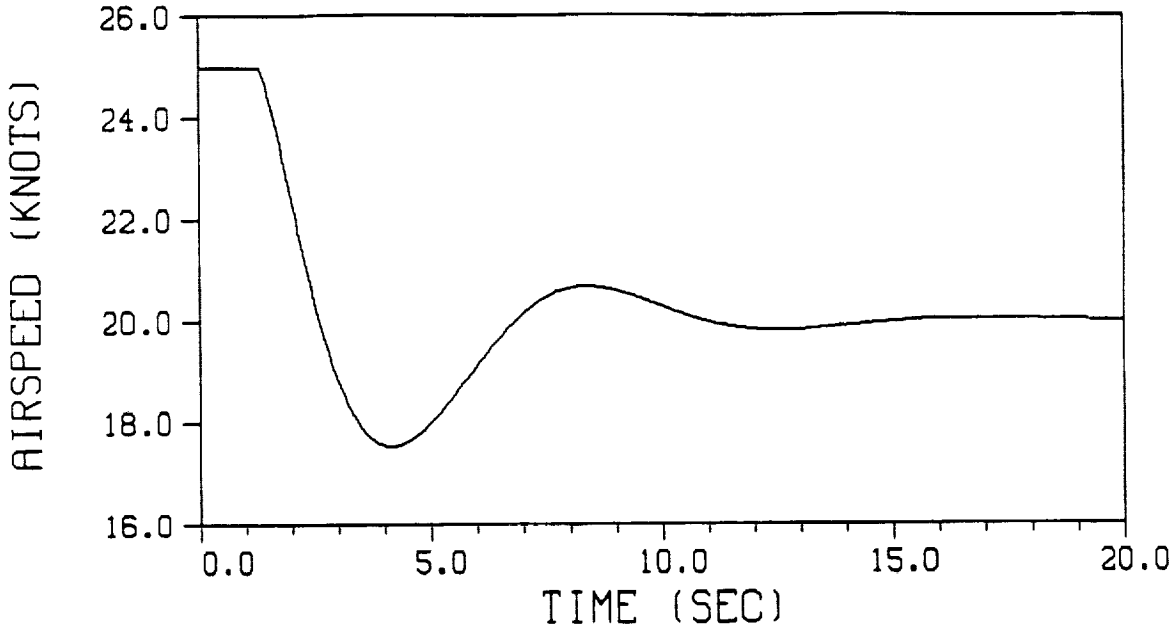

Plot V.A.3.-7. - Forward velocity response during a velocity translation maneuver by a multi-variable McRuer-Krendel pilot inserted in the Harrier AV-8B

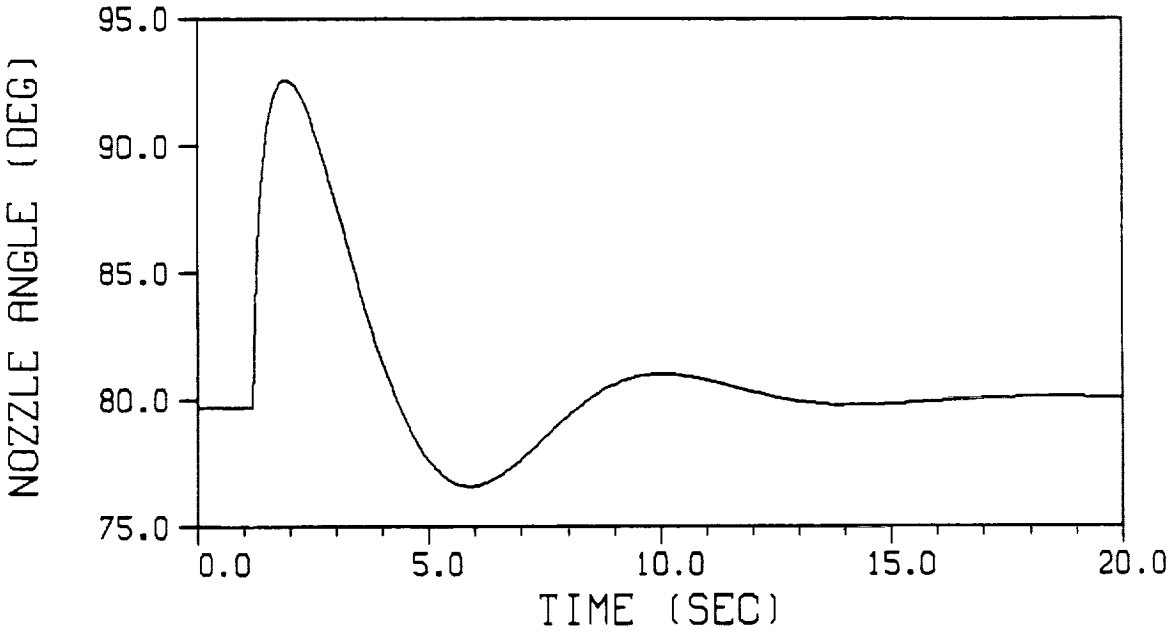

Plot V.A.3.-8. - Nozzle angle response of a multi-variable McRuer-Krendel pilot during a velocity translation maneuver in the Harrier AV-8B

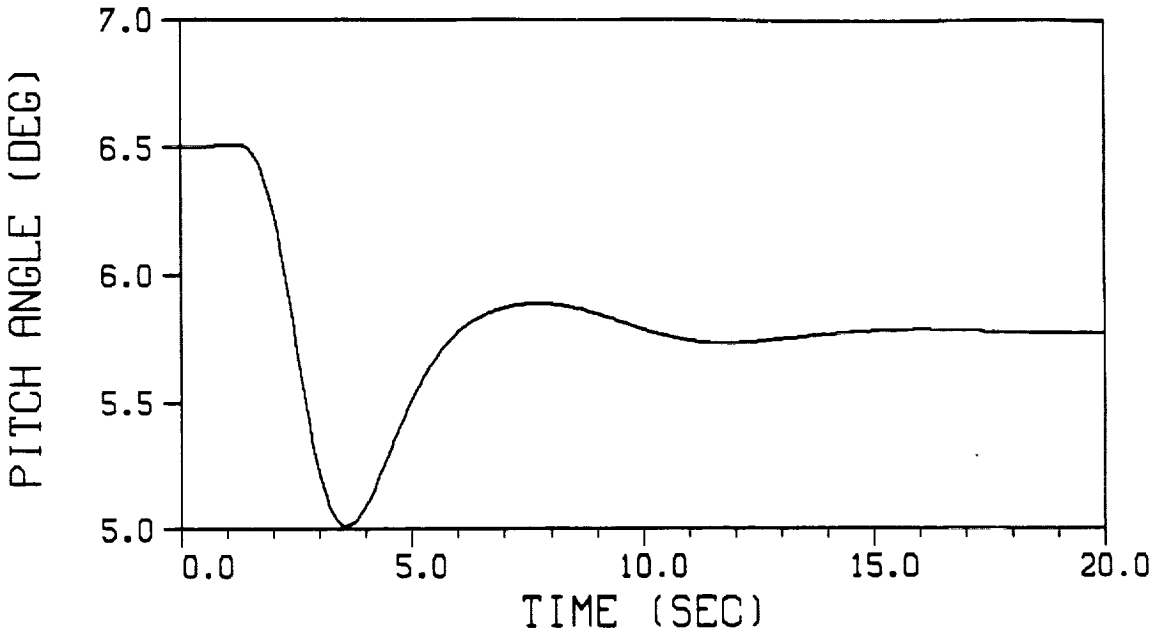

Plot V.A.3.-9. - Pitch angle response during a velocity translation maneuver by a multi-variable McRuer-Krendel pilot inserted in the Harrier AV-8B

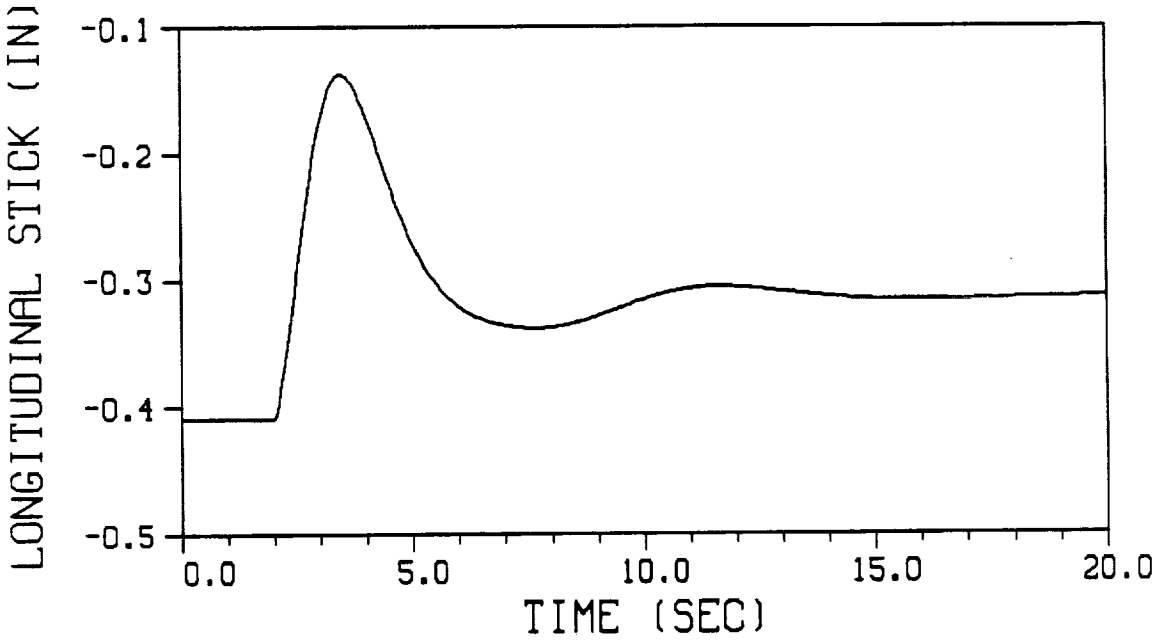

Plot V.A.3.-10. - Longitudinal stick response of a multi-variable McRuer-Krendel pilot during a velocity translation maneuver in the Harrier AV-8B

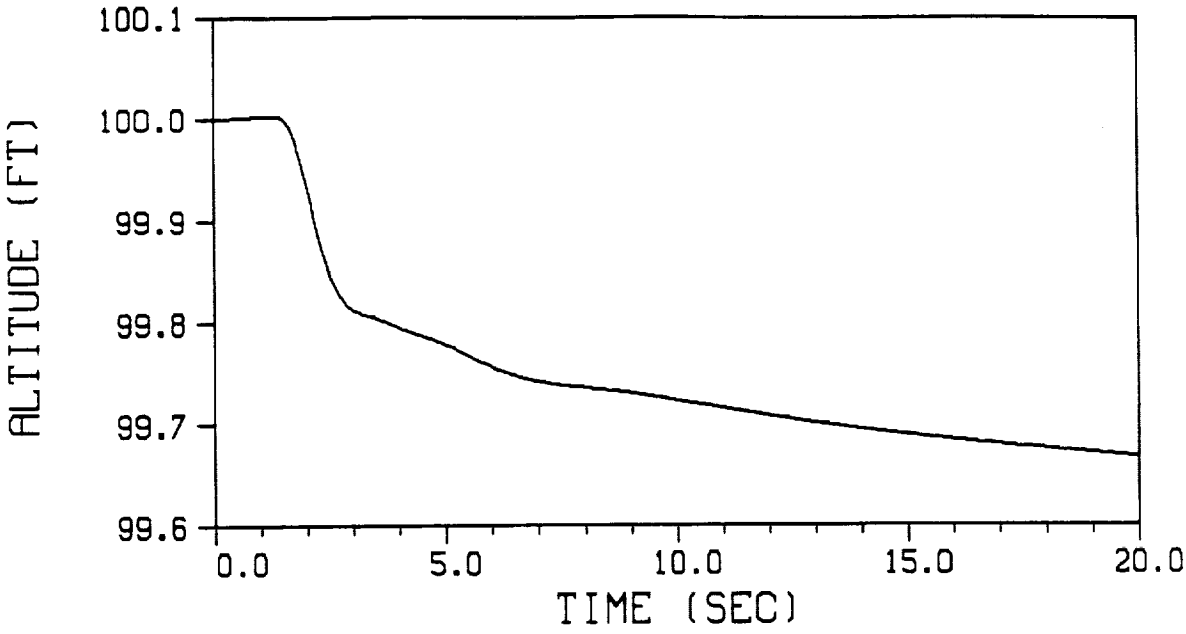

Plot V.A.3.-11. - Altitude response during a velocity translation maneuver by a multi-variable McRuer-Krendel pilot inserted in the Harrier AV-8B

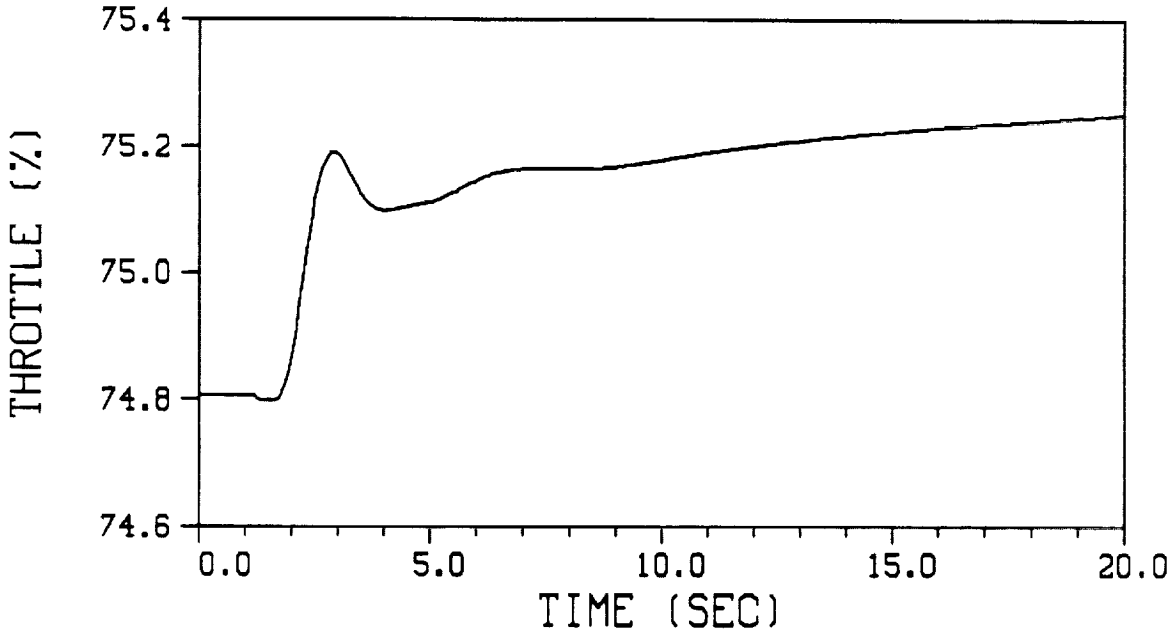

Plot V.A.3.-12. - Throttle response of a multi-variable McRuer-Krendel pilot during a velocity translation maneuver in the Harrier AV-8B

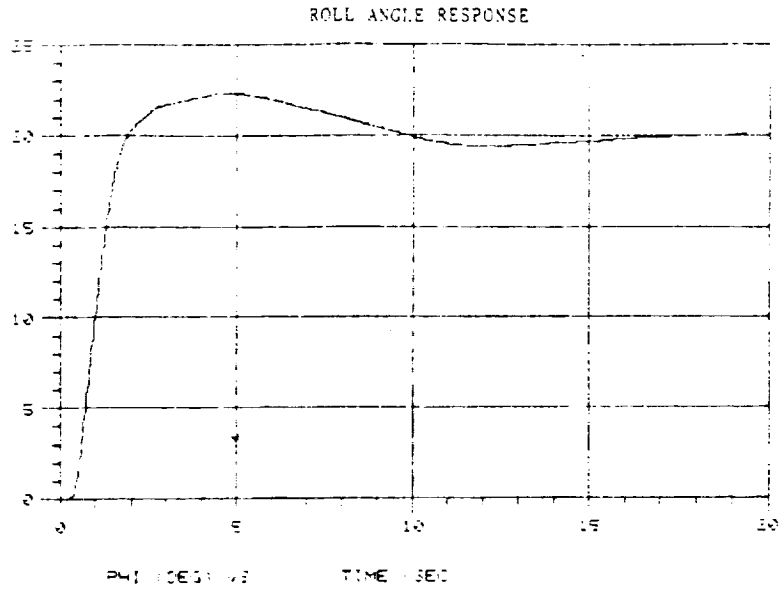

Plot V.A.3.-13. - Roll angle response during a coordinated turn maneuver by a multivariable McRuer-Krendel pilot inserted in the Black Hawk UH-60A

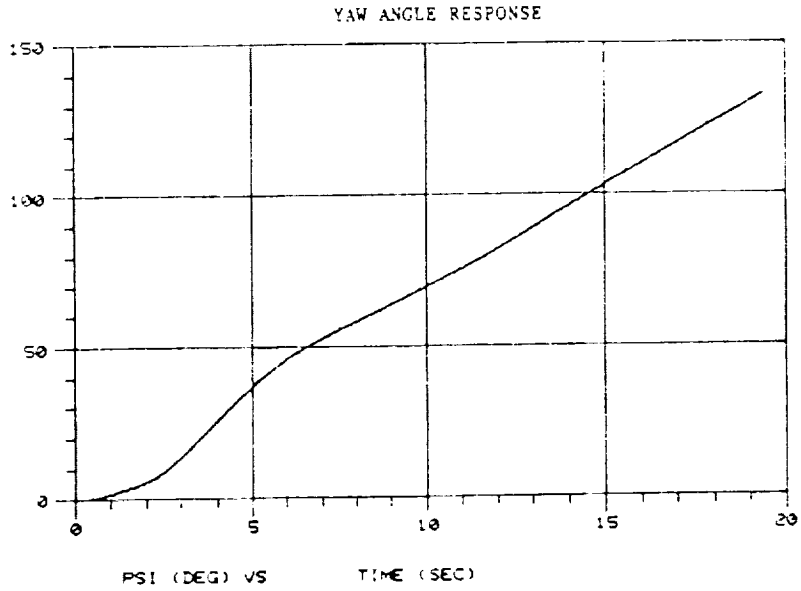

Plot V.A.3.-14. - Yaw angle response during a coordinated turn maneuver by a multivariable McRuer-Krendel pilot inserted in the Black Hawk UH-60A

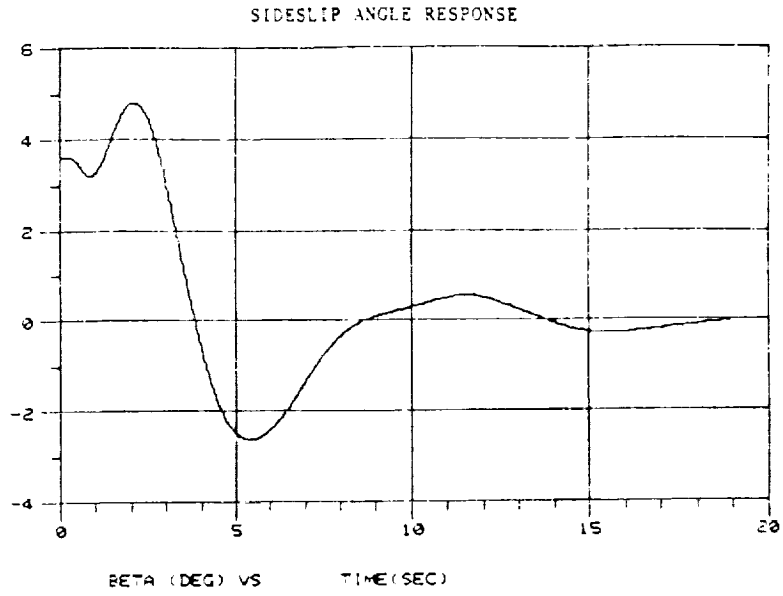

Plot V.A.3.-15. - Sideslip angle response during a coordinated turn maneuver by a multi-variable McRuer-Krendel pilot inserted in the Black Hawk UH-60A

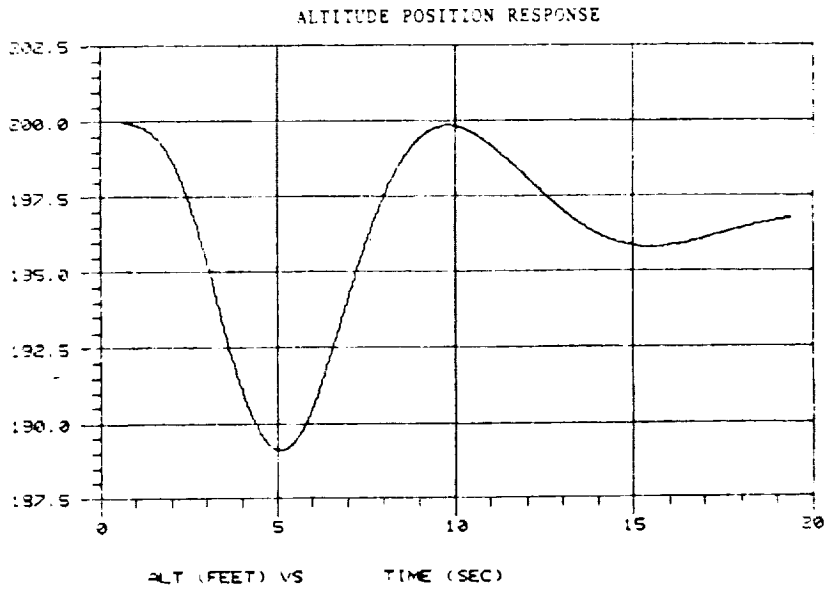

Plot V.A.3.-16. - Altitude response during a coordinated turn maneuver by a multi-variable McRuer-Krendel pilot inserted in the Black Hawk UH-60A

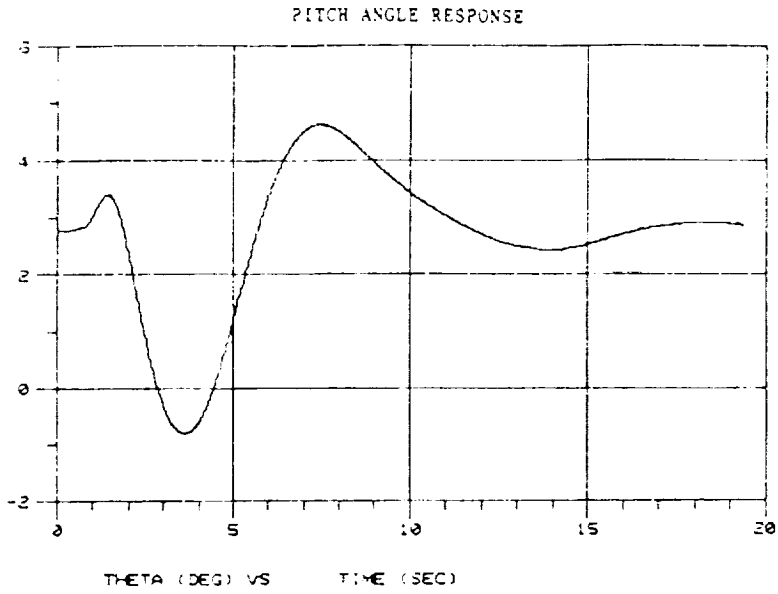

Plot V.A.3.-17. - Pitch angle response during a coordinated turn maneuver by a multi-variable McRuer-Krendel pilot inserted in the Black Hawk UH-60A

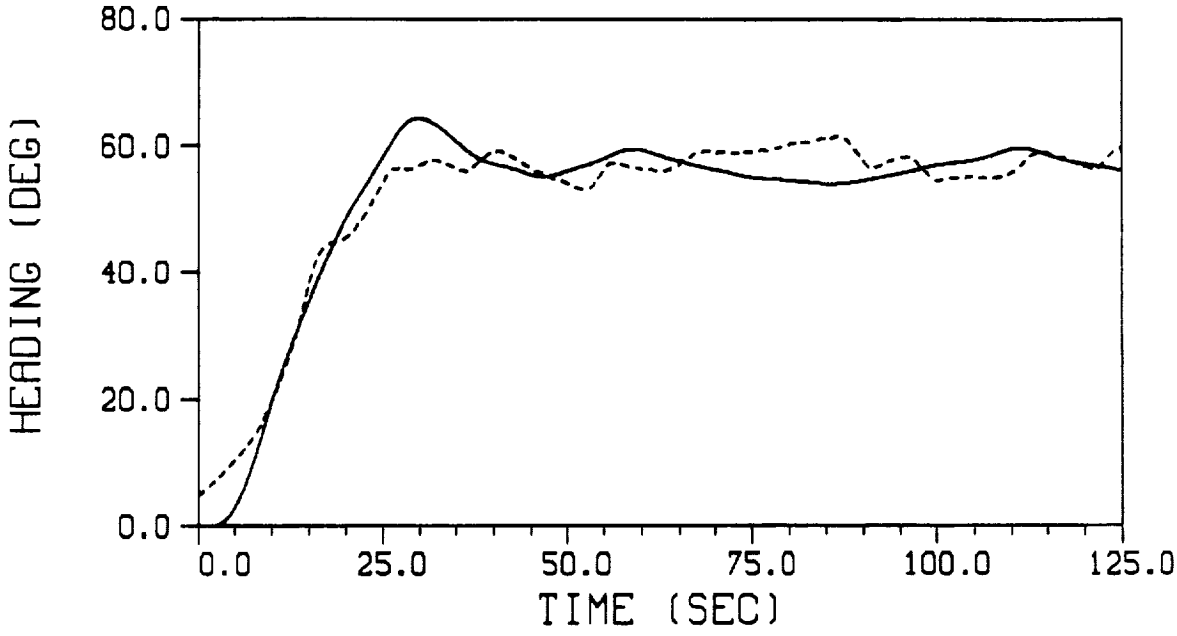

Plot V.B.4.-1. - Heading response comparison of the OCM pilot and piloted flight data during the vertical tracking maneuver.

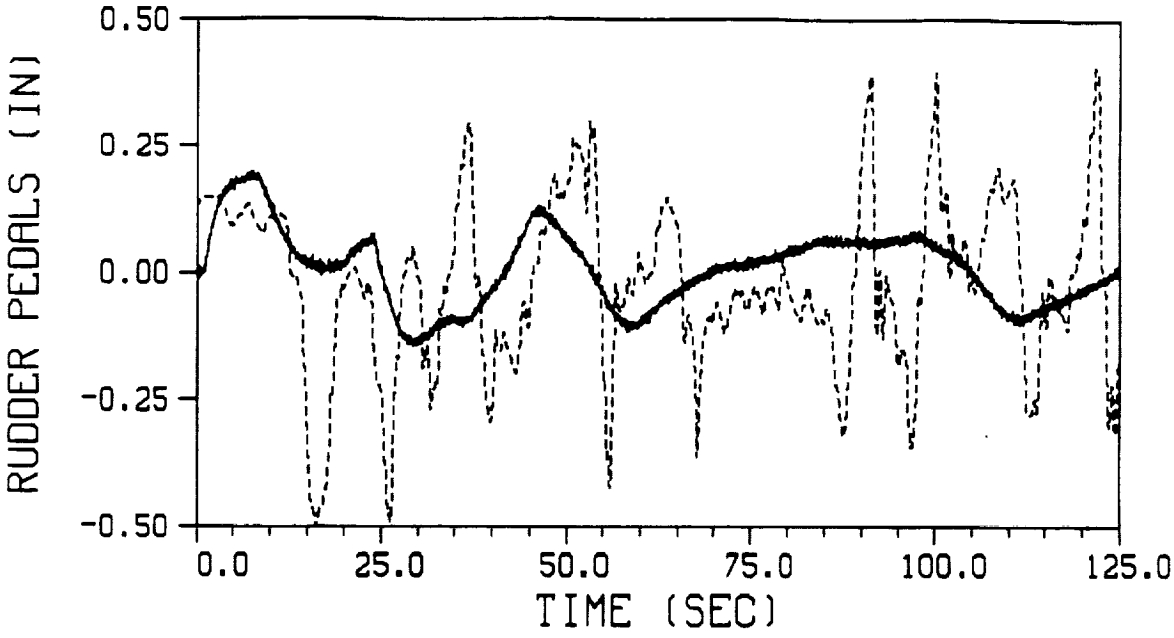

Plot V.B.4.-2. - Rudder pedal deflection response comparison of the OCM pilot and piloted flight data during the vertical tracking maneuver.

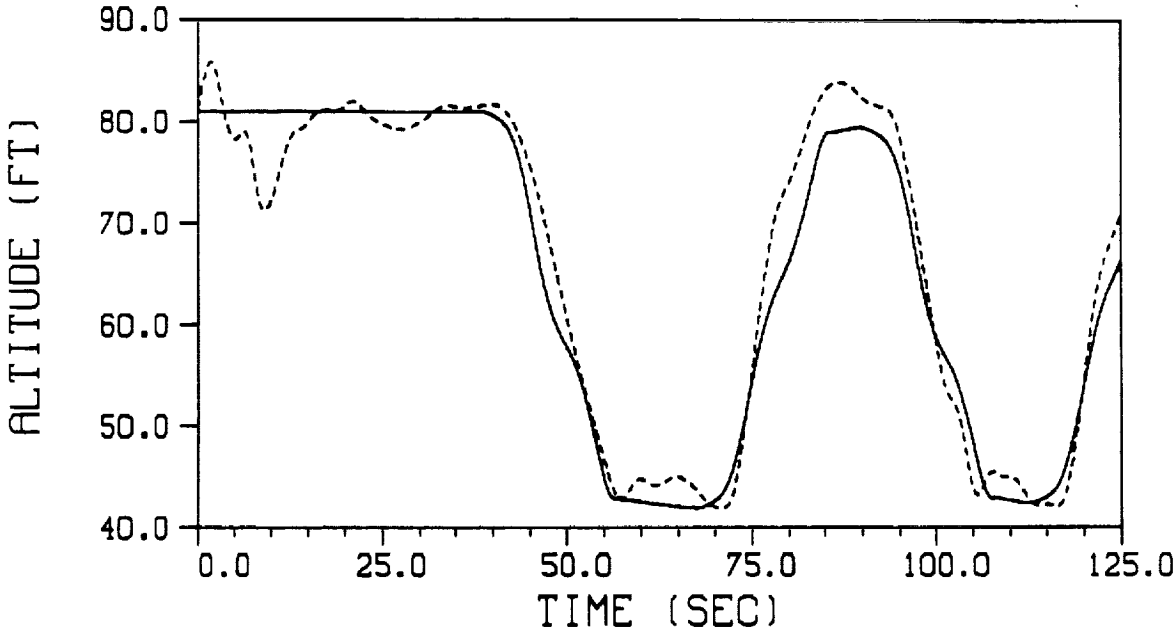

Plot V.B.4.-3. - Altitude response comparison of the OCM pilot and piloted flight data during the vertical tracking maneuver.

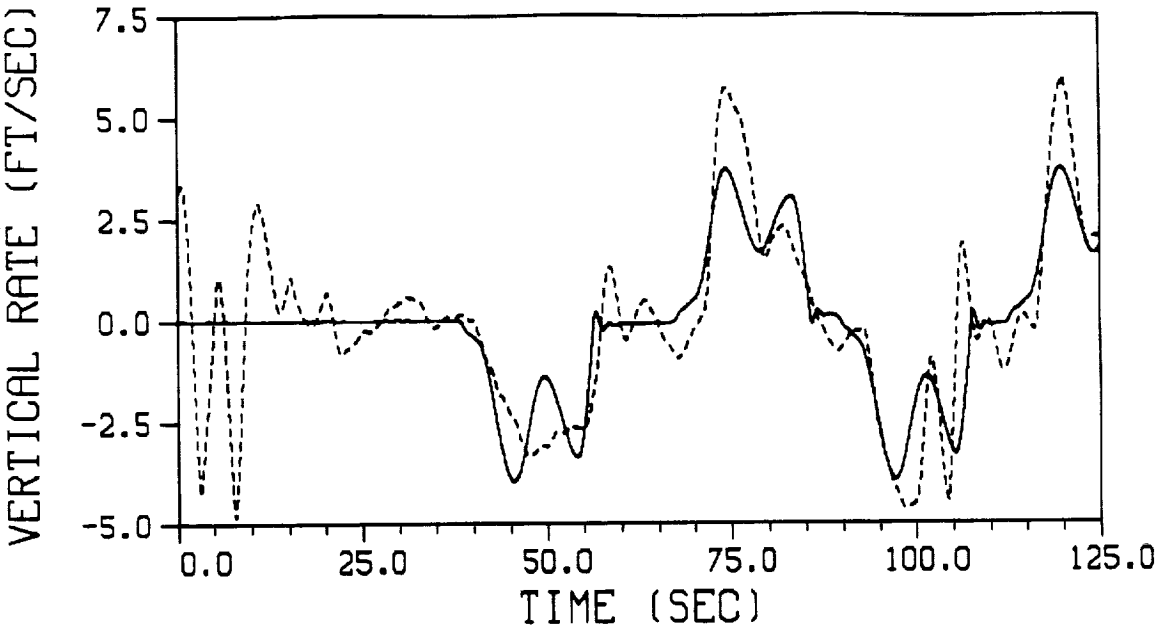

Plot V.B.4.-4. - Vertical rate response comparison of the OCM pilot and piloted flight data during the vertical tracking maneuver.

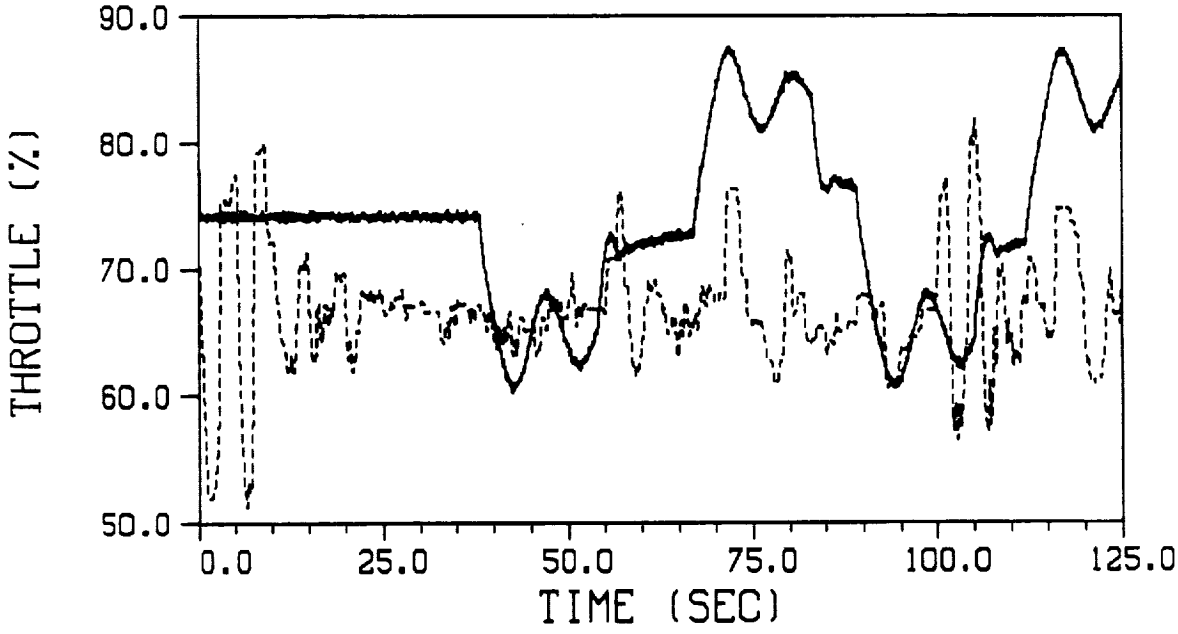

Plot V.B.4.-5. - Throttle deflection response comparison of the OCM pilot and piloted flight data during the vertical tracking maneuver.

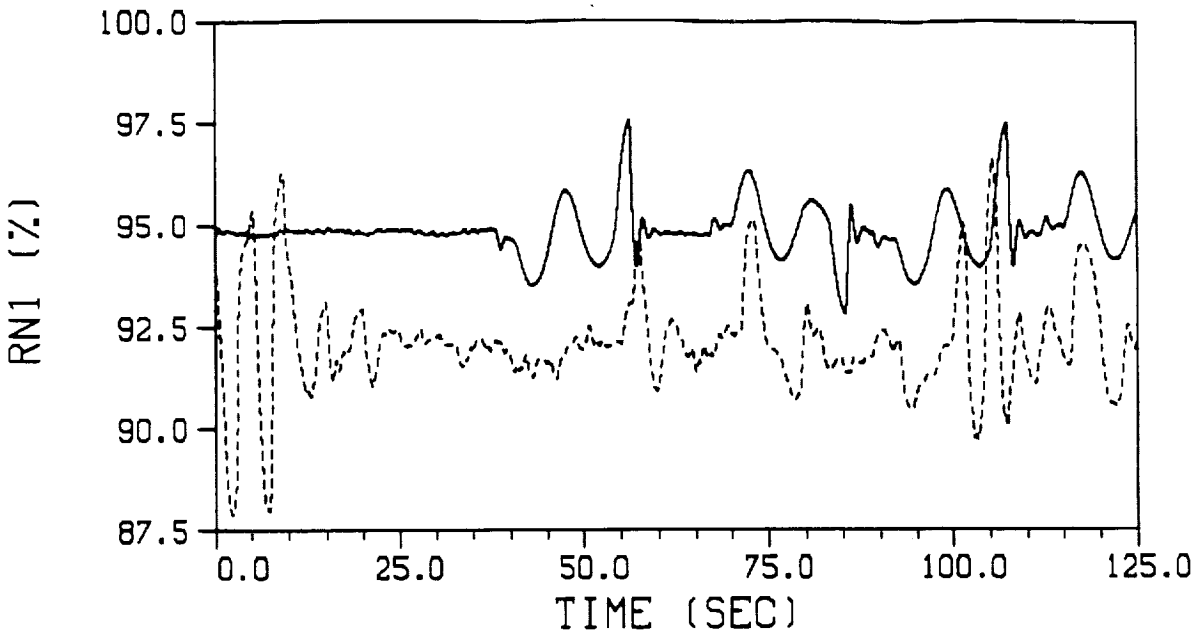

Plot V.B.4.-6. - Engine speed comparison of the OCM pilot and piloted flight data during the vertical tracking maneuver.

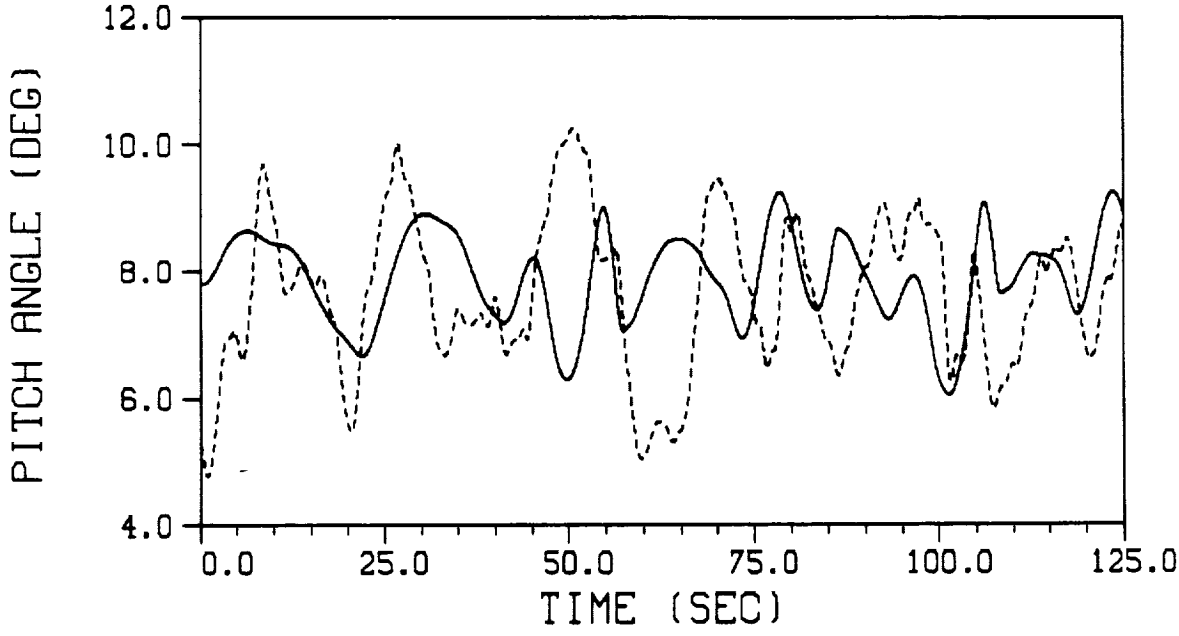

Plot V.B.4.-7. - Pitch angle response comparison of the OCM pilot and piloted flight data during the vertical tracking maneuver.

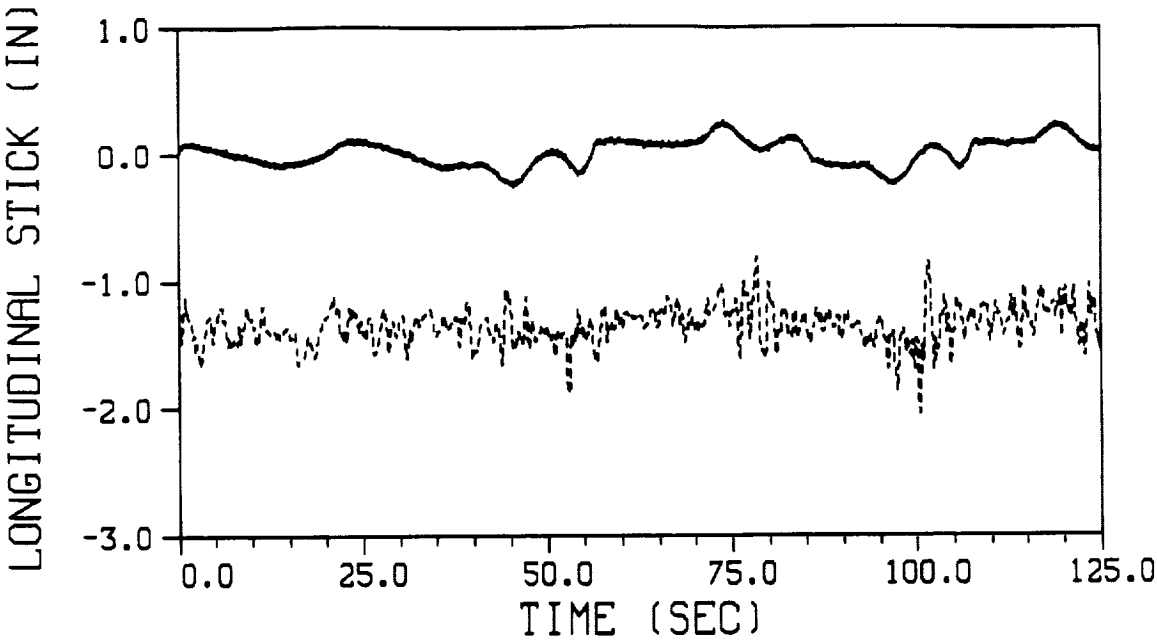

Plot V.B.4.-8. - Longitudinal stick operation comparison of the OCM pilot and piloted flight data during the vertical tracking maneuver.

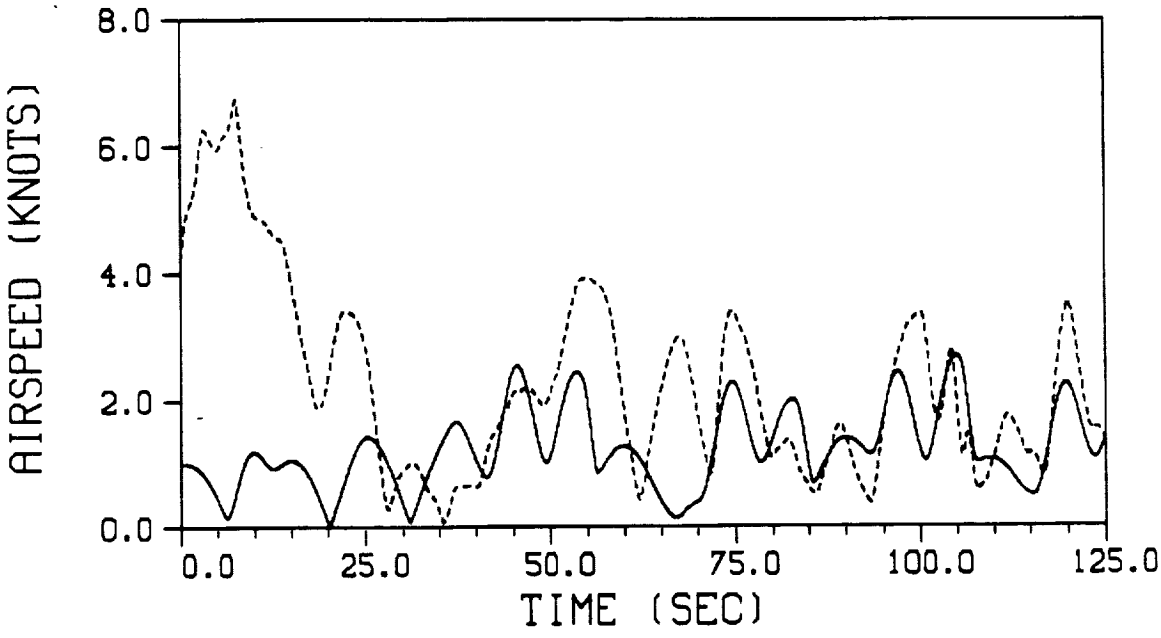

Plot V.B.4.-9. - Airspeed response comparison of the OCM pilot and piloted flight data during the vertical tracking maneuver.

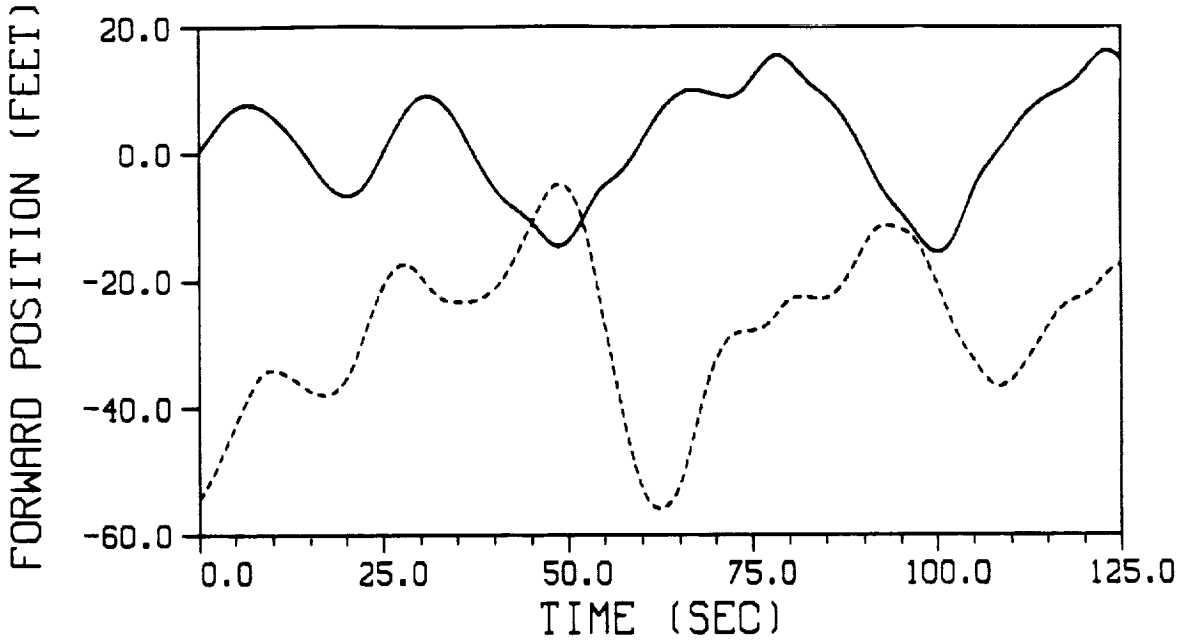

Plot V.B.4.-10. - Longitudinal position comparison of the OCM pilot and piloted flight data during the vertical tracking maneuver.

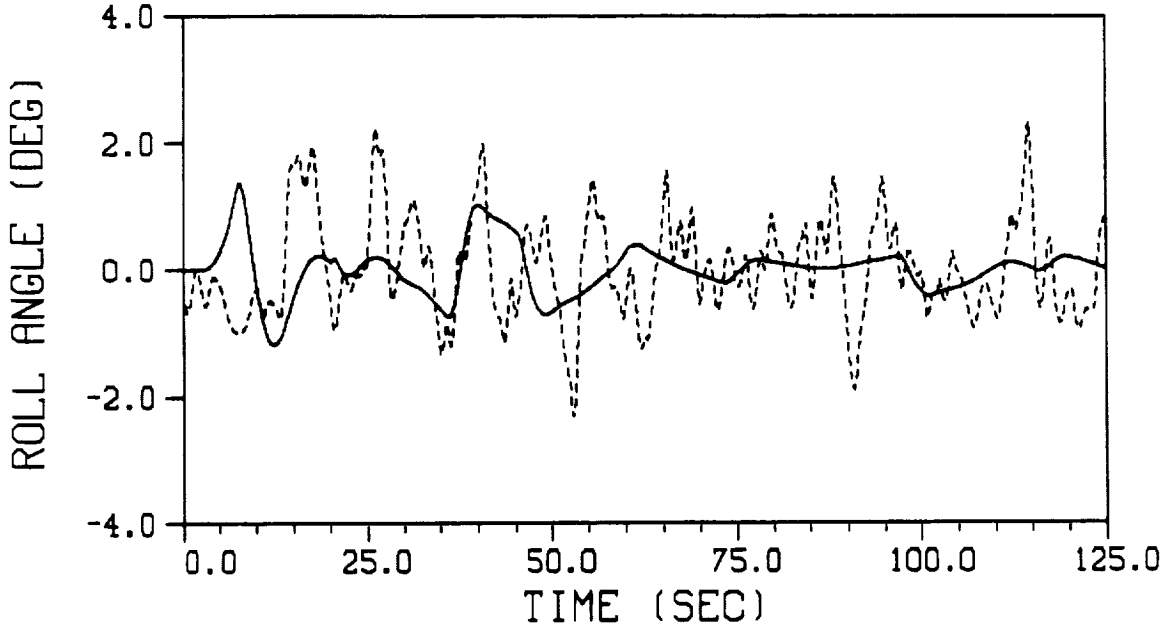

Plot V.B.4.-11. - Roll angle response comparison of the OCM pilot and piloted flight data during the vertical tracking maneuver.

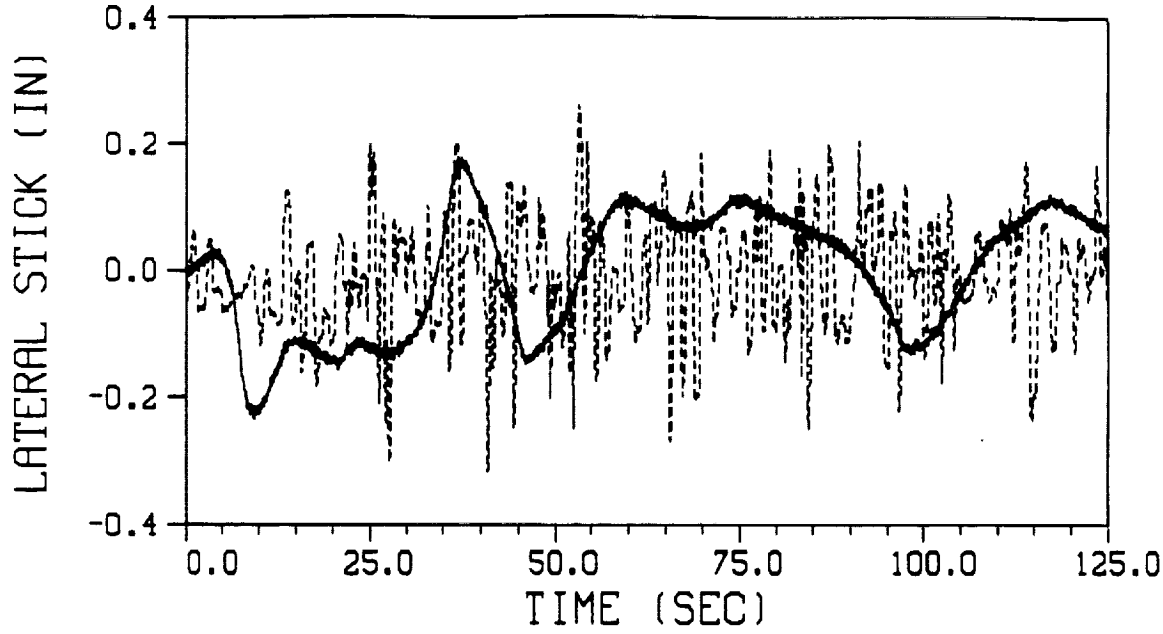

Plot V.B.4.-12. - Lateral stick operation comparison of the OCM pilot and piloted flight data during the vertical tracking maneuver.

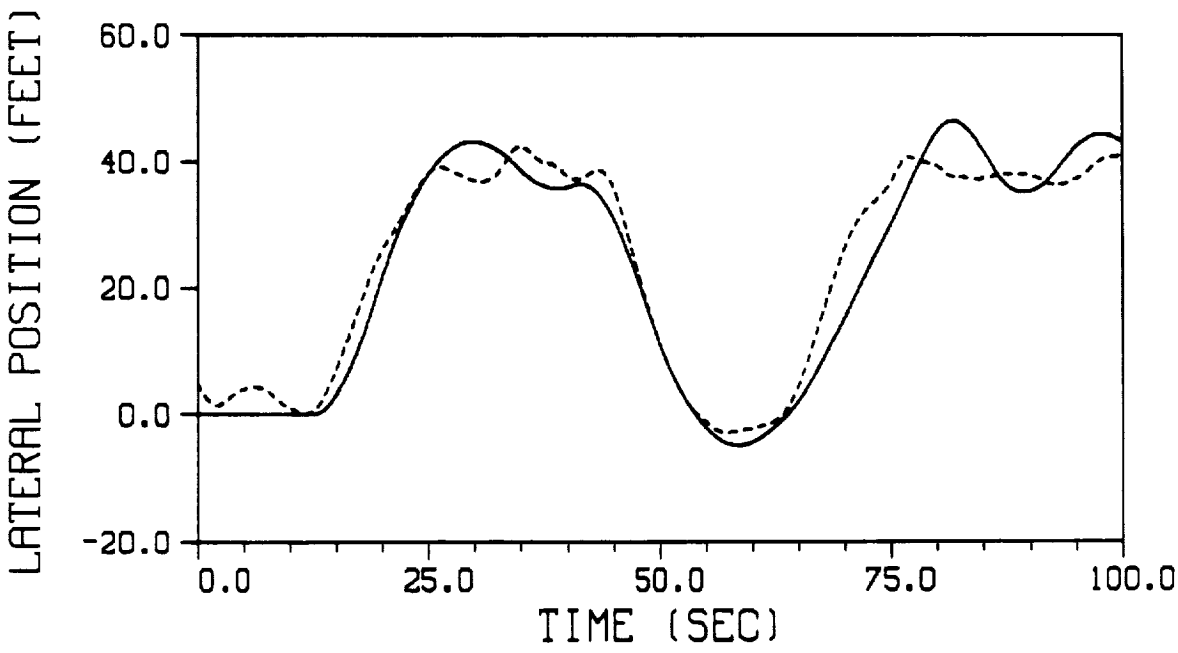

Plot V.B.4.-13. - Lateral position response comparison of the OCM pilot and piloted flight data during the lateral tracking maneuver.

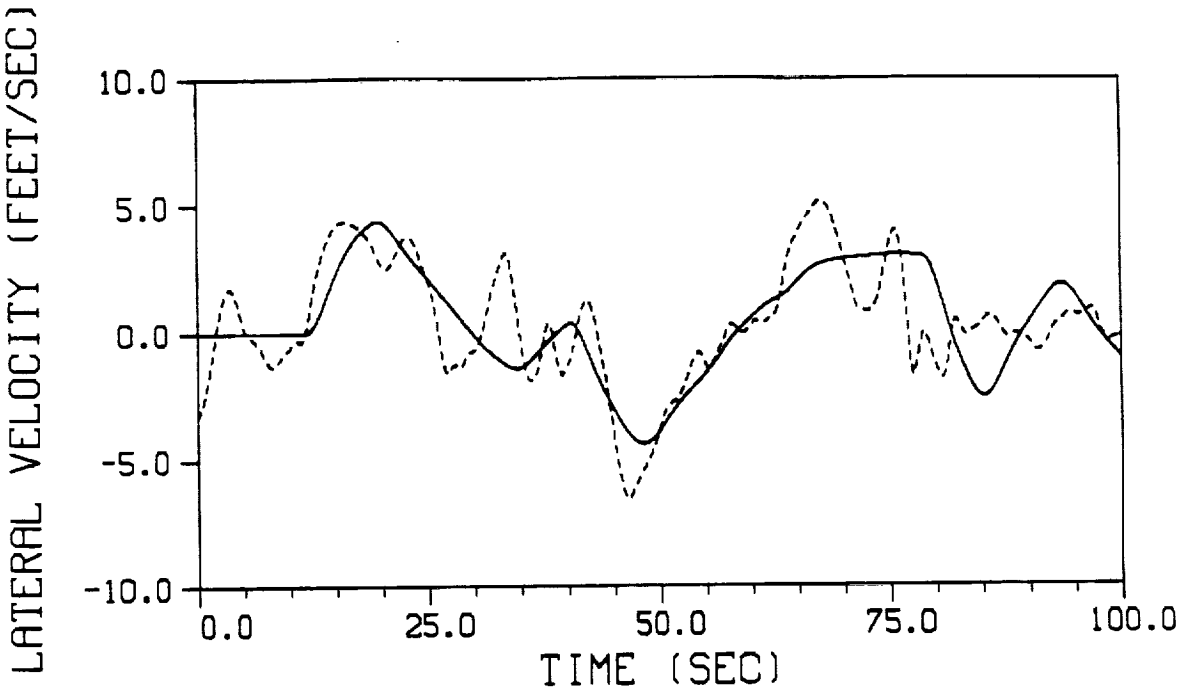

Plot V.B.4.-14. - Lateral velocity response comparison of the OCM pilot and piloted flight data during the lateral tracking maneuver.

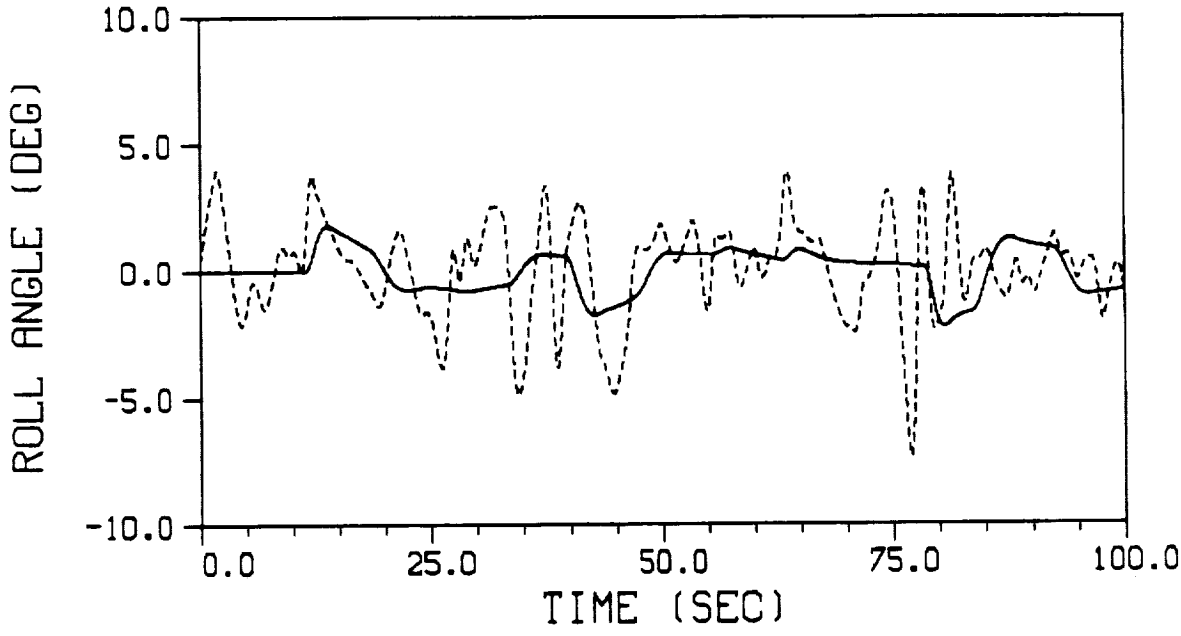

Plot V.B.4.-15. - Roll angle response comparison of the OCM pilot and piloted flight data during the lateral tracking maneuver.

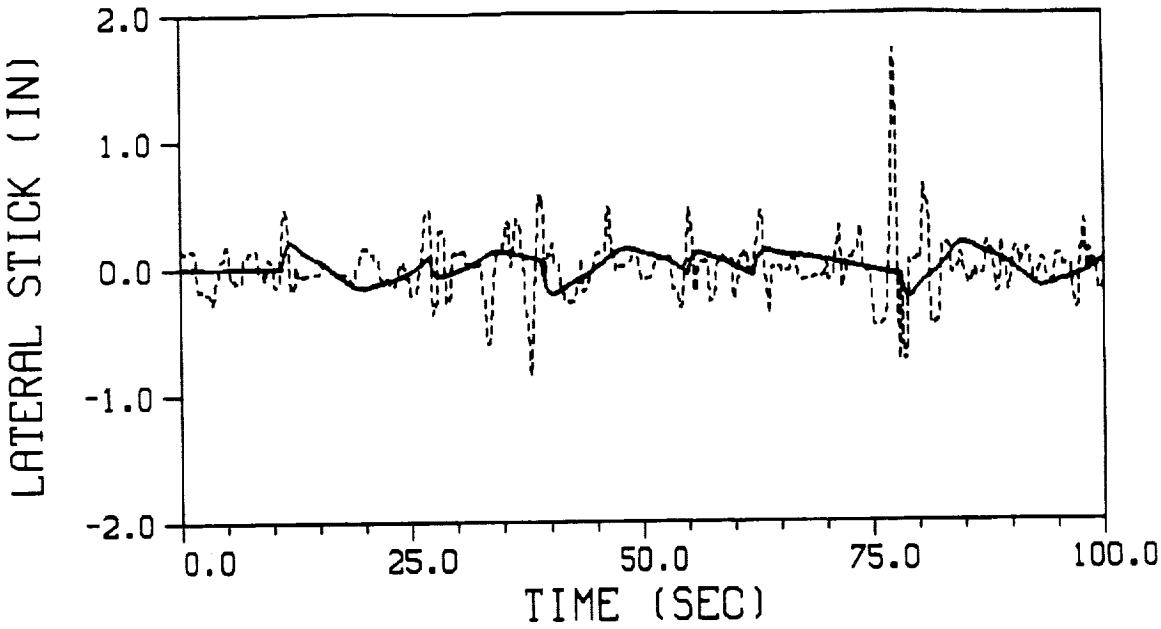

Plot V.B.4.-16. - Lateral stick operation comparison of the OCM pilot and piloted flight data during the lateral tracking maneuver.

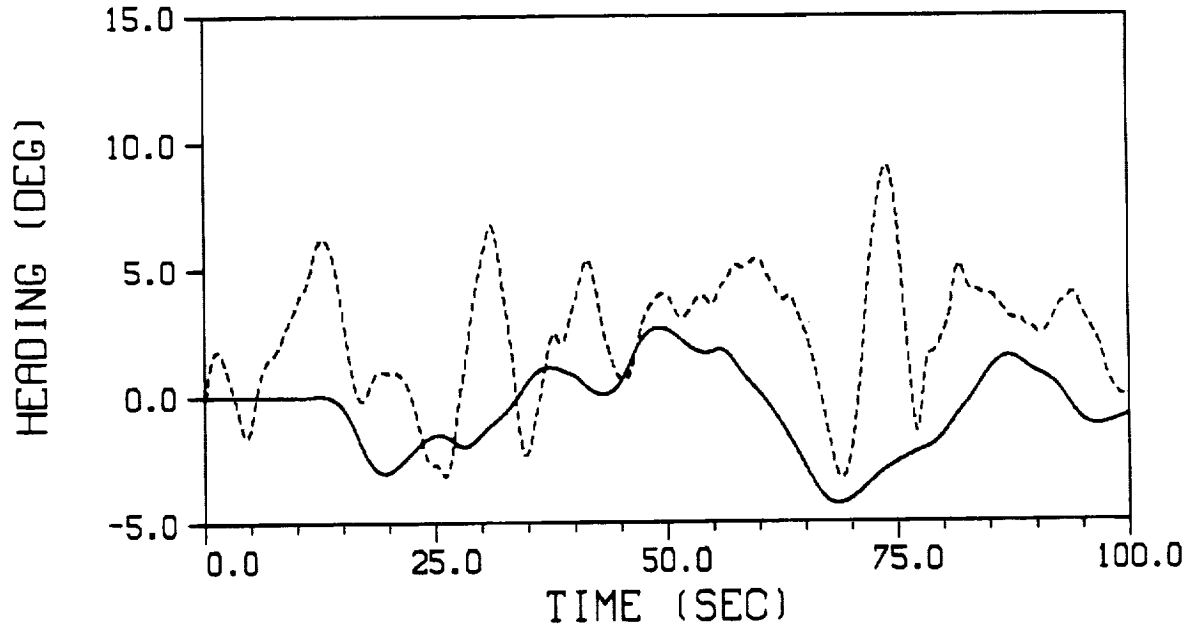

Plot V.B.4.-17. - Heading angle response comparison of the OCM pilot and piloted flight data during the lateral tracking maneuver.

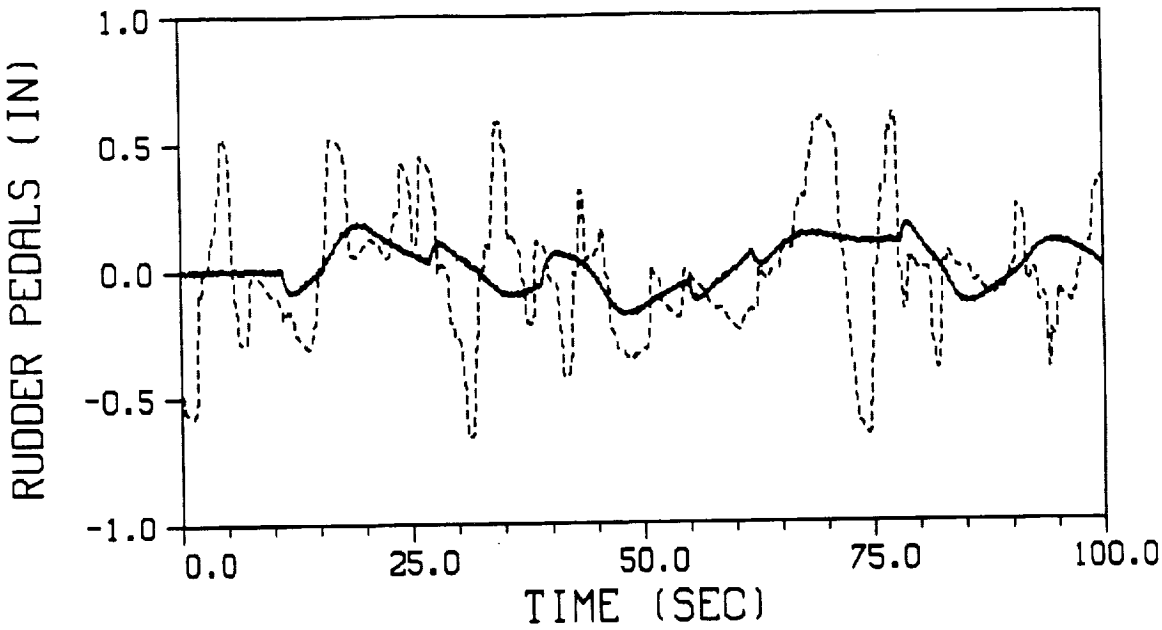

Plot V.B.4.-18. - Rudder pedal operation comparison of the OCM pilot and piloted flight data during the lateral tracking maneuver.

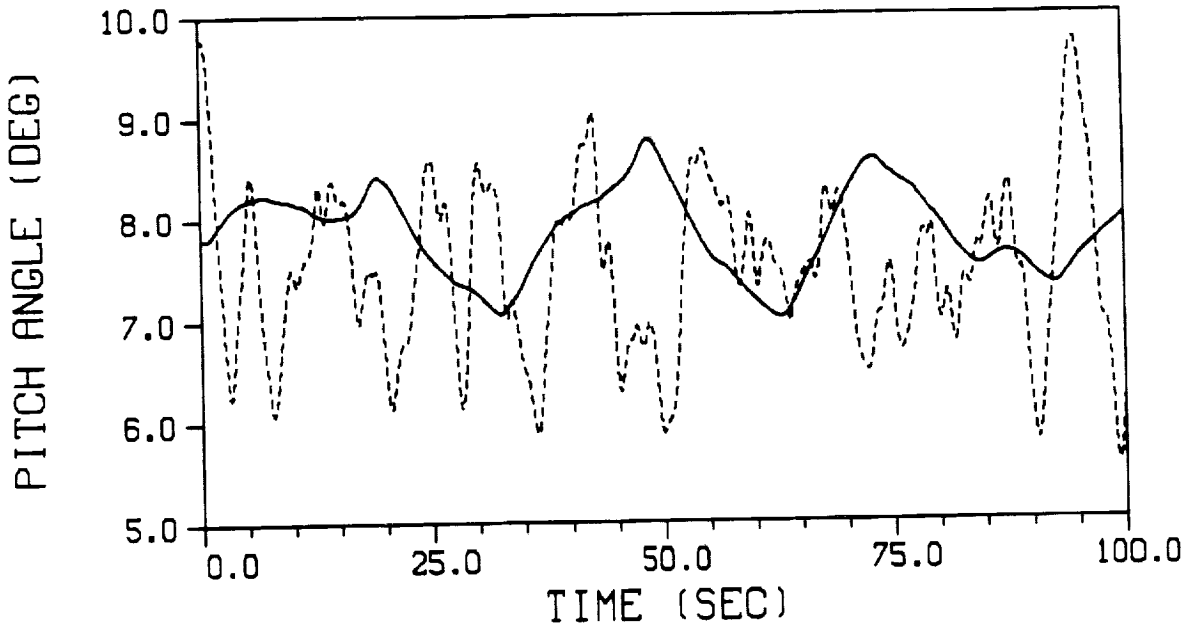

Plot V.B.4.-19. - Pitch angle response comparison of the OCM pilot and piloted flight data during the lateral tracking maneuver.

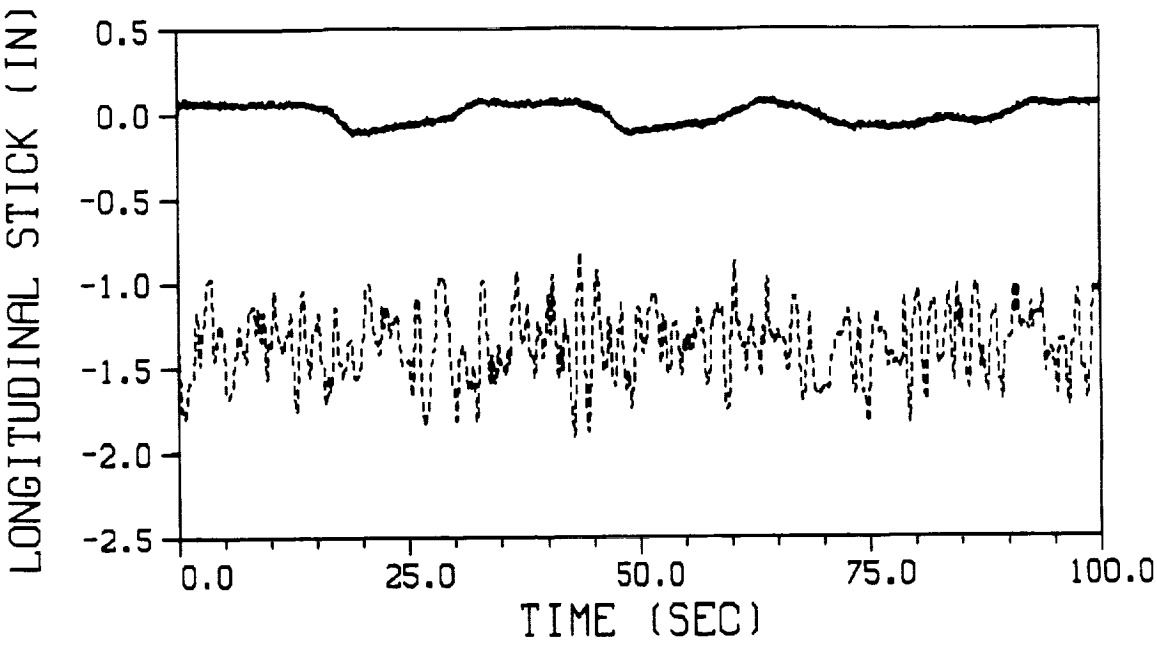

Plot V.B.4.-20. - Longitudinal stick operation comparison of the OCM pilot and piloted flight data during the lateral tracking maneuver.

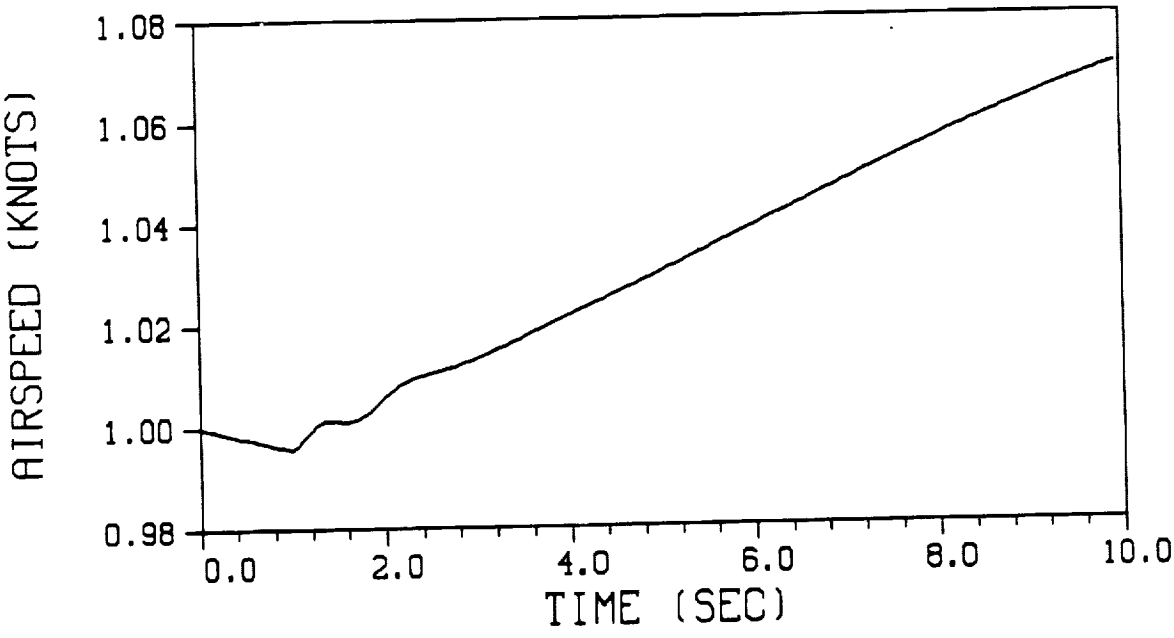

Plot B.1.-1. - Forward velocity response of the Harrier AV-8B due to a 10 percent positive impulse of the throttle.

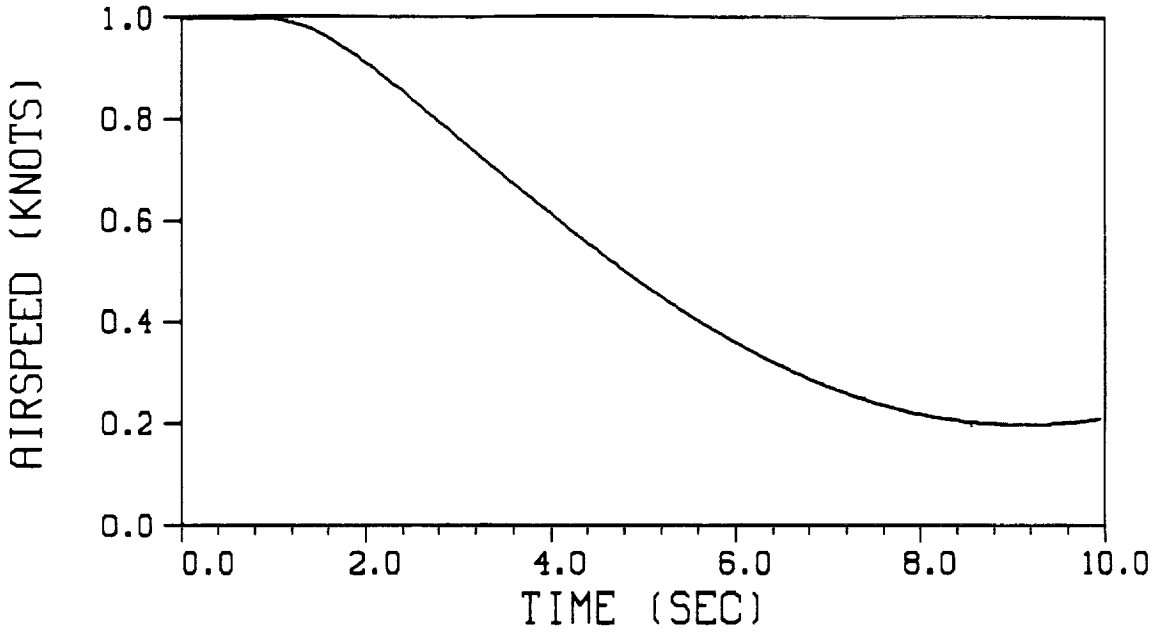

Plot B.1.-2. - Forward velocity response of the Harrier AV-8B due to a 1 inch impulse on the longitudinal stick while in a near hover.

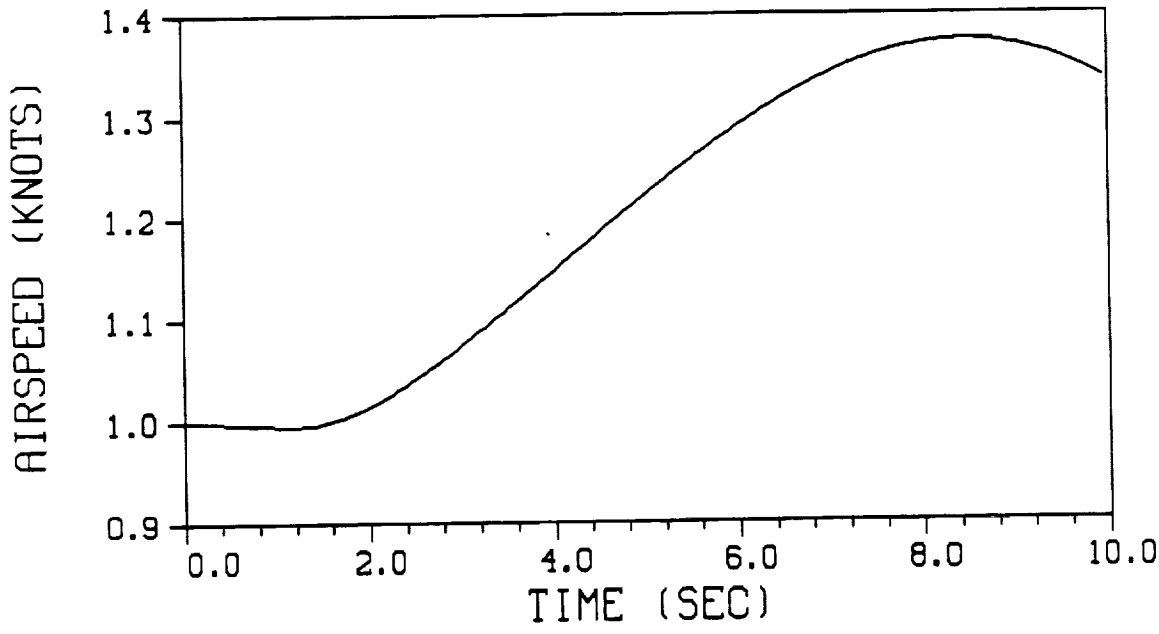

Plot B.1.-3. - Short period response of the Harrier AV-8B forward velocity due to an impulse of the lateral stick.

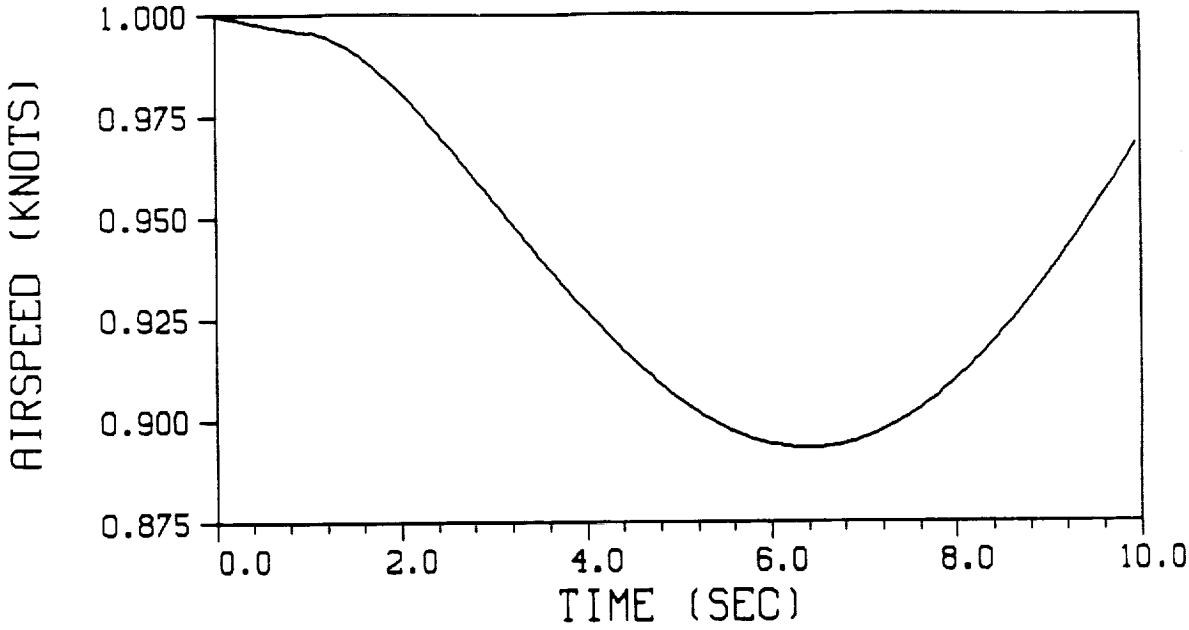

Plot B.1.-4. - Short period response of the Harrier AV-8B forward velocity due to an impulse of the rudder pedals.

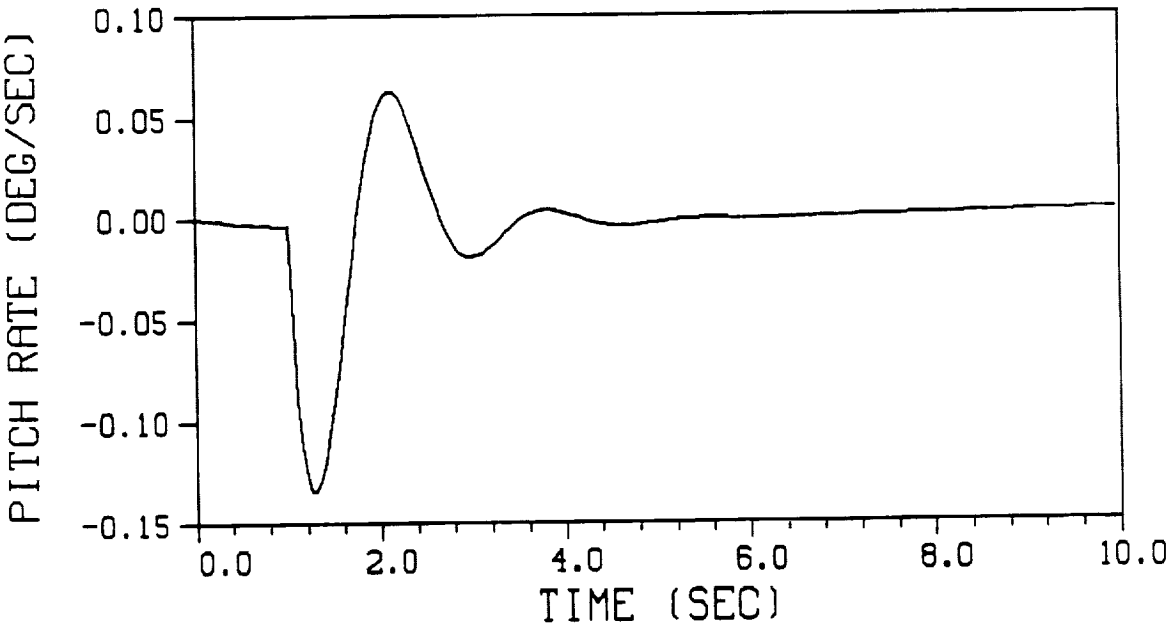

Plot B.1.-5. - Simulation model pitch rate response of the Harrier AV-8B due to a 10 percent impulse of the throttle.

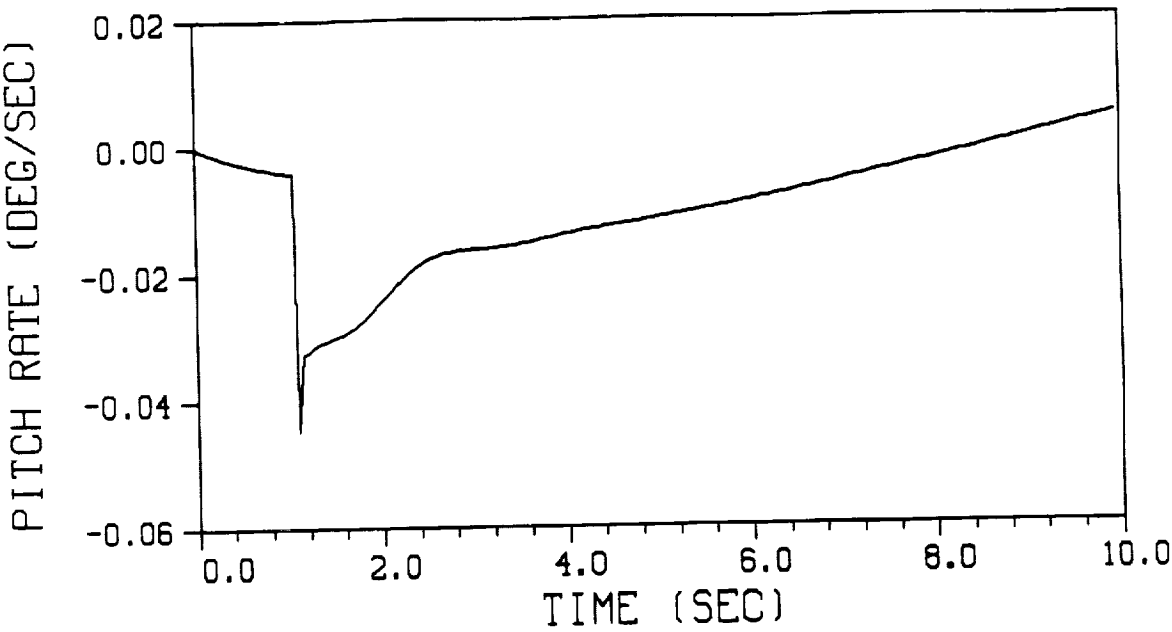

Plot B.1.-6. - Simulation model pitch rate response of the Harrier AV-8B due to a 5 degree impulse of the nozzle angle.

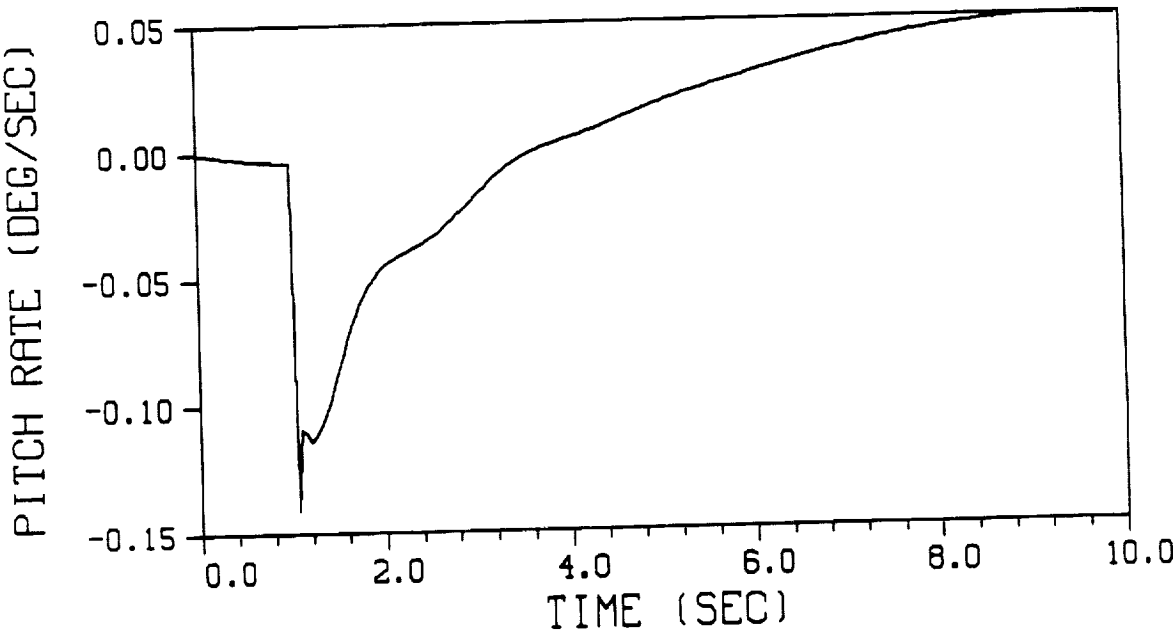

Plot B.1.-7. - Short period response of the Harrier AV-8B pitch rate due to an impulse of the lateral stick.

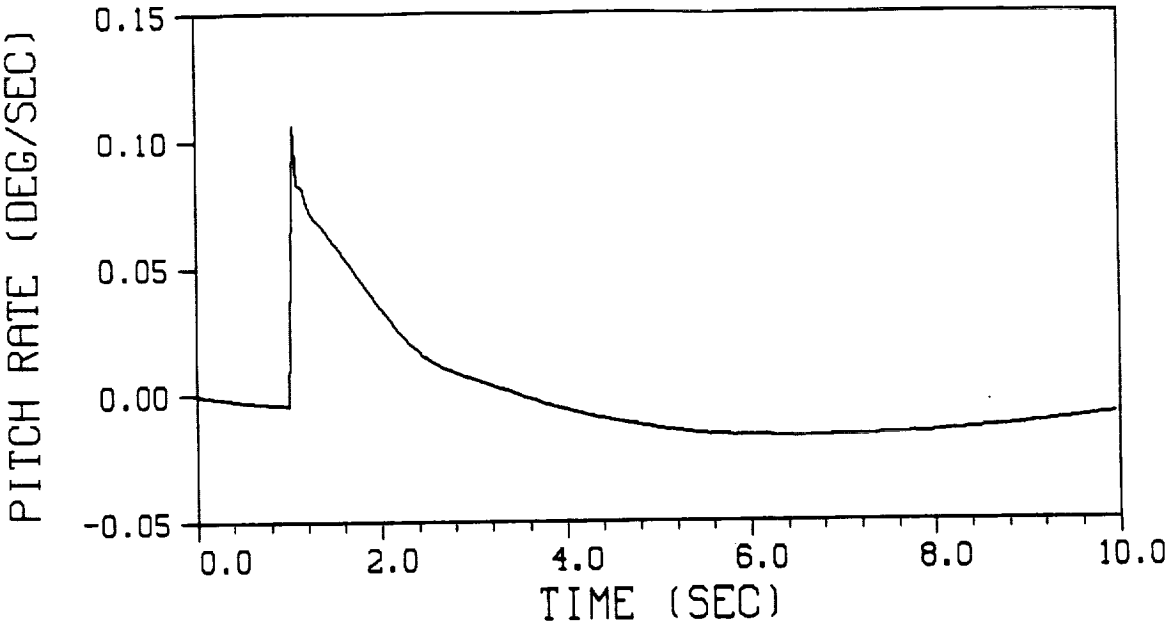

Plot B.1.-8. - Short period response of the Harrier AV-8B pitch rate due to an impulse of the rudder pedals.

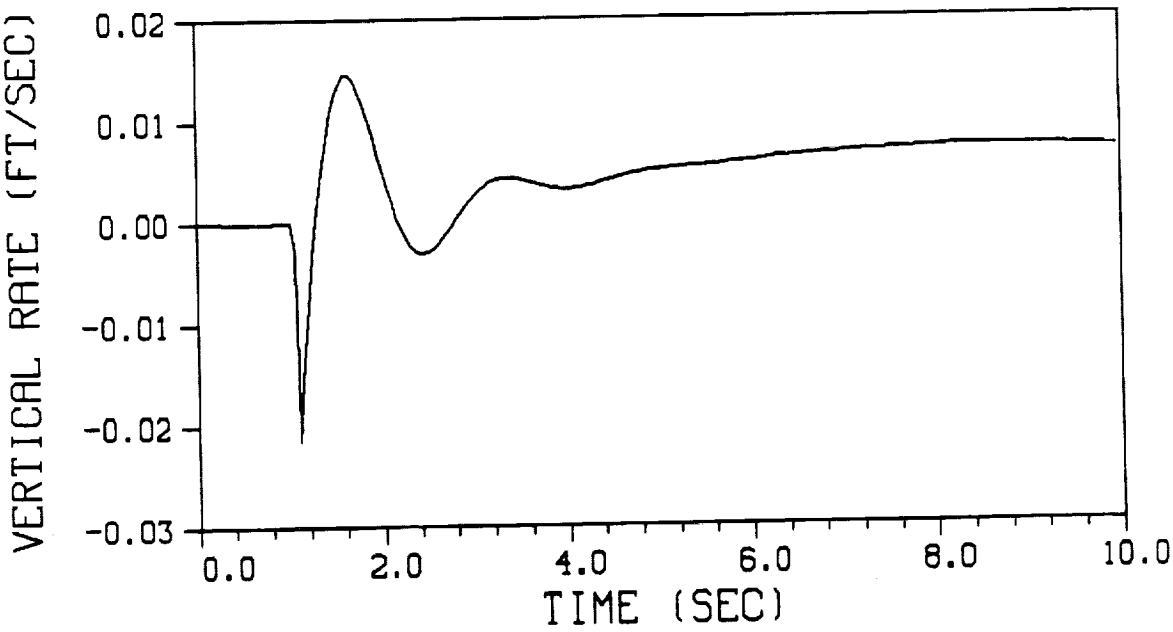

Plot B.1.-9. - Simulation model vertical rate response of the Harrier AV-8B due to a 1 inch impulse of the longitudinal stick.

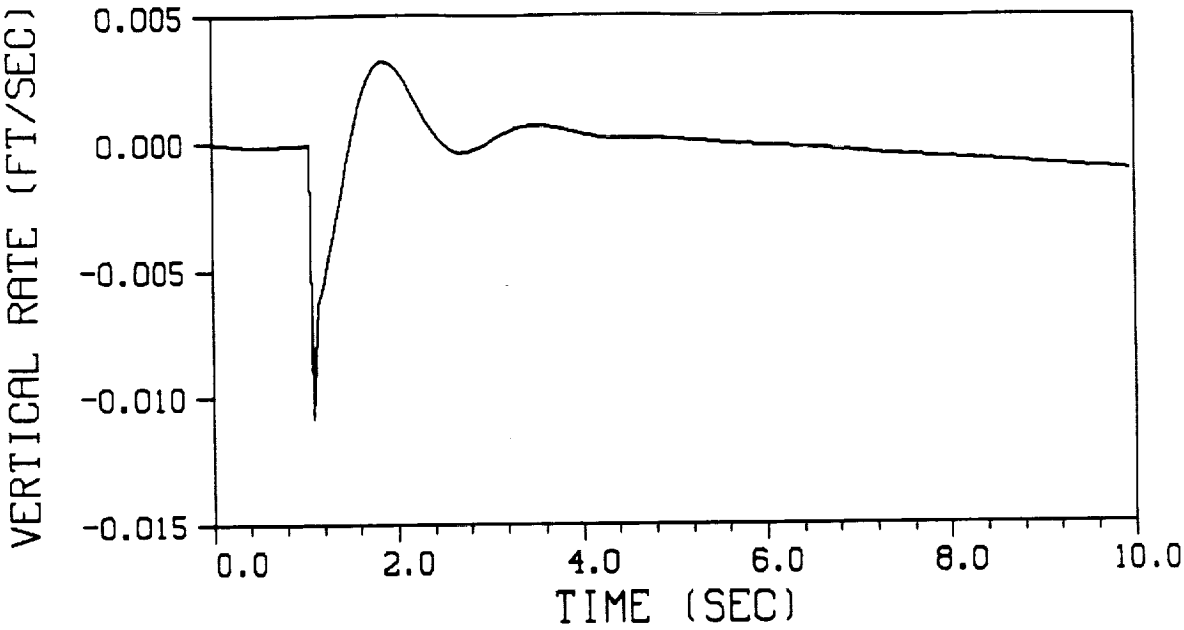

Plot B.1.-10. - Simulation model vertical rate response of the Harrier AV-8B due to a 5 degree impulse of the nozzle angle.

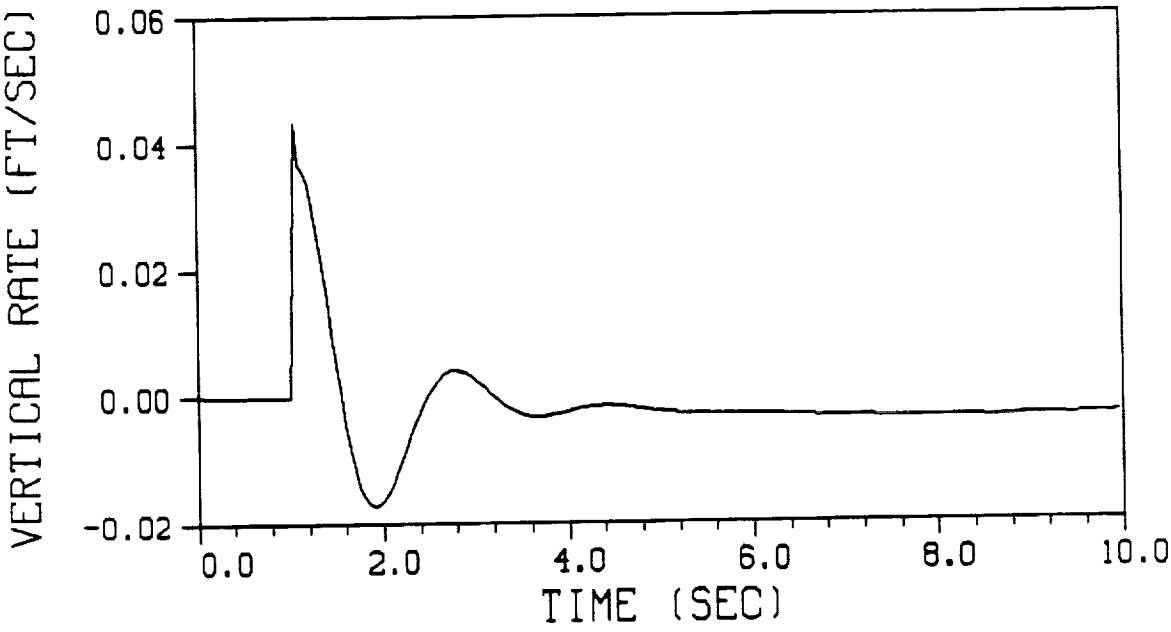

Plot B.1.-11. - Short period response of the Harrier AV-8B vertical rate due to an impulse of the lateral stick.

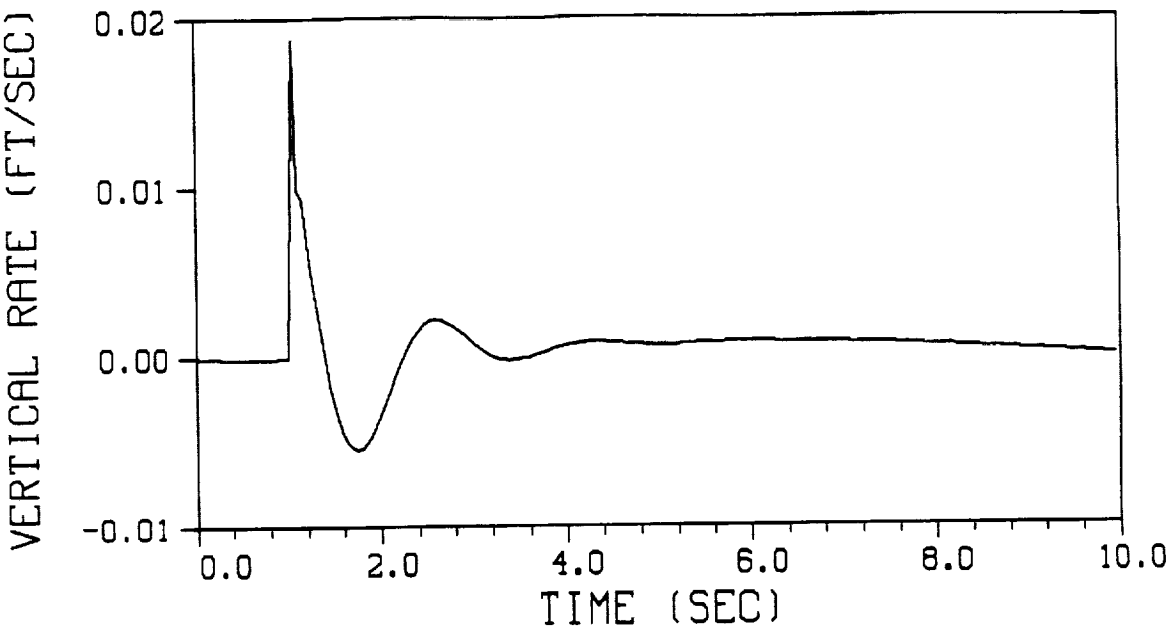

Plot B.1.-12. - Short period response of the Harrier AV-8B vertical rate due to an impulse of the rudder pedals.

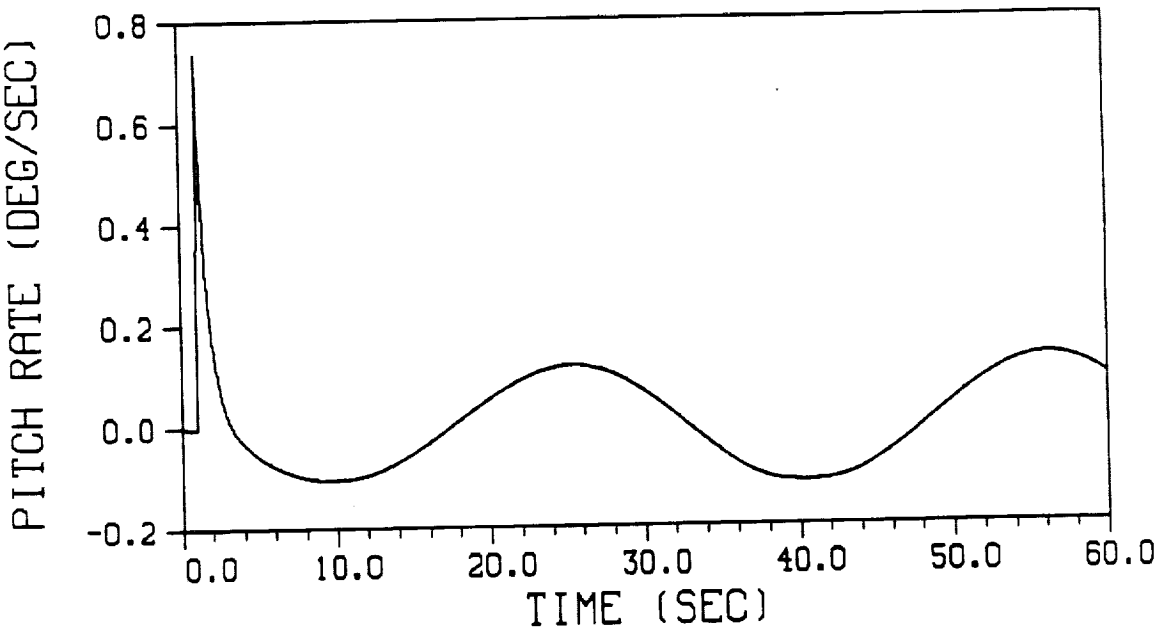

Plot B.1.-13. - Pitch rate response of the Harrier AV-8B due to an impulse of the longitudinal stick at a near hover.

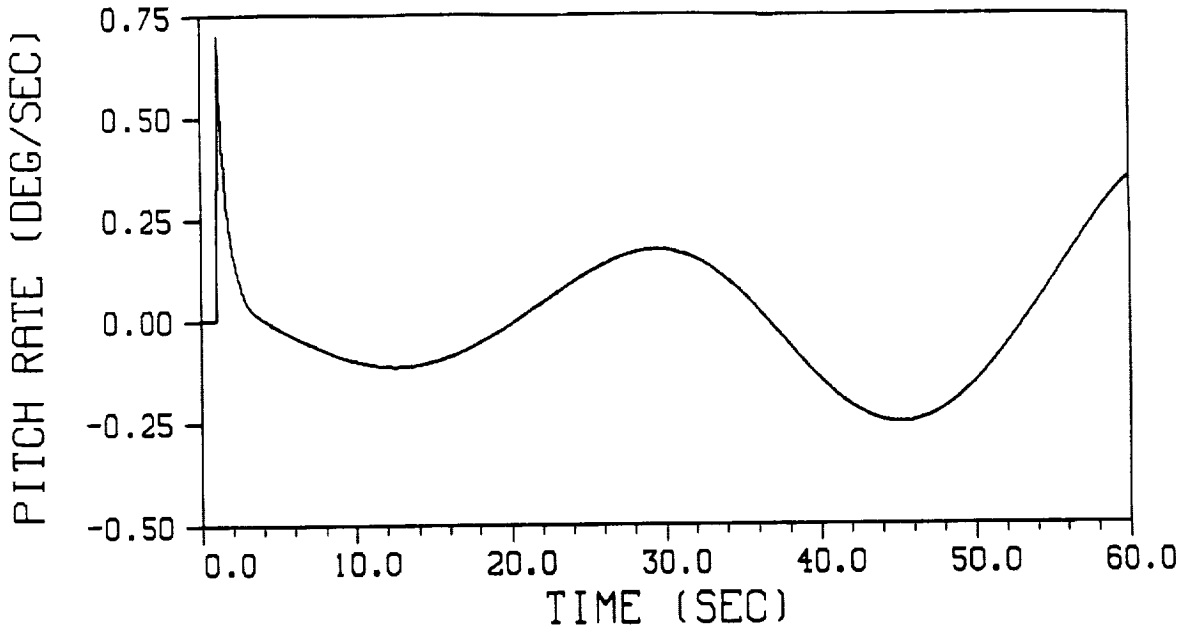

Plot B.1.-14. - Pitch rate response of the Harrier AV-8B due to an impulse of the longitudinal stick at 10 knots.

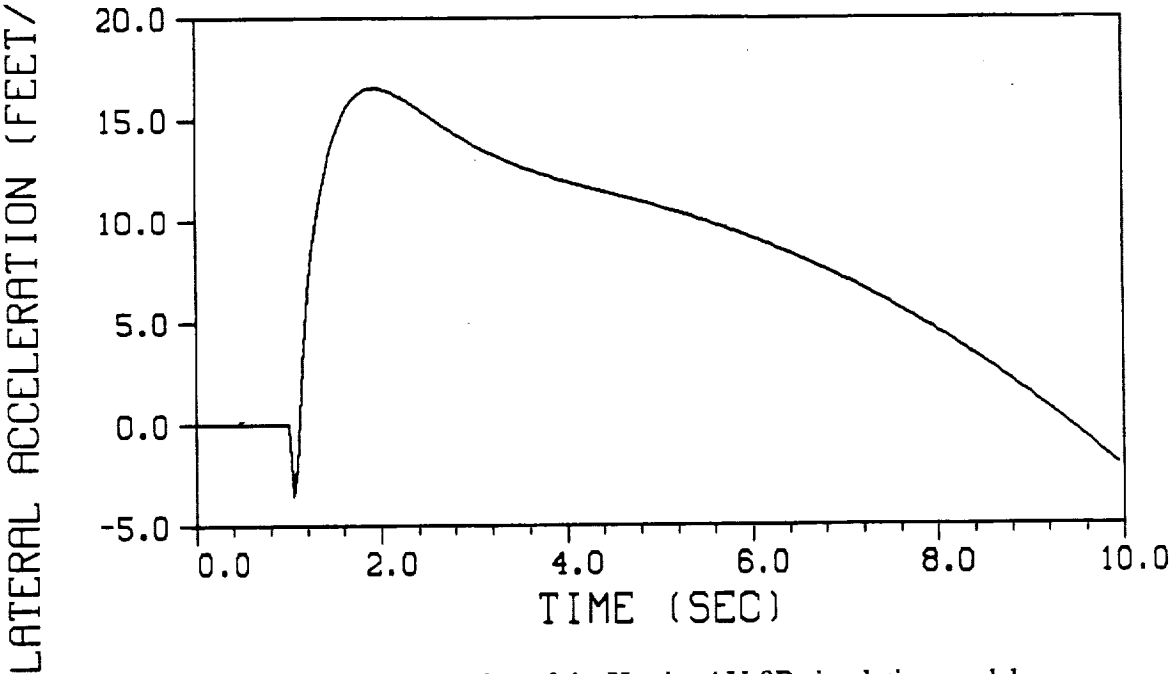

Plot B.1.-15. - Lateral acceleration of the Harrier AV-8B simulation model program due to the roll angle of Plot B.1.-16.

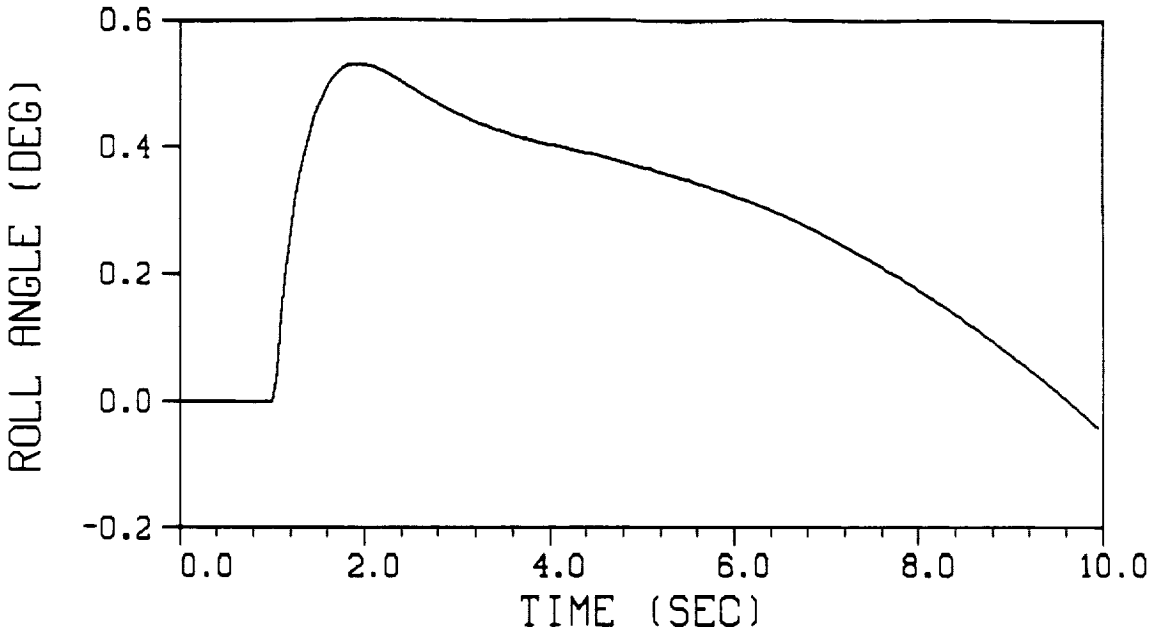

Plot B.1.-16. - Roll angle perturbation of the Harrier AV-8B due to an impulse of the lateral stick

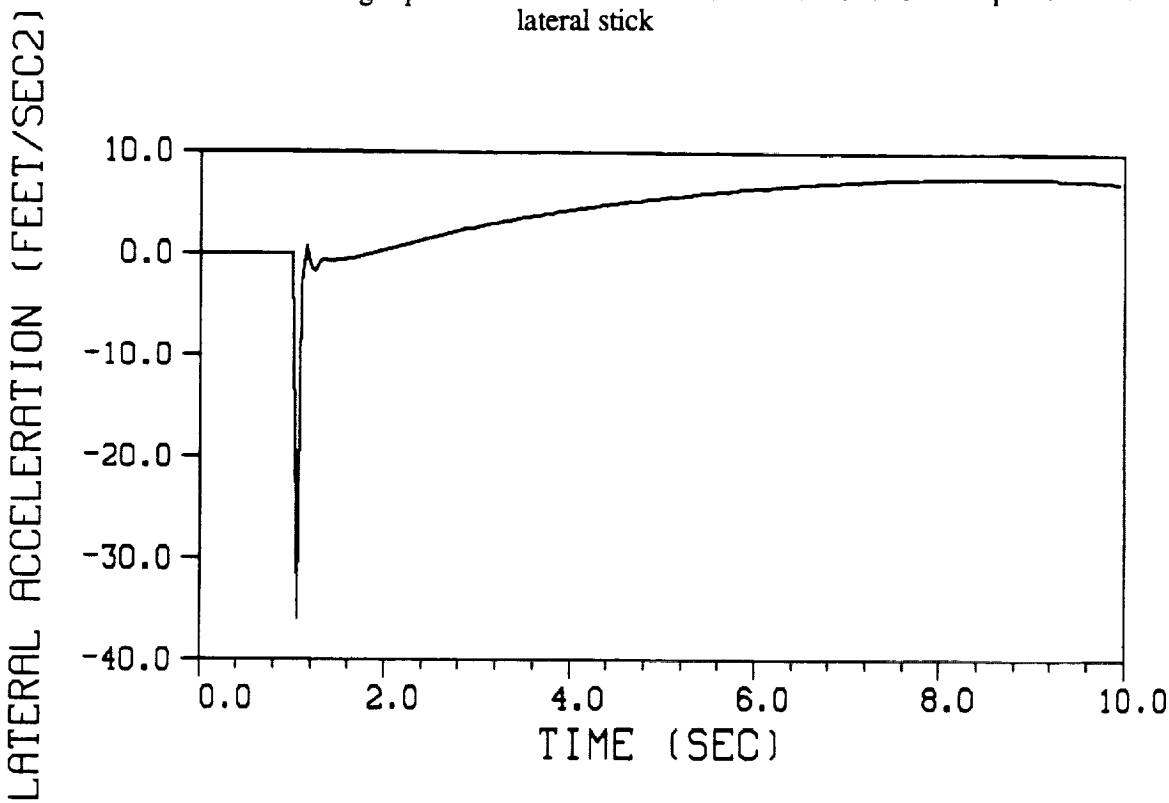

Plot B.1.-17. - Lateral acceleration of the Harrier AV-8B due to an impulse of the rudder pedals.

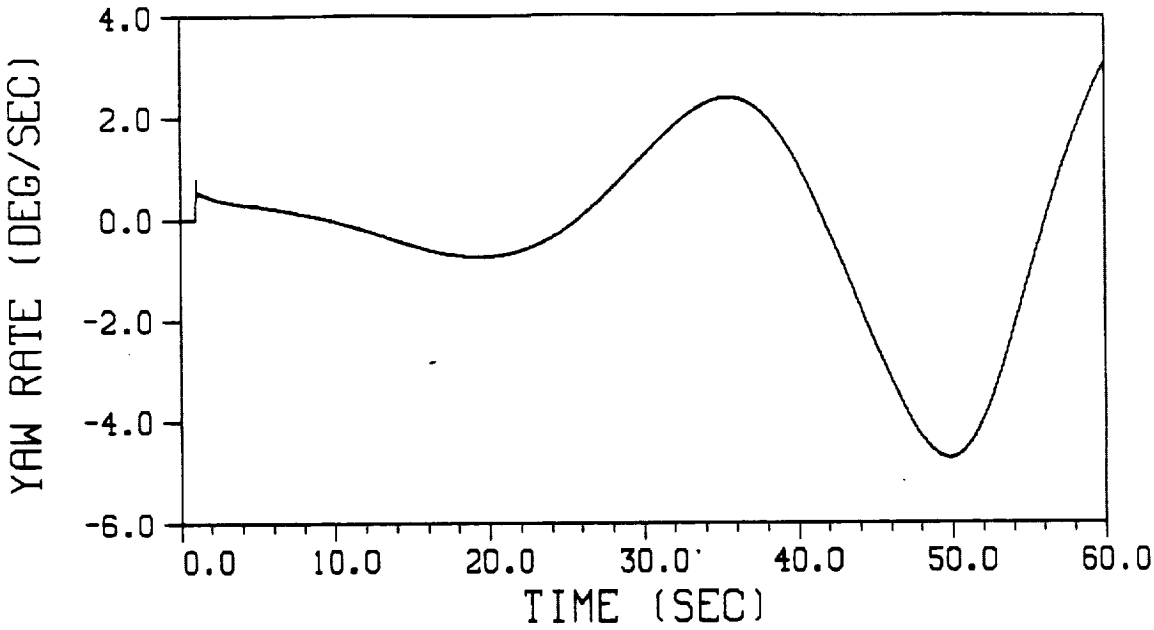

Plot B.1.-18. - Yaw rate response of the Harrier AV-8B due to an impulse of the rudder pedals.in a near hover.

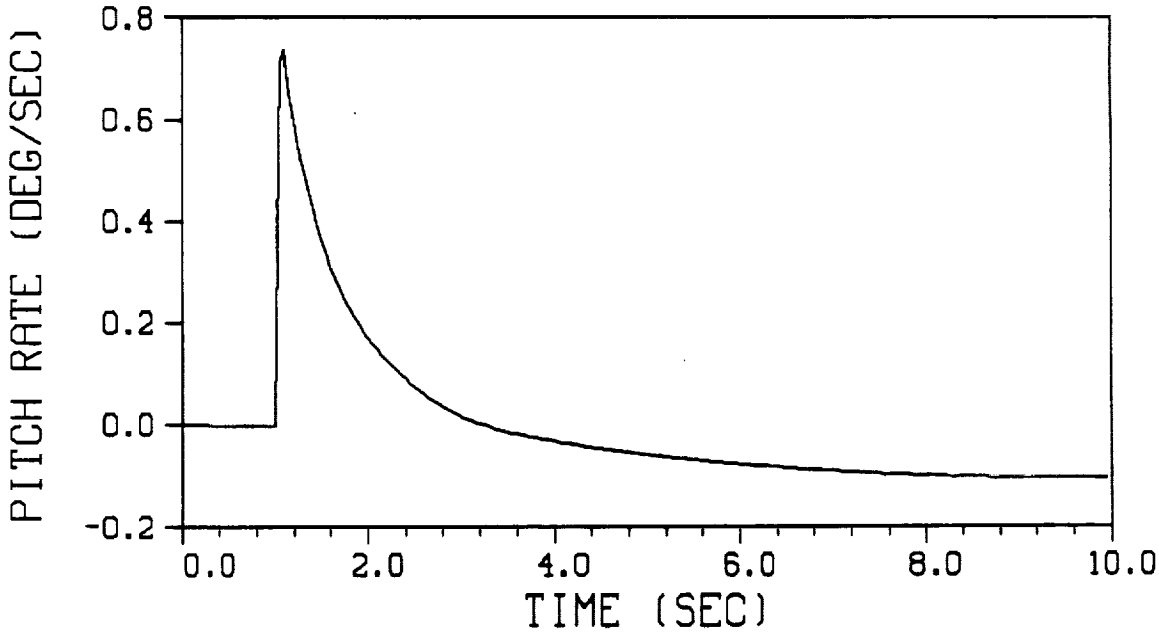

Plot B.2.-1. - Short period dynamics of the Harrier AV-8B pitch rate response due to an impulse of the longitudinal stick in a near hover.

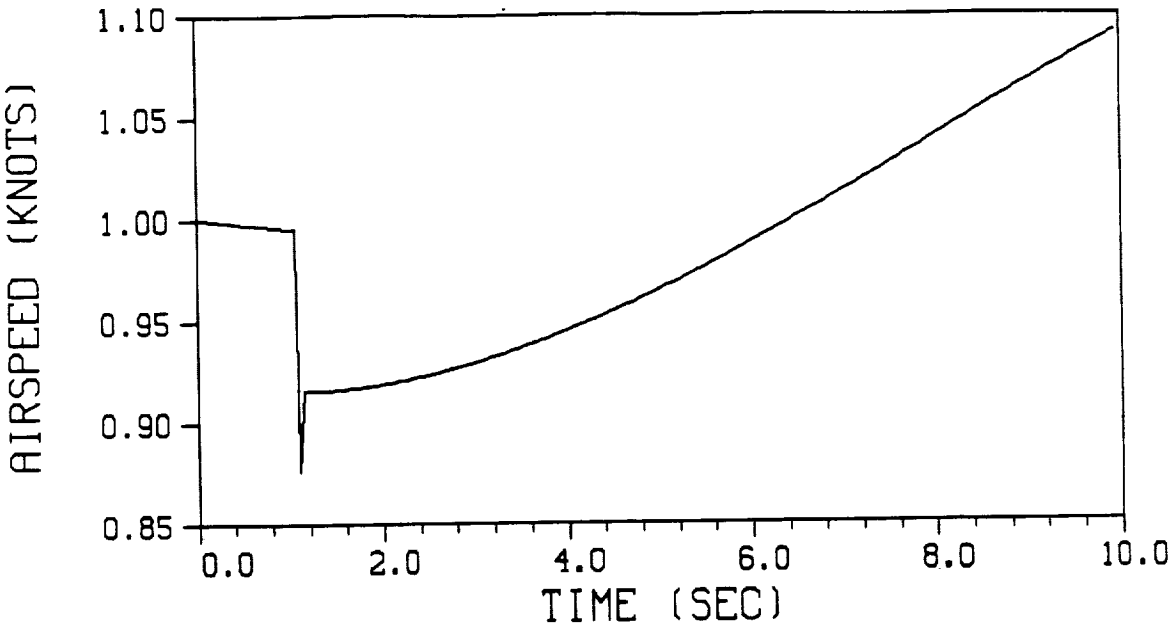

Plot B.2.-2. - Short period dynamics of the Harrier AV-8B forward velocity due to a 5 degree impulse of the nozzle angle at a near hover.

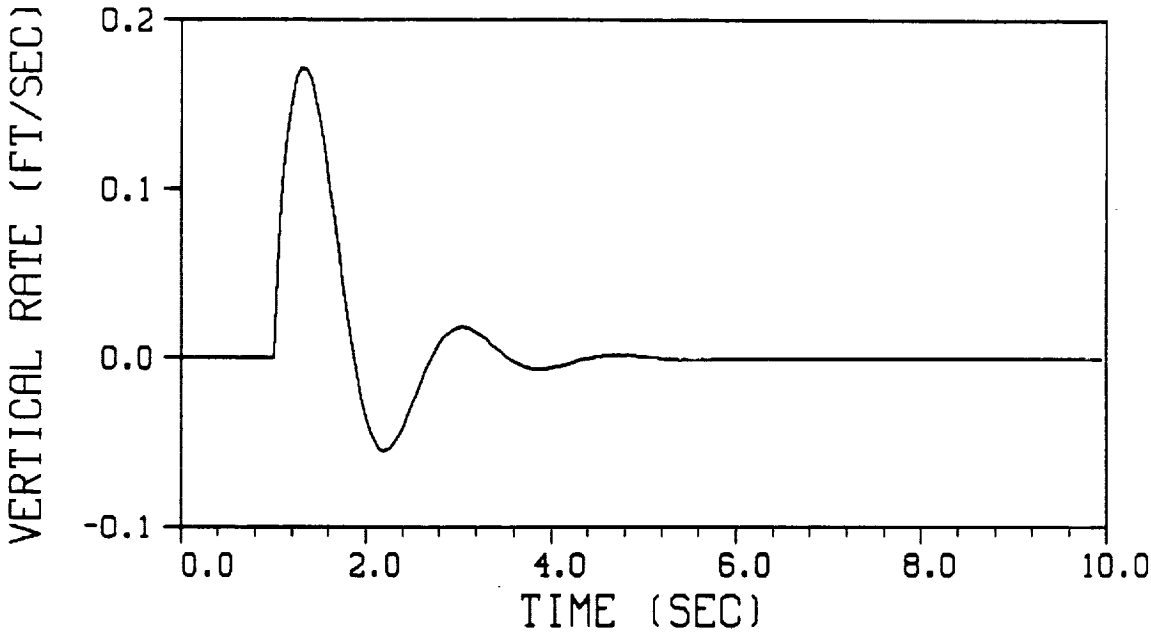

Plot B.2.-3. - Short period response of the Harrier AV-8B vertical rate due to an impulse of the throttle at a near hover.

Plot B.2.-4. - Short period response of the Harrier AV-8B engine speed due to an impulse of the throttle.

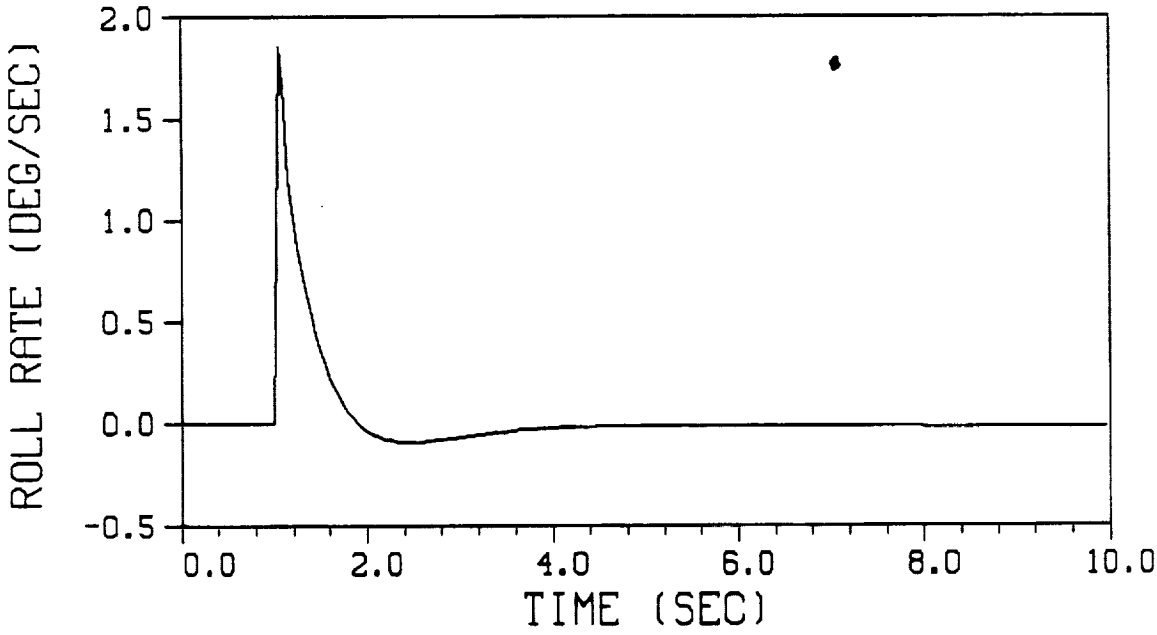

Plot B.2.-5. - Short period dynamics of the Harrier AV-8B roll rate due to an impulse of the lateral stick at a near hover.

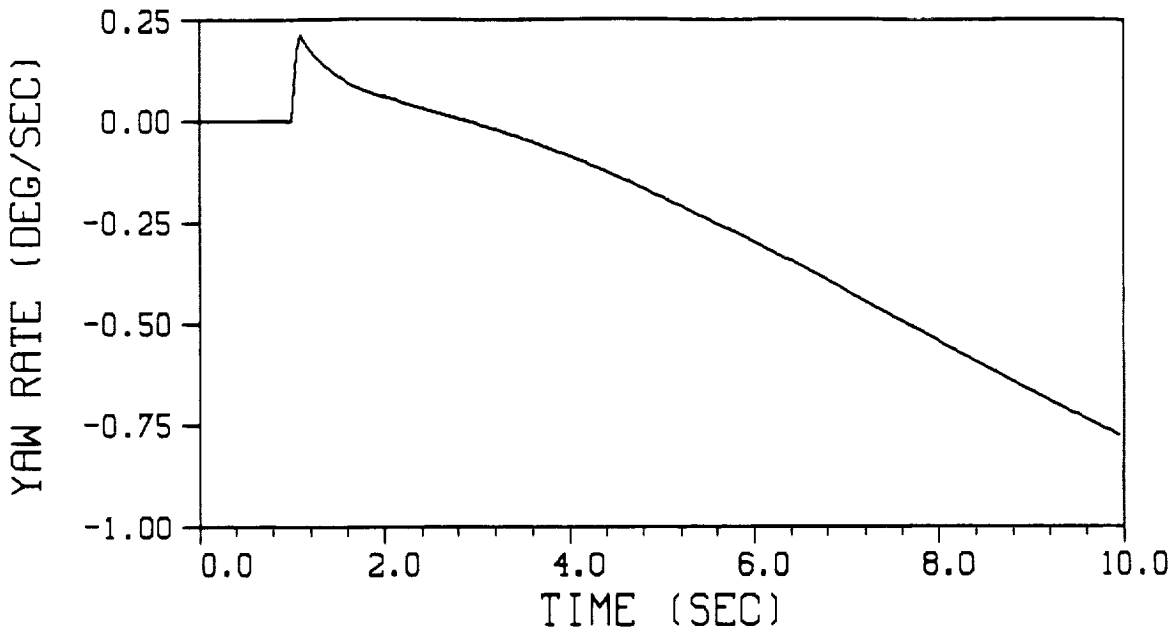

Plot B.2.-6. - Short period dynamics of the Harrier AV-8B yaw rate due to an impulse of the lateral stick at a near hover.

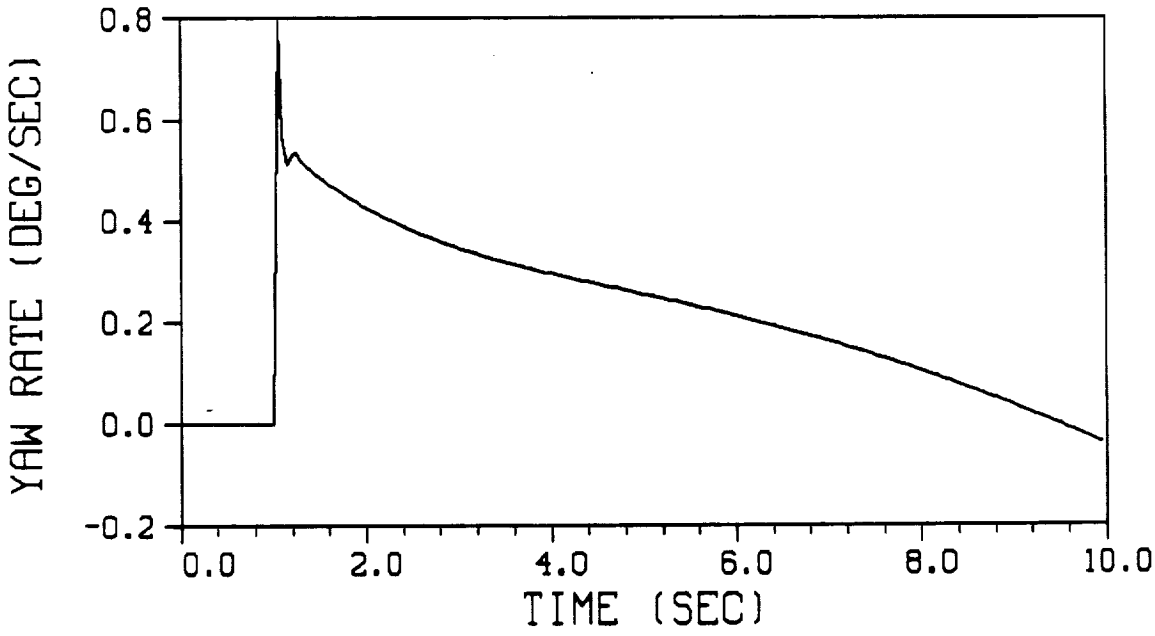

Plot B.2.-7. - Short period response of the Harrier AV-8B yaw rate due to an impulse of the rudder pedals at a near hover.

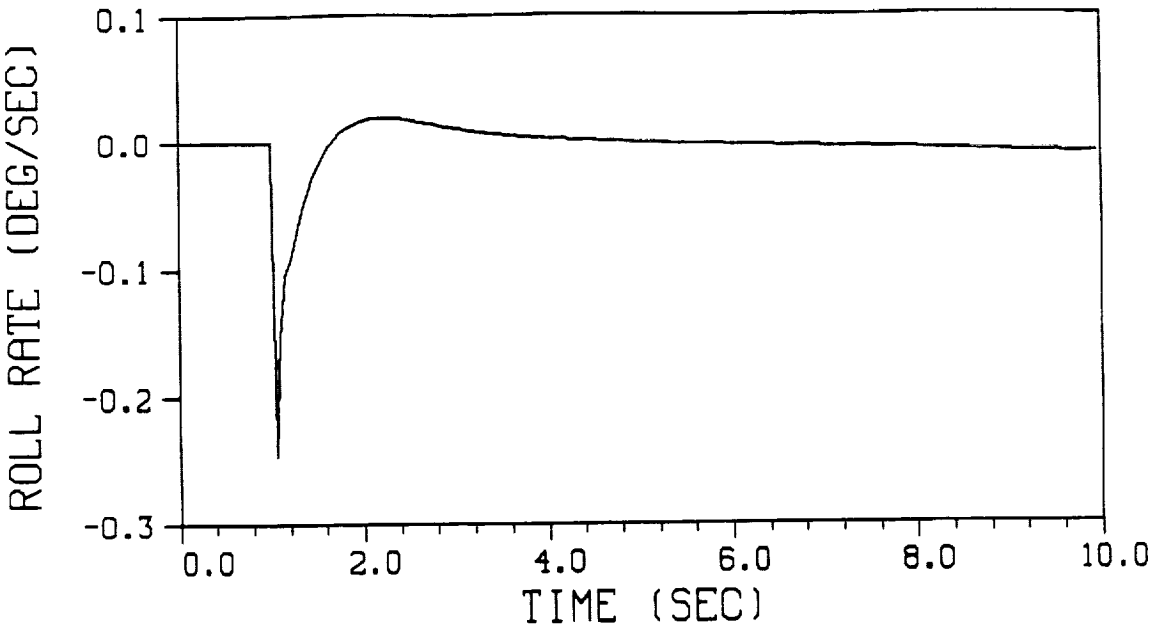

Plot B.2.-8. - Short period response of the Harrier AV-8B pitch rate due to an impulse of the rudder pedals at a near hover.